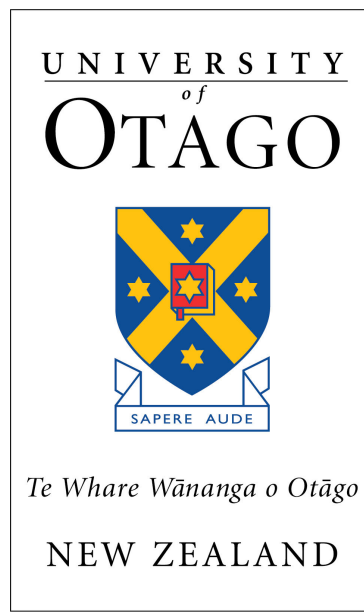


The Establishment and Characterisation of Gastric
Organoids as a Model for Hereditary Diffuse Gastric
Cancer



Yasmin Nouri

A thesis submitted in partial fulfilment of the degree:

Master of Science

Department of Biochemistry

University of Otago, Dunedin New Zealand

Abstract

Cancer is an exceptionally complex disease which requires an appropriately sophisticated model to facilitate its research. Organoids are 3D structures generated from stem cells, which recapitulate a target organ. These spherical cell cultures have the delicate organisation of the *in vivo* tissue, albeit on a smaller, simpler scale. Organoids are emerging in the field as invaluable tools for studying normal organogenesis and disease. Additionally, they can be used as an intermediate step between 2D cell lines and animal models in drug screens. This project describes the establishment and characterisation of mouse-derived gastric organoids as a disease model and medium-throughput drug screening tool for E-cadherin negative (*CDH1*^{-/-}) hereditary diffuse gastric cancer (HDGC). Their primary use will be to identify drugs that can be used as chemopreventative treatments for HDGC.

Organoids were cultured using an air-liquid interface (ALI) method from the gastric stem cells of conditional *Cdh1* knockout mice. *Cdh1* deletion was induced by co-culturing with endoxifen. Immunofluorescence and confocal microscopy have been used in the characterisation of the organoids and to validate the efficacy of *Cdh1* knockout. For drug screening, organoids were first exposed to the drug 48h post-seeding, and effects were recorded at 24 h intervals for 96 h.

Our gastric organoids harbour functional populations of epithelial cells and proliferating stem cells. They are spherical and cystic in shape, containing an inner lumen surrounded by epithelium. *Cdh1*-negative cells accumulate in the lumen of the organoids, possibly due to their impaired cell-cell adhesion ability relative to the *Cdh1*-positive cells. ARQ-092 and MK2206, both pan-AKT inhibitors, have been shown to reduce growth and induce death in the organoids in a synthetic lethal manner, validating their use as a drug screening tool for the development of a treatment for HDGC.

Acknowledgements

I would like to firstly thank my supervisor, Professor Parry Guilford, for your guidance throughout the duration of this project. Your unwavering optimism and support has not only made this thesis possible, but also one of the most enjoyable, formative and interesting experiences of my life. Thank you for your kindness and the incredible generosity you've shown towards me with your time. I feel very lucky to have worked with you this year. Long live the Kererū.

Another huge thank you goes to the SL group for the support (both academic and otherwise) that you've provided. I am so grateful to have been part of such a wonderfully dedicated and supportive group of scientists. Also thank you to the wider CGL group for making the lab such a great place to be. Thank you for all the advice, the friendship and mostly importantly, the many Bird Dogs.

Thank you to my wonderful friends and family for everything. The phone calls, the messages, the visits – none of it has gone unappreciated. A very special thank you to Rosie, my best friend and my biggest support – I couldn't have done this without you. Time for an Aperol Spritz I think.

Lastly, a very important thank you to the whanau involved in HDGC research. You are the 'why' that stayed at the forefront of my mind for the entirety of this project. Thank you for allowing us to go on this journey with you – every day we get a little bit closer to our end goal.

List of abbreviations

°C – Degrees Celsius	h – Hour(s)
µg – Micrograms	H&E – Haematoxylin and eosin
µL – Microliters	HDGC – Hereditary Diffuse Gastric Cancer
µm – Micrometre	iPSC – Induced pluripotent stem cell
µM – Micromole(s) per litre	KO – Knockout
2D – Two dimensional	LBC – Lobular breast cancer
3D – Three dimensional	LN ₂ – Liquid nitrogen
ALI – Air liquid interface	MFB11 – Myofibroblast cell line
ADB – Antibody diluting buffer	mL – Millilitre(s)
BB – Blocking buffer	mm ³ – Millimeters cubed
C57BL/6 – C57 black 6 mouse	mM – Millimole(s) per litre
cm – centimetre	PBS – Phosphate buffered saline
DAPI – 4',6-diamidino-2-phenylindole	PDO – Patient-derived organoid
DGC – Diffuse gastric cancer	PFA – Paraformaldehyde
DMEM-F12 – Dulbecco's modified Eagle's medium and F12	siRNA – Small interfering ribonucleic acid
DMSO – Dimethyl sulfoxide	RNAi – Ribonucleic acid interference
DNA – Deoxyribonucleic acid	rpm – Revolutions per minute
FHS – Foetal horse serum	SC – Stem cell
FBS – Foetal bovine serum	WT – Wildtype
GPCR – G protein-coupled receptor	

List of Figures

1.1 – Organisation of gastric glands	15
1.2 – Schematic diagram of the PI3K/AKT pathway	34
2.1 – Diagram of bridge mounting set up for organoid microscopy	46
2.2 – Diagram of the four plate conditions for each drug screening experiment	48
3.1 – Typical growth pattern of organoids from day 0-5	51
3.2 – Primary tissue that has failed to generate organoids	52
3.3 – Visualisation of the organoids through fluorescence and confocal imaging	54
3.4 – A comparison of fluorescence and confocal imaging	55
3.5 – Induced (KO) organoids display successful induction of Cdh1 knockout	57
3.6 – Uninduced (WT) organoids show consistent E-cadherin expression	58
3.7 – Growth pattern of TdTomato-expressing organoids	61
3.8 – Immunofluorescence of TdTomato-expressing organoids	63
3.9 – E-cadherin deficient cells cluster in the inner lumen of the organoid	65
3.10 – TdTomato fluorescence increases over time	67
3.11 – Confocal images of organoids with and without collagen	69
3.12 – Ki67 staining in organoids showing proliferating cells	71
5.1 – DMSO tolerance screening in the organoids	82
5.2 – Representative brightfield images of organoids exposed to ARQ-092 and controls	85
5.3 – Percentage change in area of organoids from day 2-6	88
5.4 – Bar graph showing % Change in area of organoids exposed to ARQ-092 for 96 h	89

5.5 – Confocal images of DMSO control organoids	90
5.6 – Confocal images of uninduced (WT) organoids exposed to ARQ-092	91
5.7 – Confocal images of induced organoids exposed to ARQ-092	93
5.8 – Representative brightfield images of organoids exposed to MK2206 and controls	95
5.9 – Data showing the percentage change in area of organoids from day 2-6	98
5.10 – Bar graph showing Change in area of organoids exposed to MK2206 for 96 h	99
5.11 – Confocal image of an uninduced (WT) organoid exposed to MK2206	100
5.12 – Confocal images of induced organoids exposed to MK2206	101
5.13 – Brightfield images of organoids exposed to Vorinostat and controls	103
5.14 – Confocal image of an uninduced (WT) organoid exposed to Vorinostat	106
5.15 – Confocal images of induced organoids exposed to Vorinostat	107
5.16 – Brightfield images of organoids exposed to MBCD and controls	110
5.17 – Confocal image showing a KO water control organoid after 6 days of growth	116
5.18 – Confocal image of an uninduced (WT) organoid exposed to MBCD	117
5.19 – Confocal imaging of induced (KO) organoids after being exposed to MBCD	118

List of Tables

2.1 – Concentration of components in collagen gel culturing kit organoid model	42
2.2 – Primary and secondary antibody dilutions used in immunofluorescence	45
3.1 – Approximate percentage of knocked out cells in a sample of organoids	59

Table of Contents

ABSTRACT	3
ACKNOWLEDGEMENTS	5
LIST OF ABBREVIATIONS	6
LIST OF FIGURES	7
LIST OF TABLES	9
TABLE OF CONTENTS	10
CHAPTER 1: INTRODUCTION.....	14
1.1 GASTRIC CANCER	14
1.1.1 <i>Introduction</i>	14
1.1.2 <i>Subtypes</i>	14
1.1.3 <i>Stomach anatomy</i>	15
1.2 HEREDITARY DIFFUSE GASTRIC CANCER	16
1.2.1 <i>Introduction</i>	16
1.2.2 <i>CDH1 Function</i>	17
1.2.3 <i>CDH1's Role in Cancer</i>	18
1.2.4 <i>CDH1's Role in HDGC</i>	18
1.2.5 <i>Onset</i>	19
1.2.6 <i>Progression</i>	20
1.2.7 <i>Current clinical management</i>	20
1.3 SYNTHETIC LETHALITY	22
1.3.1 <i>Introduction</i>	22
1.3.2 <i>Possible Synthetic Lethal Candidates</i>	24
1.4 CURRENT MODELS FOR HDGC	25

1.4.1 2D cell lines	26
1.4.2 Animal models	27
1.5 ORGANOIDS	28
1.5.1 Introduction	28
1.5.2 Gastric organoids.....	29
1.5.3 Organoid culture methods.....	30
1.5.4 Conditional knockout mice.....	31
1.6 PI3K/AKT PATHWAY	32
1.6.1 Overview and role in cancer	32
1.7 AIMS.....	35
CHAPTER 2: MATERIALS AND METHODS	36
2.1 LIST OF REAGENTS.....	36
2.2 LIST OF EQUIPMENT	37
2.3 SOFTWARE	38
2.4 ETHICS	38
2.5 MYOFIBROBLAST CULTURE.....	39
2.5.1 Myofibroblast passage	39
2.5.2 Myofibroblast freezing.....	40
2.5.3 Myofibroblast resurrection	40
2.6 ORGANOID CULTURE	40
2.6.1 Mouse euthanasia and stomach extraction	40
2.6.2 Organoid seeding.....	41
2.7 ORGANOID INDUCTION	43
2.7.1 Knockout induction	43
2.7.2 Knockout efficacy calculations.....	44
2.8 IMMUNOFLUORESCENCE	44
2.8.1 Staining.....	44
2.8.2 Bridge mounting	45

2.8.3 <i>Brightfield and Fluorescence microscopy</i>	46
2.8.4 <i>Confocal microscopy</i>	47
2.9 DRUG SCREENING	47
2.9.1 <i>DMSO toxicity testing</i>	47
2.9.2 <i>Drug treatment</i>	47
2.9.3 <i>Quantification of organoid viability</i>	49
2.9.4 <i>Statistical analysis</i>	49
CHAPTER 3: OPTIMISATION RESULTS	50
3.1 ORGANOID ESTABLISHMENT AND GROWTH	50
3.2 OPTIMISATION OF IMAGING TECHNIQUES	53
3.3 <i>CDH1</i> KNOCKOUT INDUCTION.....	55
3.4 ESTABLISHMENT OF TdTOMATO ORGANOIDS	60
3.5 IMMUNOFLOURESCENCE OPTIMISATION: COLLAGENASE.....	68
3.6 KI67 STAINING	71
3.7 CD44 STAINING.....	73
3.8 CONCLUDING REMARKS	73
CHAPTER 4: OPTIMISATION DISCUSSION.....	74
CHAPTER 5: DRUG SCREENING RESULTS.....	81
5.1 DMSO TOLERANCE.....	81
5.2 DRUG SCREENING PROTOCOL	84
5.3 ARQ-092.....	84
5.4 MK2206	95
5.5 VORINOSTAT	103
5.6 MBDC.....	110
5.7 CONCLUDING REMARKS	119
CHAPTER 6: DRUG SCREENING DISCUSSION	120
CHAPTER 7: CONCLUDING REMARKS AND PROJECT SIGNIFICANCE.....	126

REFERENCES	128
APPENDIX A	140
A.1 REAGENT PREPARATIONS	140
A.1.1 Antibody diluting buffer	140
A.1.2 Blocking buffer	140
A.1.3 Phosphate buffered saline (PBS).....	140
A.1.4 Myofibroblast freezing medium	140
A.1.5 Trypsin preparation	140

Chapter 1: Introduction

1.1 Gastric Cancer

1.1.1 Introduction

Gastric cancer, encompassing both intestinal and diffuse subtypes, is the fourth most common cancer worldwide and the second leading cause of cancer-related deaths (Nadauld & Ford, 2013). Rates of gastric cancer vary drastically between countries, but are generally highest in Eastern Asia and lowest in North America and Africa (Torre et al., 2015). This geographical variation can be largely attributed to regional differences in diet, food storage and rates of *Helicobacter Pylori* infection (Parkin, 2006). Despite ongoing clinical and scientific research, gastric cancer persists as a highly prevalent disease with a generally poor prognosis. Treatment advancement is relatively slow, due to a lack of understanding surrounding the exact molecular changes that underpin the development of the disease, resulting in a poor 5-year survival rate of under 25% (Ferlay et al., 2010). Part of the difficulty in understanding and treating gastric cancer is that it is a multifactorial disease, with many genetic and environmental risk factors contributing to its carcinogenesis.

1.1.2 Subtypes

The two histologically distinct gastric cancer subtypes as defined by the Lauren classification (Lauren, 1965), intestinal and diffuse, differ in their primary risk factors as well as their morphology, epidemiology and molecular mechanisms of development (Nadauld & Ford, 2013). Intestinal-type gastric cancer is more prevalent as an aging disease, has stronger links to environmental risk factors and a more differentiated phenotype, while diffuse-type generally has a younger age of onset, inherited risk factors, and a diffuse phenotype (Poultsides &

Norton, 2015). Diffuse-type is the less common form of the two subtypes, accounting for approximately 30% of all gastric cancer cases (Oliveira et al., 2009).

1.1.3 Stomach anatomy

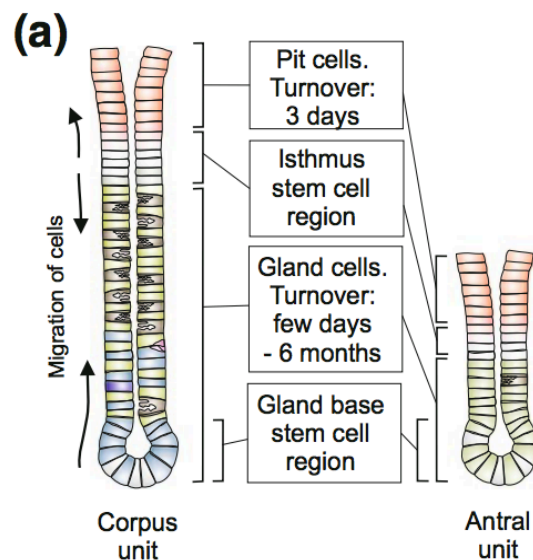


Figure 1.1 | Organisation of gastric glands. A) Each gland is divided into four regions: the pit, isthmus, gland neck and gland base. Stem cells reside in the isthmus and gland base, where they divide and differentiate, renewing the various cell types of the gland. Adapted from Pompaiah & Bartfield, 2017.

Mutations that cause dysregulation of the stem cell population within the gastric gland are often at the root of gastric cancer. The inner stomach wall is lined by columnar epithelial cells, organised into deep crater-like indentations called gastric pits (Fig. 1.1). Each gastric gland acts like a conveyer belt; a production line of various differentiated cells, all being generated from a meticulously regulated population of stem cells within the gland. The turnover of cells in the gastric gland is both continuous and tightly regulated. Each cell type is renewed at a different rate, ranging from 3 days to 6 months (Pompaiah & Bartfield, 2017). Moreover, the turnover rate within each cell type is dynamic, gaining or losing speed depending on the needs

of the gastric environment at any given time. This enormous regenerative burden sits on the shoulders of the small stem cell population harboured within the gastric pits. When this tightly regulated system malfunctions, the effects are substantial and widespread.

1.2 Hereditary Diffuse Gastric Cancer

1.2.1 Introduction

Although the vast majority of both intestinal- and diffuse-type gastric cancers are sporadic, a few percent of diffuse-type cases are caused by an autosomal dominant gastric cancer predisposition syndrome called Hereditary Diffuse Gastric Cancer (HDGC) (Fitzgerald et al., 2010; Guilford et al., 1998). HDGC has been genetically defined by the presence of an inactivating, germline mutation in the tumour suppressor gene *CDHI* (Guilford et al., 1999), although occasional mutations in other genes with related function, such as *CTNNA1*, have been reported (Hansford et al., 2015).

The clinical criteria to trigger mutation screening in gastric cancer cases is currently as follows:

- Families where two or more members develop gastric cancer (one diffuse type) at any age.
- Anyone who presents with diffuse gastric cancer (DGC) before the age of 40.
- Families with at least one case of both DGC and lobular breast cancer (LBC), one before the age of 50.

Screening could also be considered in patients presenting with bilateral or familial LBC before the age of 50, patients with precursor signet ring cell carcinoma lesions and patients presenting with DGC who also have a cleft lip/palate (van der Post et al., 2015).

Overall, New Zealand has a relatively low incidence of gastric cancer. However, the New Zealand Māori population, which comprises 15% of the total population, harbours rates of gastric cancer more than three times higher than that of the non-Māori population (Ministry of Health, 2015). In further contrast to the general population, the predominant subtype being presented within Māori is diffuse, and the age of onset is on average 10 years younger than that of non-Māori. It has recently been reported that this disproportionately high prevalence can be partly attributed to the increased frequency of germline mutations in the *CDHI* gene in New Zealand Māori (Hakkaart et al., 2018).

1.2.2 *CDHI* Function

The *CDHI* gene is located on chromosome 16q22.1 and spans over 100 kB. It has a 2.6 kb coding sequence, which is divided into 16 exons (Dunbier & Guilford, 2001). The protein product of *CDHI*, Epithelial cadherin (E-cadherin), is a type I cadherin, and the founding member of the cadherin superfamily. E-cadherin's primary role in the body is to act as an adhesive protein between cells in epithelial tissue. First cloned and fully characterised in 1995, E-cadherin is defined as a calcium-dependent epithelial cell-cell adhesion glycoprotein (Bex et al., 1995). It has an extracellular domain for intercellular adhesion, a single-pass transmembrane region and a highly conserved intracellular domain (Grunwald, 1993; Takeichi, 1991). The extracellular domain forms homophilic bonds with E-cadherin molecules on neighbouring cells, while the cytoplasmic domain interacts with the actin cytoskeleton via catenins, along with other transmembrane and cytoplasmic proteins (Briehner & Yap, 2013; Kemler, 1993). The inter- and intracellular interactions that E-cadherin forms are the core of adherens junctions – strong, dynamic links between neighbouring cells.

In addition to its role in cell adhesion and cytoskeletal organisation, E-cadherin also acts to transduce mechanical stress across the cell membrane and trigger intracellular signalling

cascades, initiating many integral growth, proliferation and survival pathways (Berx et al., 1995; Lecuit & Yap, 2015). Furthermore, it plays a crucial role in the contact inhibition of cell growth and programmed cell death. Epithelial cells continually proliferate until they have occupied a defined area – a process that is especially active during embryogenesis and wound healing. Once the defined area has been sufficiently occupied with epithelial tissue, growth signals are repressed and proliferation pathways are inhibited, halting growth (Kim, Koh, Chen, & Gumbiner, 2011). This contact inhibition of cells, along with controlled cell death, is crucial to the maintenance and correct function of complex tissues and is the basis of E-cadherin's classification as a tumour suppressor.

1.2.3 *CDHI*'s Role in Cancer

E-cadherin's role as a tumour suppressor gene means that silencing mutations and downregulation of E-cadherin expression can result in cells displaying poor differentiation, strong invasive potential, loss of polarity and mesenchymal phenotypes (Berx et al., 1995; P. Carneiro et al., 2012; Menke & Giehl, 2012). For these reasons, it is often correlated with poor prognosis in various epithelial cancers. E-cadherin promoter studies have shown negative regulation throughout tumour progression, further affirming the inverse relationship between the normal expression of E-cadherin and human malignancy (Berx et al., 1995). Notably, somatic mutations in the E-cadherin gene have been strongly linked with sporadic diffuse-type gastric cancers and lobular breast cancer (Dunbier & Guilford, 2001).

1.2.4 *CDHI*'s Role in HDGC

Those born with a heterozygous inactivating mutation in *CDHI* have a 70% chance of developing DGC in their lifetime, as well as an additional 40% chance of LBC (Hansford et al., 2015; van der Post et al., 2015). In 1998, *CDHI* was identified as the primary gene responsible for HDGC. Genetic linkage analysis and sequencing were used to identify

inactivating *CDHI* mutations in three Māori families harbouring high rates of diffuse gastric cancer (Guilford et al., 1998). Age of onset for diffuse gastric cancer in these families was exceptionally low. The majority of those with clinically apparent stomach cancer were under 40, with the youngest patient dying at only 14 years of age (Guilford et al., 1998).

Although there are no dominant mutational hotspots in *CDHI*, over 155 germline mutations have been identified in different HDGC families (Hansford et al., 2015), and it is estimated that there are now over 500 known HDGC families worldwide (P. Guilford, pers. comm.). There is no known correlation between the type and location of *CDHI* mutation and cancer phenotype (Guilford, Humar, & Blair, 2010).

1.2.5 Onset

It is a heterozygous inactivation of *CDHI* that predisposes mutation carriers in HDGC families to developing DGC; homozygous loss of *CDHI* is embryonically lethal (Guilford et al., 2010). Cells that develop into HDGC-related cancers have undergone somatic inactivation of the second copy of *CDHI*, which can happen at any point throughout the mutation carrier's life. It is thought that this inactivation occurs largely through epigenetic mechanisms, including DNA promoter hypermethylation. Cells with a homozygous loss of *CDHI* are devoid of E-cadherin, and therefore have disrupted cellular function in many integral growth, survival and proliferation pathways.

After the second copy of *CDHI* has been lost, the onset of gastric cancer is typified by the development of stage T1a signet ring cell carcinomas (Guilford et al., 2010). These carcinomas are initially relatively indolent, displaying lower rates of proliferation than surrounding non-malignant cells. As many as several hundred T1a foci have been observed in a single patient (Charlton et al., 2004).

1.2.6 Progression

Following the initial development of multifocal T1a signet ring cell carcinomas, a small proportion of these cancers progress to higher stage (Guilford, 1999). Lacking the tumour suppressing function of E-cadherin, these cells adopt an invasive phenotype, where their poorly defined cell architecture allows them to infiltrate the underlying stroma. The timing of this process is unclear, as evidence suggests that there is an undefined period of dormancy after the initial development of a signet ring cell carcinoma (Barber et al., 2008). Once the cancer does begin to progress, the process is often rapid.

Cancer progression is often aligned with a transition of the cells into a mesenchymal phenotype (Egeblad et al., 2010). This process is known as epithelial to mesenchymal transition (EMT) and is a well-established hallmark of cancer advancement. The phenotypic change causes the cells to lose polarity, gain migratory and invasive abilities and resist apoptosis. Specifically, the down regulation of E-cadherin as a crucial epithelial cell-cell adhesion protein results in β -catenin being released from its usual membrane-bound position. Free β -catenin is translocated to the nucleus where it is responsible for the activation of signalling pathways, such as *WNT*, that promote cell motility and prevent adhesion. This process ultimately provides the cells with the ability to metastasise (Egeblad et al., 2010). In cancers such as HDGC where the loss of E-cadherin plays a causal role, and expression is lost early on in cancer progression, tumours display an almost permanent mesenchymal phenotype (Guilford et al., 1998; Yang & Weinberg, 2008).

1.2.7 Current clinical management

As it stands, the only treatments available to those born with a *CDHI* mutation contain significant drawbacks. The clinical management of HDGC begins with genetic counselling and predictive testing for mutation(s) in the *CDHI* gene from approximately 16 years of age for

those in known HDGC families (van der Post et al., 2015). These are typically families who have presented with one or more cases of diffuse gastric cancer or lobular breast cancer, especially those with early-onset cases. It is also recommended that regardless of family history, individuals presenting with DGC below the age of 40 should be screened for germline *CDHI* mutations (Poultsides & Norton, 2015).

Family members identified as carrying a *CDHI* mutation must then consider their treatment options, which are outlined below.

1.2.7.1 Surveillance

Patients can opt for a surveillance strategy, where they undergo regular endoscopies and biopsies – usually annual – to monitor for the presence of cancerous gastric signet ring cells. However, the histological nature of HDGC is diffuse, in that its onset is defined by small, unevenly distributed malignant foci which spread below an intact mucosa and are therefore difficult to detect. Moreover, the number of these foci can vary significantly between individual patients. In a study of six patients from three HDGC kindred in New Zealand, the number of foci in each individual stomach ranged between 4-318 (Charlton et al., 2004). In another study of nine HDGC cases, gastrectomy specimens contained between one and 161 individual foci, many of which were underlying the normal mucosa (Carneiro et al., 2004). For these reasons, the surveillance strategy, though beneficial in its relatively low-impact nature, is imperfect. Even with rigorous check-ups, the early-stage signet ring cells can be missed by endoscopy. This has been reported in multiple case studies, where patients receive negative biopsy results despite having extensive DGC (Huntsman et al., 2001). If advanced disease is missed, the patient's prognosis is generally poor. By the time the cancer has become clinically apparent, the 5 year survival rate is a dismal 10% (Poultsides & Norton, 2015). For these reasons, it is

recommended that individuals who test positive for a *CDHI* mutation, regardless of endoscopic findings, should consider a prophylactic gastrectomy (Fitzgerald et al., 2010).

1.2.7.2 Prophylactic gastrectomy

The second treatment option, though more effective than the former, is not without its own caveats. Due to the wide distribution of signet ring cells throughout the stomach, the only sure way of eliminating all risk of HDGC is to surgically remove the entire stomach. Patients can therefore opt for a gastrectomy. Although preferable to gastric cancer, this procedure can have a long-term detrimental impact on the patient's quality of life. It is a technical procedure that harbours many immediate and long-term risks. Although overall mortality from the surgery is only 1-2%, almost all patients experience often severe side effects, including diarrhoea, weight loss, fatigue, iron and Vitamin B₁₂ deficiencies, and difficulty eating (Norton et al., 2007). Therefore, there is an urgent need for a highly effective, relatively non-invasive treatment for HDGC.

1.3 Synthetic Lethality

1.3.1 Introduction

Ideally, a chemoprevention strategy will be developed for HDGC, where patients can take a regular dose of highly specific chemotherapy to prevent the onset of the HDGC phenotype. This therapy would utilise a compound that selectively kills cancerous cells while leaving normal cells largely unharmed. However, the development of such a drug is no small undertaking. For starters, cancerous cells, though stand out in phenotype, are often only subtly different genetically from their non-cancerous equivalents. In addition to this, further difficulties arise when the gene in question is a tumour suppressor with a loss of function mutation, rather than an oncogene with a gain of function mutation. The fully or partially

silenced products of mutated tumour suppressors are pharmacologically elusive. Drugs are typically designed to inhibit proteins, so the pharmacologic restoration of a silenced function is fundamentally difficult (Iglehart & Silver, 2009). The circumvention of this problem lies within the strategic targeting of cellular vulnerabilities – an approach known as synthetic lethality.

Originally defined in 1946 by geneticists working on the fruit fly, synthetic lethality describes the relationship between two genes, where the loss of one gene does not impact cell viability, however the additional loss of the second gene will induce cell death (Dobzhansky, 1946). This concept has since been thoroughly explored, revealing itself as a promising new area for cancer therapy development (Chan et al., 2011; Ferrari, Lucca, & Foiani, 2010; Kaelin, 2009).

Processes crucial to cell survival are often achieved through multiple redundant cell signalling pathways (Lord, Tutt, & Ashworth, 2015). This means that the inactivation of one pathway does not necessarily result in cell death. Rather, the process is carried out by another compensatory pathway – a concept known as functional buffering. This redundancy is at the crux of why cancerous cells can survive despite major disruptions in integral signalling pathways. In cancer cells where a major pathway has been silenced, these compensatory pathways can be exploited as cellular vulnerabilities. In other words, synthetic lethal genes can be utilised as novel therapeutic targets for cancers caused by the loss of a tumour suppressor gene by inducing cell death in cancerous cells, while leaving non-cancerous cells largely unharmed.

The first synthetic lethal relationship to be utilised as an anticancer therapy was established in 2005 between the genes *BRCA1/2* and polyADP ribose polymerase (*PARP*) (Bryant et al., 2005; Farmer et al., 2005). This led to the development of *PARP* inhibitors as a

chemotherapeutic drug for breast cancer, which exploit the vulnerabilities surrounding DNA repair in *BRCAl/2* negative breast cancer cells. More recently, several other synthetic lethal relationships have been discovered and explored as potential therapeutic targets, such as the tumour suppressor *P53* with *ATR*, a key determinant of replication fork stability (Reaper et al., 2011; Ruzankina et al., 2009; Sangster-Guity, Conrad, Papadopoulos, & Bunz, 2011). In the case of HDGC, potential synthetic lethal drug targets are genes implicated in pathways that compensate for the homozygous loss of *CDHI*. A particular focus will be put on genes where pharmacologic inhibition will be easily attainable, such as those coding for kinases and other enzymes (Kaelin, 2005).

Synthetic lethality provides a novel approach to the field of cancer therapy, which in some areas has fallen into a state of stagnancy. It is a solution to the frustrations of crippled or silenced tumour suppressor genes, previously deemed undruggable. It competes with the idea that a new mutation is a cancer cell's strength, a new barrier to treatment, instead allowing them to be seen as potential lethal vulnerabilities to be exploited. Treatment development using this approach can be rapid, either through using new compounds uncovered with chemical screens, or by utilising existing compounds and licenced drugs for even faster implementation (Lord et al., 2015).

1.3.2 Possible Synthetic Lethal Candidates

The identification of novel synthetic lethal targets can be done through an extensive screening process. The goal of a synthetic lethal screen is to reveal genes which when chemically inhibited or transcriptionally silenced, inhibit cells harbouring the genetic mutation of interest – usually a tumour suppressor gene.

The inherent complexity of cell signalling networks make synthetic lethal interactions difficult to predict. However, high throughput RNAi screening has been used as an unbiased approach to identify genes in a synthetic lethal relationship with *CDHI* (Telford et al., 2015). Previous work at the Cancer Genetics Laboratory has been done to identify potential synthetic lethal candidates for *CDHI*, as well as compounds capable of inducing the synthetic lethal effect.

Both an siRNA screen targeting 18,120 genes and a known drug screen of 4,057 drugs have been completed. These screens identified many lead synthetic lethal candidates, including G-protein coupled receptor (GPCR) signalling proteins and cytoskeletal proteins (Telford et al., 2015). Subsequent drug screening and bioinformatic work has built on this, helping to identify the *PI3K/AKT* cell survival signalling pathway as a key pathway in maintaining *CDHI* negative cell viability, and therefore a potential target for synthetic lethal drugging (Bougen-Zhukov et al., 2019, manuscript in preparation). This pathway is described in more detail in section 1.6.

1.4 Current models for HDGC

Cancer is an exceptionally complex disease, which requires appropriately sophisticated models to facilitate its research. Unfortunately, models of human cancers often struggle to recapitulate the incredibly diverse and ever-changing nature of *in vivo* cancerous tissue, while maintaining a suitable level of throughput. As a result of this, for a long time the price paid for complexity was reduced throughput. Researchers had to jump between simple, high throughput disease models such as transformed 2D cell lines, and complex, low throughput animal models in order to gain a more complete understanding of the disease.

1.4.1 2D cell lines

Transformed 2D cell lines are a well-established and thoroughly validated model for cancer. They provide a platform for the study of cancer in human cells and are easily manipulated, robust, tractable and rapidly expandable (Neal & Kuo, 2016). Their ability to be genetically and pharmacologically manipulated with relative ease means that cell lines can model specific mutations and cancer subtypes, while providing an ideal platform for preliminary, high-throughput drug screening.

However, without undermining their significant benefits, it must be acknowledged that as models of cancer, 2D cell lines are acutely flawed. Their inherent simplicity means that they fall short of accurately depicting the true nature of cancerous tissue, which harbours high levels of heterogeneity and heavily involves the tumour microenvironment. Although easily expandable, their long-term passage inevitably causes cells to evolve and pick up mutations, which if not regulated means that eventually they will no longer be an accurate representation of the tissues from which they were derived and intend to reflect (Neal & Kuo, 2016). Furthermore, cancer-specific cell lines often have uncharacterised background mutations, which can have an effect on their drug response and impact other experimental elements in an unprecedented manner. These limitations are at the root of why numerous anti-cancer treatments developed from 2D cell line screening have failed in clinical trials (Caponigro & Sellers, 2011; Kamb, 2005).

Cell heterogeneity and extracellular matrix interactions are at the core of cancer initiation and progression (Egeblad et al., 2010). Tumours, often incorrectly thought of as a group of cancer cell clones, are in actuality an organ – albeit a structurally and functionally abnormal one – comprised of differentiated cells, stem cells, and an extracellular matrix. Understanding the complex and dynamic interactions between heterogenic cancer cells within a tumour, as well

as with their microenvironment and the body as a whole, is crucial to the development of effective cancer treatments and prevention (Egeblad et al., 2010). Ultimately, this level of heterogenic complexity cannot be obtained with 2D models. As such, despite the benefits of 2D cell modelling, the technique is inherently limited and thus can only be effectively used as a first step in disease modelling and treatment research.

As a first *in vitro* screening step in our laboratory, two isogenic *CDHI*^{-/-} cell lines have been characterised (Chen et al., 2019, manuscript in preparation). The first, MCF10A, is a human epithelial breast cell line. This is a non-cancerous cell line with a ‘clean’ genetic background, suitable for this project due to HDGC’s link to LBC. The second cell line used, NCI-N87, is a gastric cancer cell line with a high rate of background mutations. Although more challenging to work with due to its unpredictable and changeable behaviours, this cell line reflects the more complex genomic landscape of cancerous tissue.

1.4.2 Animal models

Animal models, including patient-derived xenografts and genetically-engineered mouse models, are highly complex, inhabiting the opposing end of the cancer model spectrum to 2D cell lines. They are inclusive of a tumour microenvironment and heterogenous cell populations, meaning they are a more accurate model of the cancer they are depicting in comparison to 2D cell lines – both for the study of disease and drug screening (Neal & Kuo, 2016). However, as a result of their increased complexity, they lack the easy manipulation and expandability of cell lines. In addition to this, they are time, money and resource intensive. Therefore, they cannot provide the high-throughput modelling often required in cancer research. It has been observed that the tumour microenvironment can confer drug resistance through regulating the distribution of the drug or by releasing signals that prevent cell death (Egeblad et al., 2010). Therefore, having a model that is inclusive of this microenvironment, such as an animal model,

is imperative to studying disease and developing therapies. However, to maximise efficiency in the process, they should only be used late in the piece as a near-final step, preceded by higher-throughput, more amenable models.

Modelling a disease as multi-faceted as cancer is an endlessly challenging task for scientists in the field. As discussed, there are two opposing yet complementary movements in cancer modelling at present: firstly, a push towards more complex, more representative *in vitro* models, and secondly, a drive in the other direction that moves away from using high volumes of animal models and instead explores more ethical, high-throughput options. These two movements, opposite in direction but aligned in intention, meet in the middle and ‘find themselves’ at organoids. This medium-throughput cellular model of substantial complexity fills a previously vacant research niche, providing us with a platform for novel discovery in a new wave of disease modelling.

1.5 Organoids

1.5.1 Introduction

Organoids are 3D structures comprised of both differentiated and stem cells, which in part recapitulate the organisation and function of target organs. Propagated *in vitro*, these spherical cell cultures have the delicate organisation of the *in vivo* gastric gland, albeit on a smaller, simpler scale. They can be generated from various different cell types, including induced pluripotent stem cells (iPSCs), embryonic stem cells and adult stem cells (Fatehullah, Tan, & Barker, 2016; Yin et al., 2016) – both mouse (Li et al., 2014; Seidlitz et al., 2018) and human (McCracken et al., 2014; Pompaiah & Bartfeld, 2017; Seidlitz et al., 2018). Organoids provide an easily manipulated disease model with high-throughput potential, while maintaining a relatively complex level of structure and organisation. Though they do not replace either 2D

cell lines or animal models, organoids fill their own valuable niche in disease modelling. They harbour the ability to facilitate medium throughput, specific screening of drugs, provide a more comprehensive look at disease progression and mechanisms, and can aid in the development of personalised medicine (Xu et al., 2018).

Despite their undeniable benefits, like all models, organoids do not come without limitations. There are things that they cannot tell us, and thus we should not ask of them. Their main purpose is to act as a medium-throughput, medium-complexity screening tool for novel treatments, and to allow for a closer look at disease mechanisms. Organoids cannot provide comprehensive information on the extensive effects of cancer outside of the cancer cells, nor can they tell us about any long-term or downstream drug effects. Furthermore, despite their complex structure, they still do not harbour the complete cancer microenvironment that is so crucial to the thorough study of the disease. As a result, they should be considered complementary to, rather than replacive of, current *in vitro* and *in vivo* cancer models.

In recent years, organoids have increased substantially in popularity as a research tool. At present, they have been developed for virtually every human organ, including brain (Eiraku et al., 2008; Lancaster et al., 2013), intestine (Ootani et al., 2009), breast (Simian et al., 2001), lungs (Rock et al., 2009) and stomach (Mahe et al., 2013; McCracken et al., 2014; Nadauld et al., 2014; Pompaiah & Bartfeld, 2017; Seidlitz et al., 2018).

1.5.2 Gastric organoids

In recent years, gastric organoids, or gastroids, have been used to study cancer (Li et al., 2014; Seidlitz et al., 2018; Vlachogiannis et al., 2018), as well as other diseases such as *H. pylori* infection (McCracken et al., 2014; Pompaiah & Bartfeld, 2017; Schlaermann et al., 2016). The study of gastrointestinal cancers has advanced rapidly of late, owing in part to the organoid

model, which has made the investigation of oncogenic processes significantly more accessible (Neal & Kuo, 2016). Organoids can be used to investigate many of the well-established hallmarks of cancer using various assays, including cell proliferation, cell death, resistance to growth suppression, and invasion capabilities. Furthermore, organoids have proved to be a valuable drug screening tool, both for the discovery of novel treatment compounds, for example using an organoid biobank (Van De Wetering et al., 2015), and for the pre-screening of already established treatments on patient-derived organoids (Seidlitz et al., 2018; Vlachogiannis et al., 2018). They provide a sufficiently accurate measure of the efficacy of the drug and the *in vivo* response, often reflecting the results of clinical trials more accurately than equivalent 2D cell line screens (Jabs et al., 2017). Because of this, they are one of the primary drivers behind the emerging area of personalised medicine.

1.5.3 Organoid culture methods

There are currently two primary methods used for the culture of organoids: the submerged model and the air-liquid interface (ALI) model. The submerged model requires organoids to be grown embedded in Matrigel and completely submerged with growth media (Barker et al., 2010). The ALI method is an adaption of this, where the organoids are embedded in collagen in a transwell insert, which sits in an outer well of growth media (Ootani et al., 2009). This allows the organoids to have an air supply for oxygenation, as well as a supply of liquid growth media, which diffuses through the semi-permeable bottom of the transwell insert. The collagen mimics the structure of collagen found *in vivo*, and acts as an extracellular matrix for the organoids. The air-liquid interface (ALI) method encourages the culture of epithelial-mesenchymal hybrid structures from primary tissue (Neal & Kuo, 2016), and therefore is a suitable method for generating gastroids for studying epithelial cancers such as HDGC. In comparison to the submerged model, the ALI method has been described as the system providing the most accurate recapitulation of the *in vivo* situation (Katano et al., 2013a). It

establishes a polar environment, with air exposure on one side and a source of growth factor-containing liquid on the other. This is intended to mimic the *in vivo* environment for epithelial tissue, where a lumen lies on one side and a mesenchymal layer on the other side, encouraging a polar cell phenotype.

In the ALI model, organoids are co-cultured with myofibroblast cells, also embedded in the collagen, which provide a stromal-like environment and aid in maintaining the stem cell niche (Katano et al., 2015). The endogenous factors released by the myofibroblasts facilitate the growth of the organoids without the need for exogenous growth factors added into the media. A successful ALI culture will produce 3D, spherical structures with active proliferation in both the stem and epithelial cell populations. In addition to this, there is often an accumulation of apoptotic cells in the lumen, due to the rapid turnover rate of cells within the organoids (Katano et al., 2013b).

1.5.4 Conditional knockout mice

Loss-of-function studies can be easily performed using organoids derived from the stem cells of a genetically modified mouse with a mutant target gene. Moreover, inducible systems for conditional knockout cells can be added through the insertion of a *Cre*-inducible construct into the genome. This allows for the temporal and spatial control of the expression of a target gene.

The *Cre-loxP* construct is a bacteriophage P1 recombination system that can be utilised to mutate a gene of interest in an inducible manner (Schwenk, Baron, & Rajewsky, 1995). The system uses the *Cre* recombinase enzyme to catalyse target-specific DNA recombination between two *loxP* sites. If the *loxP* sites are placed flanking an essential part of a target gene, expression of *Cre* will result in the deletion of that essential segment of target DNA, and consequently silence the gene of interest.

This system is especially useful for genes, such as *CDH1*, that are embryonic lethal when homozygously inactivated, as it allows for temporal and spacial control of the knockout (Deng, 2012). In the case of HDGC, patients are born with only a heterozygous loss of the gene and lose the second copy somatically later in life. Therefore, induction of the homozygous loss of *Cdh1* in an established organoid is comparable to HDGC's initiating step. The mutational silencing of *Cdh1* in the mice can be restricted to specific cell types determined by the promotor *Cre* is placed under. For example, in order to knock out *Cdh1* from epithelial cells, *Cre* is placed under the promotor of *Cd44*, a gene that is highly expressed in the stem cells of several epithelial tissues (Senbanjo & Chellaiah, 2017).

1.6 *PI3K/AKT* pathway

1.6.1 Overview and role in cancer

The *PI3K/AKT* pathway is a crucial regulator of cell proliferation and survival and closely linked with E-cadherin. Co-immunoprecipitation has been used to show *PI3K*'s association with E-cadherin at the adherens junction and that *AKT* is activated by cell-cell adhesion (Pece, Chiariello, Murga, & Gutkind, 1999). E-cadherin-mediated activation of the *PI3K/AKT* pathway is crucial for the repression of programmed cell-cell death signals and the regulation of cell overgrowth through contact inhibition.

Deregulatory changes in cell signalling pathways underlie the development of many cancers. The *PI3K/AKT* pathway plays an important role in the regulation of many essential cell functions, including proliferation, metabolism, growth, survival and protein translation (Tapia et al., 2014). Due to its integral role in cellular function, deregulation of this pathway is

frequently found to play a role in the development and progression of a diverse range of malignancies, including gastric cancer.

Protein expression studies have shown that the majority of proteins implicated in the *PI3K/AKT* pathway are over-expressed or phosphorylated in gastric tumour tissue, when compared to normal gastric tissue of the same patients (Tapia et al., 2014). The main exception to this is the tumour suppressor gene *PTEN*, which is downregulated. This pathway can therefore be considered as a potentially effective target for gastric cancer therapy. Specifically, *PI3K* and *AKT* have been reported as being overexpressed in 80 and 82% of cases, respectively (Ye, Jiang, Xu, Zhou, & Li, 2012). This information, along with the screening previously done in our laboratory, has flagged the *PI3K/AKT* pathway as a strong contender for synthetic lethal targeting.

In normally functioning pathways, growth factor signalling is mediated by *PI3K* through *AKT*, which activates *mTORC1* when upstream signals are activated (Tapia et al., 2014). *mTORC2* acts through negative feedback to prevent *AKT* activity. When the pathway is deregulated in cancer cells, *PI3K* and *AKT* have increased levels of activity, which results in increased *mTORC1* activity and decreased negative feedback of *mTORC2*. These changes result in an uncontrolled increase in cancer-enabling cellular functions including cell growth, proliferation, autophagy, angiogenesis and protein synthesis. Recognition of the importance of this pathway in cancer has led to the development of a new class of *mTOR*-targeting anticancer therapies that have been yielding promising results. Drugs that inhibit other components of the pathways, including *AKT* and *PI3K*, are also emerging as promising options for cancer therapies (Brown & Banerji, 2017).

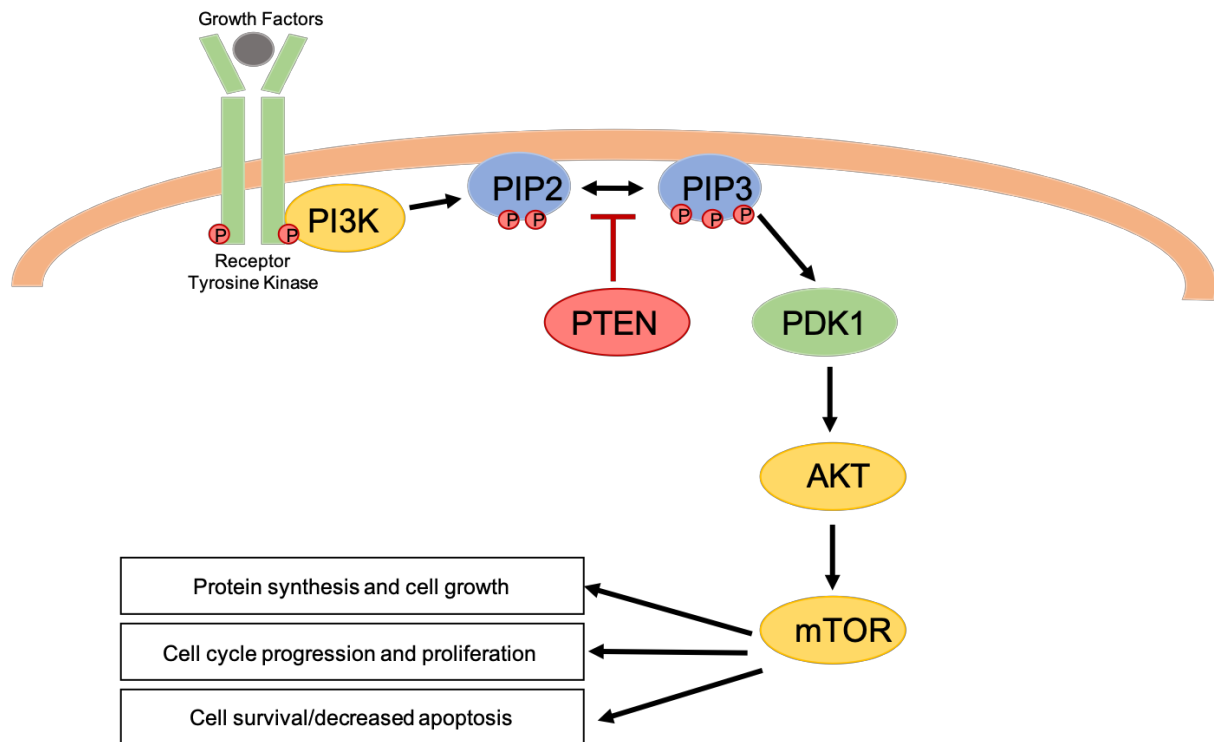


Figure 1.2 | Schematic diagram of the PI3K/AKT pathway. Growth factor signalling is mediated by PI3K through AKT, which activates mTOR when upstream signals are activated. This pathway regulates cell growth, proliferation and survival.

It is important to note that the *PI3K/AKT* pathway regulates a wide range of cellular processes, exceeding those involved in tumorigenesis. Therefore, proteins selected as therapeutic targets must be carefully chosen as to inflict minimal disruption on other integral *PI3K/AKT*-dependent process not involved in tumorigenesis. For example, due to its regulatory role on insulin metabolism, *PI3K* inhibitors have the potential to disrupt glucose homeostasis (Luo, Manning, & Cantley, 2003). A solution to this is to target proteins further downstream in the pathway, such as *mTOR*. Hence, the recent increase in popularity for *mTOR* inhibitors as cancer therapeutics.

1.7 Aims

This project aims to use gastric organoids derived from engineered mice as a model for HDGC cancer progression. This will be done through an initial optimisation phase, where organoid culture techniques and qualitative analysis methods will be assessed. Qualitative measurements will include morphology, proliferation rate and cell composition of the organoids. These will be measured using techniques such as light, fluorescence and confocal microscopy, as well as immunofluorescence staining.

The second part of this project will be a drug testing phase, where drugs that have previously been identified as potentially synthetic lethal will be applied to *Cdh1*-negative and *Cdh1*-positive organoids and their effects measured.

Ultimately, this thesis aims to prove the hypothesis that conditional *Cdh1*-knockout organoids can be used to identify synthetic lethal drugs with the potential to be used as treatments for the chemoprevention of HDGC.

Chapter 2: Materials and Methods

2.1 List of reagents

0.05% trypsin solution – Prepared in lab (Appendix A)

Antibody diluting buffer – Prepared in lab (Appendix A)

Anti-Ki67 Antibody – Abcam, USA

Anti-rat IgG (H+L), (Alexa Fluor 488) – Cell Signalling, USA

ARQ-092 – Selleckchem, USA

Blocking buffer – Prepared in lab (Appendix A)

CD44 Monoclonal Antibody – Invitrogen, USA

Chicken anti-Rabbit IgG Secondary Antibody (Alexa Fluor 594) – Invitrogen, USA

Dimethyl sulfoxide (DMSO) – Sigma-Aldrich, USA

Donkey anti-Goat IgG Secondary Antibody (Alexa Fluor 488) – Invitrogen, USA

Dulbecco's modified Eagle's medium and F12 (DMEM-F12) – Thermo Fisher Scientific, USA

Endoxifen Hydrochloride Hydrate – Sigma-Aldrich, USA

Ham's F-12 Nutrient Mix, GlutaMAX™ Supplement – Thermo Fisher Scientific, USA

Human/Mouse E-cadherin Antibody – R&D Systems, USA

Foetal bovine serum (FBS) – Invitrogen, USA

Foetal horse serum (FHS) – Invitrogen, USA

Freezing medium – Prepared in lab (Appendix A)

Gentamicin (Gibco) – Thermo Fisher Scientific, USA

Methyl- β -cyclodextrin – Sigma-Aldrich, USA
MK2206 – Selleckchem, USA
Nitta cellMatrix Collagen Gel Culturing Kit – Novachem, Australia
Paraformaldehyde (PFA) – BDH Limited, England
Phosphate buffered saline (PBS) solution – Prepared in lab (Appendix A)
ProLong Gold antifade reagent with DAPI – Thermo Fisher Scientific, USA
ProLong Gold antifade reagent without DAPI – Thermo Fisher Scientific, USA
Triton X-100 – Sigma-Aldrich, USA
Vorinostat (SAHA) – Selleckchem, USA

2.2 List of equipment

0.2 μ m hydrophilic syringe filter – Sartorius, Spain
1 mL cryovials – Nunc, Denmark
10 cm Cellstar cell culture dish – Greiner, Germany
1.5 mL Eppendorf tubes – Sigma-Aldrich, USA
30 mm Cellstar cell culture dish – Greiner, Germany
5 mL Eppendorf tubes – Sigma-Aldrich, USA
60 mm Cellstar cell culture dish – Greiner Bio-One, Germany
10 mL serological pipettes – Greiner Bio-One, Germany
15 mm cell culture dish – Greiner Bio-One, Germany
15 mL Falcon tubes – BD Biosciences, USA
22x22 mm glass cover slips – Menzel-Glaser, Germany
50 mL Falcon tubes – BD Biosciences, USA 500 mL filter system - Corning, USA
75 mL cell culture flasks – Greiner Bio-One, Germany

75x25 mm Gold Seal microscope slides – Thermo Fisher Scientific, USA

Centra 3C centrifuge – International Equipment Company, USA

CO₂ cell culture incubator – Binder, Germany

Dual chamber cell counting slides – Bio-Rad, USA

Eclipse Ti Inverted Microscope System – Nikon, USA

Eppendorf Mini Spin Plus centrifuge – Sigma-Aldrich, USA

Fuji LAS-3000 ECL Imaging System – Thermo Fisher Scientific, USA

Millicell cell culture inserts (0.4µm, 30mm) – Merck Millipore, Ireland

Mr. Frosty 5100 Cryo 1°C Freezing Container – Thermo Fisher Scientific, USA

Olympus CK2 Microscope – Olympus, New Zealand

Olympus Fluoview FV1000 Confocal Microscope – Olympus, New Zealand

TC10 Automated Cell Counter – Bio-Rad, USA

Tissue culture hood – EMAIL, Australia

Water bath – Semco, USA

2.3 Software

ImageJ – National Institute of Health, USA

2.4 Ethics

All animal procedures were approved by the University of Otago Animal Welfare and Ethics Committee (DET35/15) and were performed in accordance with University guidelines and regulations.

2.5 Myofibroblast culture

Myofibroblasts are adherent cells that are phenotypically similar to both fibroblast and smooth muscle cells. They are found in the subepithelial region of mucosal surfaces, including the gastrointestinal tract. Their role is both supportive and paracrine, aiding in the regulation of crypt structure and maintenance of the stem cell niche – hence their importance in gastric organoid culture (Hinz et al., 2007).

Myofibroblasts used here were previously isolated in our laboratory from a wildtype C57 black 6 mouse (C57BL/6) using a protocol adapted from Pastuła et al. (2016). This myofibroblast cell line (MFB11) was used for co-culture with organoids from passage 8, and no later than passage 17. MFB11 cells were cultured at 37 °C with 5% CO₂ in 75 mL cell culture flasks (Greiner). MFB11 complete culture media was made using Gibco DMEM/F-12 GlutaMAX™ (80%) supplemented with filtered (0.22 µm filter) fetal bovine serum (FBS) (20%).

2.5.1 Myofibroblast passage

MFB11 cells at 80-90% confluence were passaged. Following media aspiration, cells were washed once with 5mL phosphate buffered saline (PBS) and then incubated in 4 mL of 0.05% trypsin at 37 °C for 8 minutes. 8 mL of complete culture media was added to the flask and suspended cells transferred to a 15 mL Falcon tube. Cells were centrifuged at 700 rpm (Centra) for 5 minutes to pellet. Supernatant was then removed and cells resuspended in 1 mL of complete culture media. Cells were then counted using the TC10 automated cell counter (Bio-Rad) and re-seeded. Cells were re-seeded at 1.5×10^5 cells per 75 mL cell culture flask (approximately 1/10 of a confluent flask). Complete culture media was changed every 3 days and cells passaged every 7 days.

2.5.2 Myofibroblast freezing

For cryopreservation, cells were suspended in 1 mL of freezing media comprised of 80% complete culture media, 10% FBS and 10% Dimethyl sulfoxide (DMSO) in cryovials (Nunc). Cells were frozen down at 2×10^5 cells per cryovial. Cells were frozen to $-80\text{ }^{\circ}\text{C}$ in a Mr Frosty™ (Thermo Fisher Scientific) overnight and then transferred to liquid nitrogen (LN_2) for long term storage.

2.5.3 Myofibroblast resurrection

Frozen myofibroblast cells were removed from LN_2 and defrosted in a $37\text{ }^{\circ}\text{C}$ water bath. After defrosting, cells were immediately transferred to 15mL Falcon tubes containing 5 mL of complete culture media and pelleted by centrifugation at 700 rpm (Centra) for 5 minutes to pellet. Supernatant was then removed and cells were resuspended in 1 mL of complete culture media. Cells were seeded in 75 mL cell culture flasks (one vial into one flask) with 10 mL complete culture media. Media was changed after 24 hours to remove any residual DMSO, and then every 3 days.

2.6 Organoid culture

2.6.1 Mouse euthanasia and stomach extraction

Organoids were generated using stem cells from inducible knockout mice with a Cre-Lox system controlling both *Cdh1* and the fluorescent marker protein TdTomato under the *CD44* promoter (*CD44-cre/Cdh1^{-/-}/TdTomato*). Mouse pups were used on day 1-2 after birth.

After delivery, mice were euthanised through decapitation using a sterile single-edge razor blade in a 10 cm culture dish. Mice were then transferred to a sterile tissue culture hood for stomach extraction. A sterile pair of dissection scissors and forceps were used to remove the

mouse stomach. Forceps were used to hold the mouse in place while the scissors were used to make a small horizontal incision just above the stomach. The location of the stomach was known, as the small white organ was visible through the semi-transparent skin on the abdomen of the mouse pup. The stomach was removed through the small incision using the forceps and detached from the rest of the gastrointestinal tract using the scissors. The stomach was then placed into the lid of the 10 cm dish, where any congealed milk was expelled by pressing down gently on the stomach tissue using forceps.

Using a new pair of sterile forceps, the stomach was washed four times in four separate 30 mm cell culture dishes, each containing 100 μ L of PBS with added Gentamicin (Life Technologies) at 50 μ g/mL. The washed stomach was then placed into a 1.5 mL Eppendorf tube containing 100 μ L of PBS with Gentamicin (50 μ g/mL). Using a new pair of sterile scissors, stomach was then minced in the Eppendorf tube (approximately 15 cuts). Using a second, smaller pair of scissors, the stomach was minced further until the tissue was in pieces $< 0.5 \text{ mm}^3$. Equipment was sterilized between each individual mouse.

2.6.2 Organoid seeding

Organoids were cultured using an air-liquid interface (ALI) method (Ootani et al., 2009) to promote the development of epithelial/mesenchymal structures. This culture system is comprised of a 30 mm Millicell transwell insert (Millipore) with a raised, permeable (0.4 μ m) bottom that sits in a 60 mm cell culture dish (Greiner).

Prior to seeding stomach tissue, collagen containing MFB11 cells was prepared. 2.4 mL (1.2 mL per layer) of collagen mix was needed for each organoid dish (one stomach per dish). It was recommended that when preparing collagen, the total volume made should be 30% more

than what was required, due to the amount lost in the tube/pipette during preparation and tissue seeding.

cellMatrix™ Collagen Gel Culturing Kit (Nitta) was prepared as shown in table 2.1:

Component	Concentration (%)
cellMatrix™ collagen solution Type I-A	80
10x Ham's F-12 growth media (containing MFB11 cells)	10
Sodium bicarbonate buffer solution	10

Table 2.1 | Concentration of components in cellMatrix™ collagen gel culturing kit for use in the ALI organoid model.

To prepare the collagen mix, myofibroblast cells were first removed from their 75 mL cell culture flasks. Approximately 1×10^6 MFB11 cells were needed per organoid dish (5×10^5 per 1.2 mL layer). To remove cells, media was aspirated, cells were washed once with 5 mL phosphate buffered saline (PBS) and then incubated in 4 mL of 0.05% trypsin at 37 °C for 8 minutes. 8 mL of complete culture media was added to the flask and suspended cells transferred to a 15 mL Falcon tube. Cells were centrifuged at 700 rpm (Centra) for 5 minutes to pellet. Supernatant was then removed and cells resuspended in 1 mL of 10x Ham's F-12 growth media (Nitta collagen culturing kit). Cells were then counted using the TC10 automated cell counter (Bio-Rad).

Collagen mix was prepared on ice in either a 5 mL Eppendorf tube or 15 mL Falcon tube (depending on volume required) using the ratio in the above table. CellMatrix™ collagen

solution Type I-A was added first, followed by 10x Ham's F-12 growth media containing MFB11 cells. Depending on concentration of myofibroblast cells in F-12 growth media, additional media without MFB11 cells was added in order to make up required volume. Finally, the sodium bicarbonate buffer solution was added, and tube contents was thoroughly mixed using a 1 mL pipette. 1.2 mL of collagen mix was added to the transwell insert (sitting within 60 mm cell culture dish). This was then left to set at 37 °C for approximately 30 minutes. Remaining collagen/MFB11 mix was kept on ice until needed to prevent it from setting.

The tube containing the minced stomach tissue in PBS from section 2.6.1 was centrifuged at 800 rpm (Eppendorf) for 3 minutes. Supernatant was then removed and stomach tissue re-suspended in 1.2 mL of collagen mix. Collagen mix containing stomach tissue was then transferred to the transwell insert, pipetted gently in an even layer on top of the first layer of collagen (containing MFB11 cells but no stomach tissue). The second layer of collagen was then left to set at 37 °C for approximately 30 minutes. Once set, 3 mL of complete organoid media, comprised of F-12 GlutaMAX™ supplement (80%) and filtered (0.22 µm filter) FBS (20%), was added to the outer 60 mm dish. Dish was then placed in 37 °C incubator with 5% CO₂ to culture.

2.7 Organoid induction

2.7.1 Knockout induction

Knockout of *Cdh1*, and activation of TdTomato, is induced with the addition of endoxifen to the media (metabolite of tamoxifen). For dishes intending to harbour induced (KO) organoids, endoxifen is added to the complete organoid media (80% F-12 GlutaMAX™ supplement and 20% FBS) at a concentration of 5 µM on day 0. For control plates, an equivalent amount of DMSO was added to the media at the same timepoint.

2.7.2 Knockout efficacy calculations

To measure *Cdh1* knockout efficacy in the organoids, area measurements were taken using confocal Z-stack images. Using the Measure tool on Fiji (ImageJ), the total area of *Cdh1* negative cells within an organoid on a single confocal Z-stack image was measured in pixels, and then calculated as a percentage of the entire organoid area (excluding the lumen) in that image. This was done for 10 different Z-stack images in each organoid. The average percent knockout (mean) of the 10 images was then calculated and that value used as the approximate *Cdh1* knockout efficacy for that organoid.

2.8 Immunofluorescence

2.8.1 Staining

Transwell inserts were removed from 15 mm dishes, and remnant media rinsed from the bottom using a Pasteur pipette. One single use, sterile, stainless steel surgical blade (Swann-Morton) was then used to cut around the bottom of the insert and the collagen. Insert bottom was removed and the collagen placed on a 10 cm dish. Using two stainless steel surgical blades, segments of collagen containing the organoids being targeted for immunofluorescence were cut out. Cuts were made as close to the organoids as possible without inflicting any damage.

Small collagen segments containing organoids were placed into 1.5 mL Eppendorf tubes (1-2 segments per tube) containing 500 μ L of 4% PFA and left to fix for 30-40 minutes. PFA was then removed from the Eppendorf, followed by 3x PBS washes in the tube. Organoids were then blocked and permeabilised using 500 μ L of blocking buffer (BB) (10% FHS in PBS) and TritonX (0.5% final conc.) and left to incubate for 1 hour on a shaker in the dark at room temperature. After incubation, the blocking buffer was removed, followed by 1x PBS wash. 500 μ L Antibody diluting buffer (ADB) (10% foetal horse serum (FHS) and 2% FBS in PBS),

primary antibody and TritonX (0.1% final conc.) were then added to the Eppendorf and organoids were left to incubate overnight on a shaker in the dark at 4 °C.

Primary antibody	Dilution	Secondary antibody	Dilution
E-Cadherin (goat)	1:100	Donkey anti-goat (488)	1:1000
Ki67 (rabbit)	1:100	Chicken anti-rabbit (594)	1:1000
CD44 (rat)	1:50	Goat anti-rat (488)	1:1000

Table 2.2 | Primary and secondary antibody dilutions used in immunofluorescence on the organoids.

ADB, primary antibody and TritonX were removed from the tube, followed by 3x PBS washes. 500 mL ADB and secondary antibody (1:1000) were added to the tube, and organoids were left to incubate for 2 hours on a shaker in the dark at room temperature. Organoids were then washed 5x with PBS, and 3-4 drops of ProLong Gold antifade reagent with DAPI (Thermo Fisher) added to the tubes. Organoids were left to incubate in ProLong Gold with DAPI for approximately 15 minutes while bridge mounts were set up.

2.8.2 Bridge mounting

Collagen segments containing organoids were mounted on 25x75 mm microscope slides using a bridge mounting method. Bridge mounting utilises two pillar coverslips to reduce the extent to which organoids are flattened under the top coverslip. The small elevation of the top coverslip accommodates the height of the collagen (approximately 1 mm). For the supportive pillars, two 22x22 mm coverslips were placed at either end of the slide, held down using one drop of ProLong Gold antifade reagent without DAPI (Thermo Fisher). A segment of collagen

containing organoids was then transferred from the Eppendorf tube to the centre of the slide using a wide-bore pipette, and two drops of ProLong Gold antifade reagent with DAPI (Thermo Fisher) were placed on top. A final 22x22 mm coverslip was then placed on top of the organoid sample, slightly raised by the two underlying coverslips to allow for the height of the collagen segment. After 30 minutes, the perimeter of the slide was sealed with transparent nail varnish and left to dry for approximately 1 hour before microscopy.

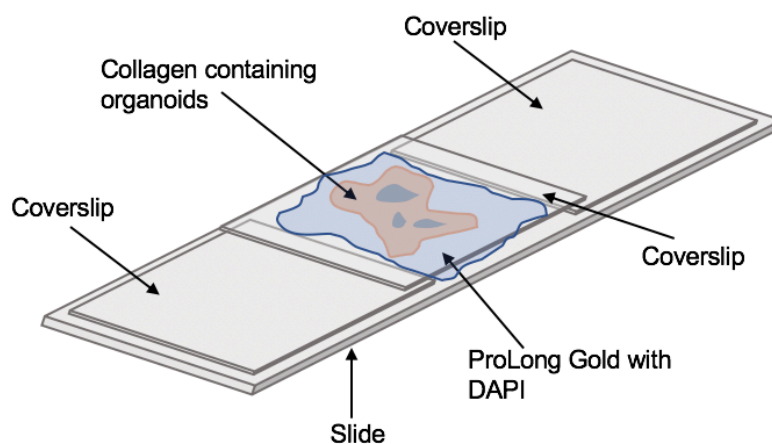


Figure 2.1 | Diagram of bridge mounting set up for organoid microscopy.

2.8.3 Brightfield and Fluorescence microscopy

All brightfield and fluorescence microscopy was done on an Eclipse Ti Inverted Microscope System (Nikon) using the Fuji LAS-3000 ECL Imaging System (Thermo Fisher Scientific). During organoid culture, daily brightfield images were taken to track growth. Images were taken of organoids in the transwell insert without removing them from the 60 mm dish. Additional fluorescence imaging using the TRIT-C filter was also carried out to track TdTomato fluorescence in the *CD44-cre/Cdh1^{-/-}/TdTomato* mice during growth.

Following immunofluorescence, images were taken of fixed and stained organoids on each microscope slide. For imaging of E-cadherin and CD44 (both 488), the FIT-C filter was used. For imaging of Ki67 (594) and endogenous TdTomato (581), the TRIT-C filter was used. DAPI nuclei staining was imaged using the UV filter.

2.8.4 Confocal microscopy

Confocal microscopy was carried out using the Olympus Fluoview Confocal Microscope. For each organoid, between 20-30 Z-stack images were taken, depending on the size of the organoid.

2.9 Drug screening

2.9.1 DMSO toxicity testing

To test DMSO tolerance, four dishes of organoids were first cultured using the method described in section 2.6. On day 2 of culture, DMSO was added to the complete culture media at a different concentration in each dish (0.2%, 0.1% and 0.05%). One dish was left untreated. Organoids were then placed in a 37 °C incubator with 5% CO₂ to culture. Brightfield images were taken every 24 hours using the inverted microscope.

2.9.2 Drug treatment

For drug screening experiments, organoids were established as described in section 2.6. From initial seeding on day 0, organoids were cultured using complete culture media. For plates needing *Cre* induction, endoxifen was added to the media at a final concentration of 5 μM from day 0.

For each drugging experiment, four cultures were set up as shown in Figure 2.2:

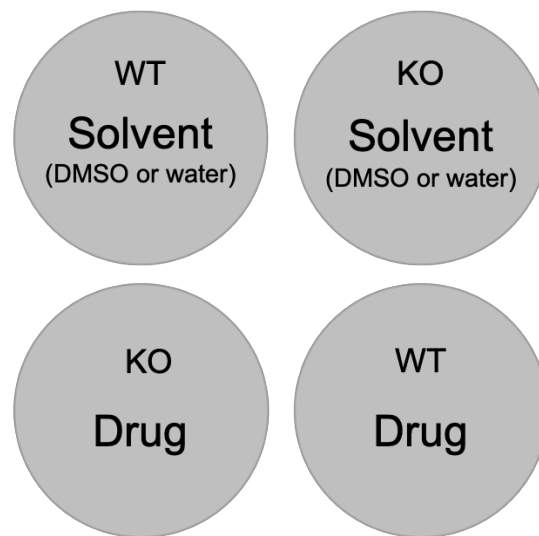


Figure 2.2 | Diagram of the four plate conditions for each drug screening experiment.

Organoids were left to culture in a 37 °C incubator with 5% CO₂ for 48 h. After 48 h, media was removed and substituted for media containing the drug or solvent at the required concentration, determined using the IC₅₀ values from initial 2D screening in our laboratory. Endoxifen was not replenished for plates containing KO organoids.

Plates were imaged using the inverted microscope every 24 hours to track growth. After the organoids had been exposed to the drug for 96 hours (day 6 of growth) they were fixed analysed using immunofluorescence (section 2.8).

2.9.3 Quantification of organoid viability

Brightfield images taken using the inverted microscope were analysed to quantify the effect of the drug. Using the measure tool on Fiji (ImageJ), the area of each organoid was outlined and measured on both the day 2 (0 h after drugging) and day 6 (96 h after drugging) images. These two measurements were then used to calculate the total percentage increase in growth for each organoid. Both the raw data and the averages could then be plotted on line and bar graphs, respectively.

2.9.4 Statistical analysis

Statistical analysis on organoid size was performed using a Wilcoxon rank-sum test, a nonparametric alternative to the two sample t-test. This is also known as the Mann-Whitney U test and is used for independent samples, differing from the Wilcoxon signed-rank test, which is used for paired samples. Analysis was done with the `{stats}` package on R, using the function `wilcox.test`.

Chapter 3: Optimisation Results

The conditional *Cdh1* knockout organoids developed here are the first of their kind as a model for HDGC. The goal for this phase of the project was to optimise an array of different staining and imaging techniques to use in the characterisation of these novel organoids.

Prior to beginning lab work, it was clear there were several challenges. Organoids of this nature, with a conditional *Cdh1* knockout, are entirely novel to the field, and therefore require considerable characterisation. Although there are similar *Cre*-inducible mouse models with which to compare the knockout efficiency, which is highly variable (Leonhard, Roelfsema, Lantinga-Van Leeuwen, Breuning, & Peters, 2008; Mirantes et al., 2013), there are none that used this exact system and CD44 promoter to drive *Cdh1* knockout in organoids. Further, we did not know how the knockout would impact the growth or stability of the organoids.

3.1 Organoid establishment and growth

To begin with, it was necessary to gain an understanding of the basic growth pattern of the organoids under our normal conditions. To do this, organoids were cultured from conditional knockout mice using the method described in section 2.6 and imaged in brightfield. After five biological replicates, a common growth pattern between the organoids was identified.

Approximately 20 organoids could be developed and sustained from a single stomach in one dish, virtually all of which followed the same growth pattern (Fig. 3.1): 24h after primary tissue was seeded in the collagen, small, transparent cystic-like structures began to appear where organoids will eventually develop – usually in the centre of a segment of tissue. For a segment

of primary tissue to generate an organoid, it must contain a substantial population of gastric stem cells. Furthermore, there needs to be a small population of mesenchymal cells projecting outwards from the surface of the organoid to aid in growth factor production and delivery for the stem and progenitor cells (Katano et al., 2013b; Ootani et al., 2009). These myofibroblast populations and their potential origins are discussed further in Chapter 6. The transparent cysts present on day 1 begin to rapidly expand, forming spherical organoid structures within 48 hours. The organoids continued to increase in size by approximately 0.1-0.4 mm each day, eventually plateauing out around day 5-6 when they typically measure 0.5-1.5 mm in diameter.

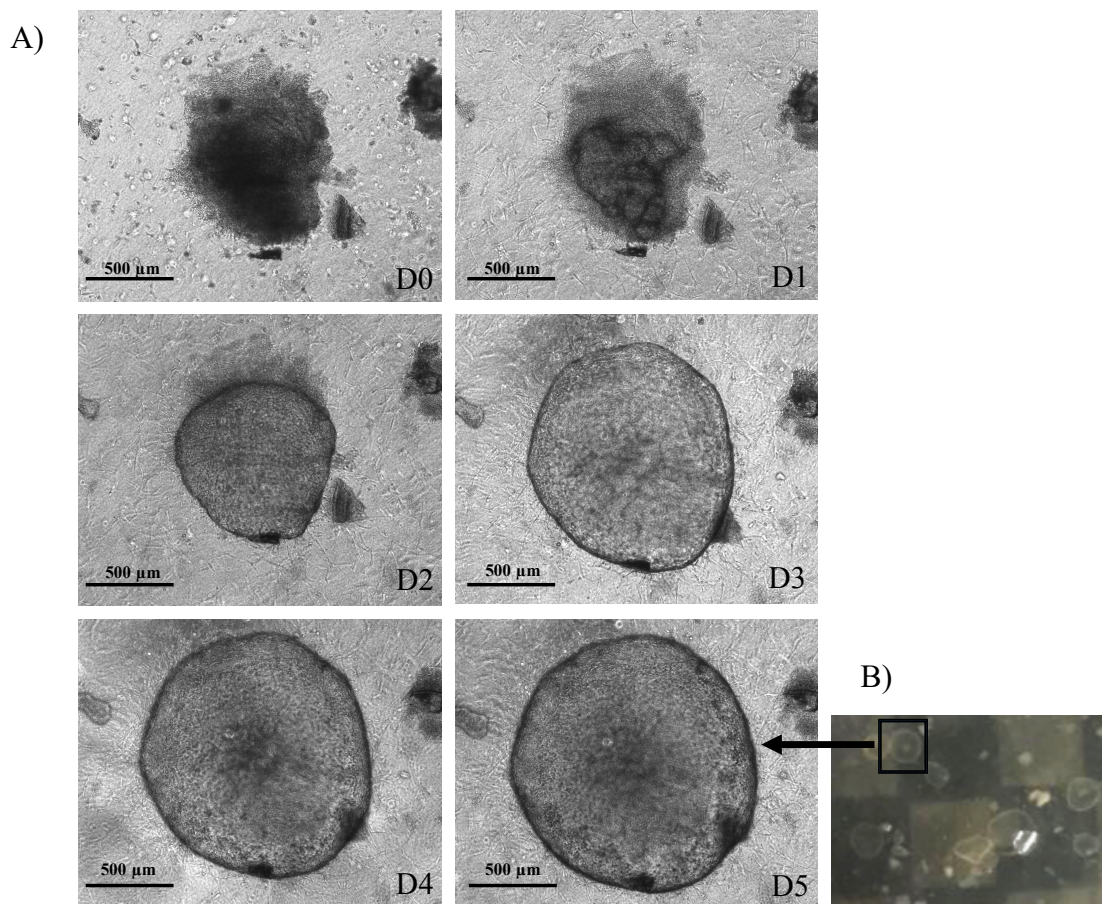


Figure 3.1 | Typical growth pattern of organoids from day 0-5. A) A representative organoid displaying the common growth pattern seen throughout the project. From primary tissue on Day 0, the beginnings of cystic structures form within 24 hours, which then go through a phase of rapid growth. Organoids expand into large, 3D spherical structures, reaching approximately 1.5mm in size by day 5. After day 5, growth continues at a decreased rate. **B)** By day 5, organoids are visible in the collagen as transparent, spherical structures.

The cystic structure of the organoids is a mimic of *in vivo* gastric glands, which contain a monolayer of epithelial cells facing into a lumen. To keep experiments consistent, it was necessary to be able to clearly distinguish organoids from other tissue. It was determined that any structure that retained a prominent core of dark, opaque primary tissue should not be considered as an organoid. This included segments of primary tissue with a surrounding layer of rounded, transparent tissue or budding growths of stem cells (Fig. 3.2), as without a lumen they do not accurately reflect *in vivo* gastric cellular structure and organisation.

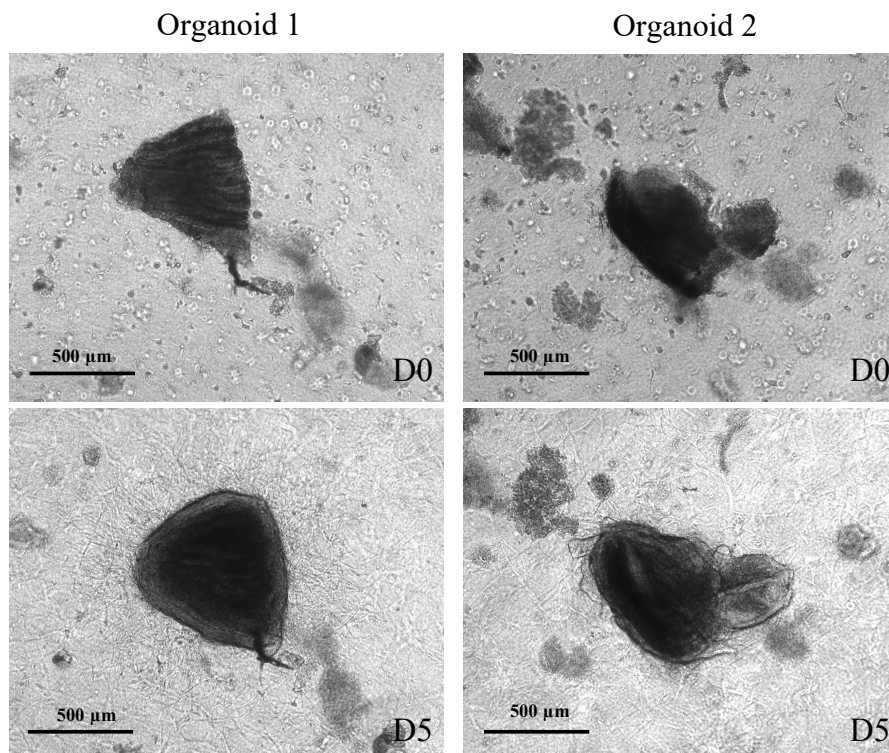


Figure 3.2 | Primary tissue that has failed to generate organoids. Two segments of primary tissue (1 and 2) imaged in brightfield on day 0 and day 5. Tissue has generated a surrounding layer of rounded semi-transparent tissue (1) and small budding stem cell growths (2). However, no cystic organoid structures have developed.

3.2 Optimisation of imaging techniques

After establishing an idea of what normal growth looked like in the organoids, suitable imaging techniques needed to be identified for use in subsequent experiments. Fluorescence imaging on an inverted microscope is adequate for gaining general insights, however it does not display anything beyond the outer surface of the organoid. Gaining a detailed understanding of the complete morphology of the organoids was an integral part of characterisation, so fluorescence imaging using a confocal microscope was explored as a method for the visualisation of both the surface and the centre of the organoid.

The organoids in Figure 3.3 were all cultured for 3 days and stained with an E-cadherin antibody (488 - green) and DAPI (blue) using the immunofluorescence protocol in section 2.8. Two dishes were stained, one induced (KO) and one uninduced (WT), both containing approximately 10 organoids. Induced (KO) organoids are described fully in section 3.3.

Figure 3.3A shows two organoids, one uninduced (WT) and one induced (KO), both imaged on the inverted fluorescence microscope. The images clearly show successful knockout in the induced (KO) organoid (right) and the complete staining of E-cadherin in the uninduced (WT) organoid (left). However, the inner lumens of the organoids are not visible. Figure 3.3B shows one uninduced (WT) organoid imaged using a confocal microscope. In contrast to Figure 3.3A, these images show both the hollow centre of the organoid (left), as well as the surface.

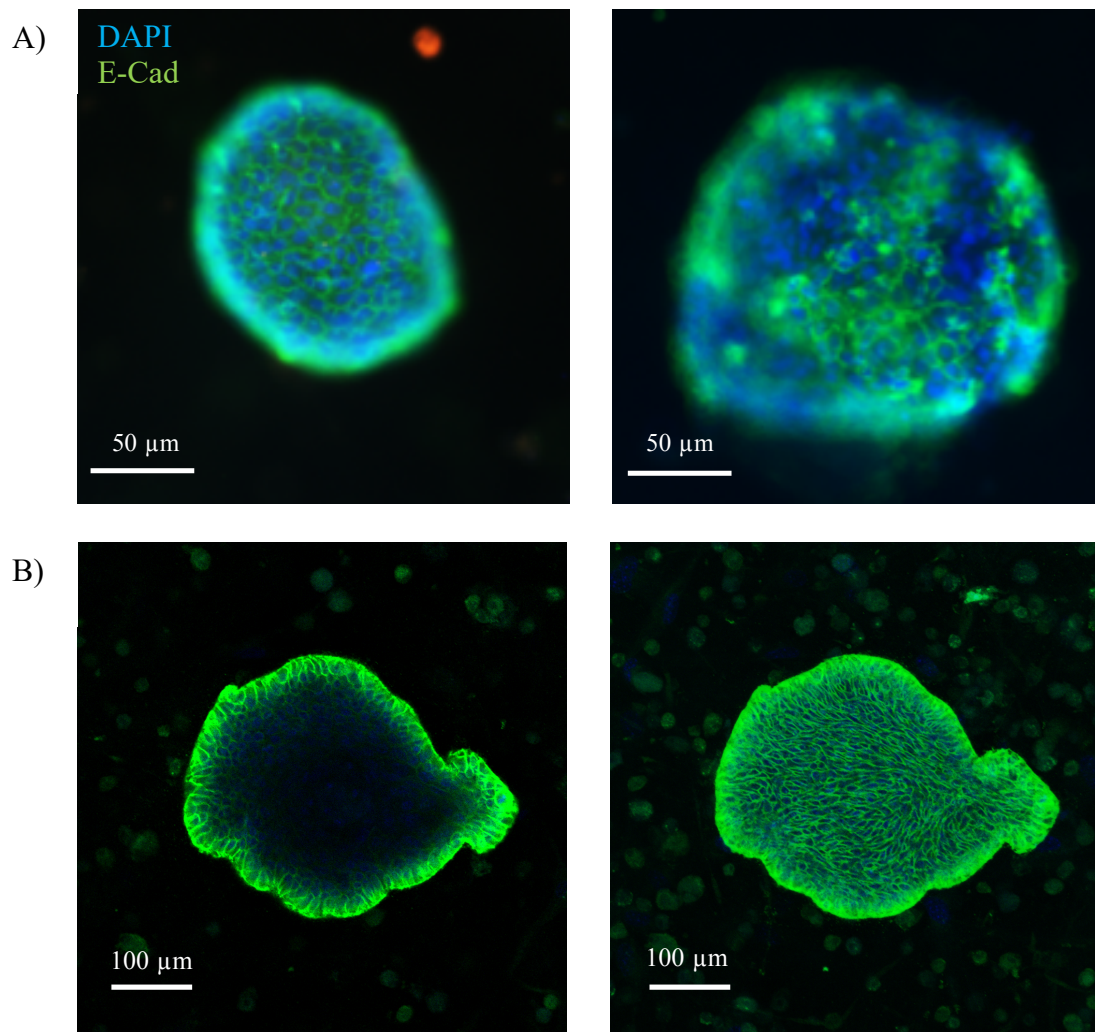


Figure 3.3 | Visualisation of the organoids through fluorescence imaging. **A)** Fluorescence imaging on an inverted microscope showing two organoids displaying immunofluorescence associated with the nuclei (DAPI – blue) and E-cadherin (488-green). Images show the general shape of both organoids, as well as the approximate knockout efficiency of E-cadherin in the induced organoid (pictured right). **B)** Fluorescence imaging on a confocal microscope showing one organoid displaying immunofluorescence associated with the nuclei (DAPI – blue) and E-cadherin (488-green). Both a slice through the hollow centre (left) and the outer surface (right) can be viewed.

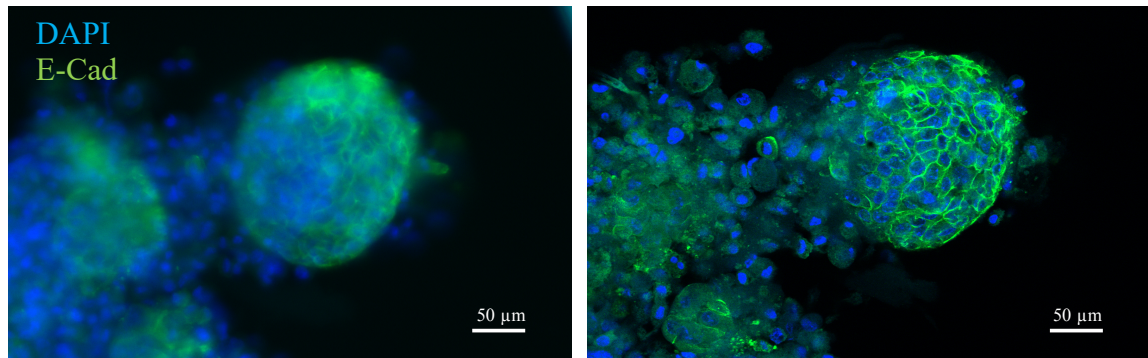


Figure 3.4 | A comparison of fluorescence imaging using an inverted and confocal microscope. One organoid showing immunofluorescence associated with E-cadherin (488-green) and DAPI (blue) imaged on both an inverted microscope (left) and confocal microscope (right). There is a distinct increase in resolution of the small organoid with the use of confocal microscopy. Single cells are more defined and overall organoid morphology and cell composition can be seen with increased clarity.

3.3 *Cdh1* knockout induction

The organoids used throughout this project were generated from 1-2 day old mice harbouring conditional *Cdh1* mutations (*CD44-cre/Cdh1^{-/-}*). These mice were designed so that induction with endoxifen (a metabolite of tamoxifen) would lead to the expression of the *Cre* recombinase in *CD44*-expressing cells, leading to a homozygous frameshift deletion in *Cdh1*. This system circumvents the issue of the embryonic lethal phenotype caused by a homozygous *Cdh1* knockout. Here, I have tested the functionality of this construct.

For the initial knockout experiment, two dishes were set up, each with the tissue of one mouse stomach seeded in the collagen. Endoxifen was added to the media of one dish from 0 hours post-seeding at a concentration of 5 µM. Organoids were then left to grow for 5 days before being fixed and stained with an E-cadherin antibody (488-green) and DAPI (blue) using the

immunofluorescence protocol described in section 2.8. The organoids were then imaged using the confocal microscope to analyse the knockout of E-cadherin.

Confocal imaging of approximately eight organoids, four of which are pictured in Figure 3.5, showed successful knockout of E-cadherin, the degree of which varied markedly between individual organoids. Moreover, knockout occurred in seemingly random clusters, and no organoids appeared to have complete knockout. Uninduced organoids had a wildtype phenotype and displayed E-cadherin staining throughout the entire structure (Fig. 3.6). E-cadherin staining had a regular, lattice-like appearance, consistent with the localisation of E-cadherin to the adherens junctions at the cell membrane. There was variation in the general shape of the organoids – not all are exactly spherical – however this variation occurs in both induced (KO) and uninduced (WT) organoids, so cannot be attributed to the knockout itself.

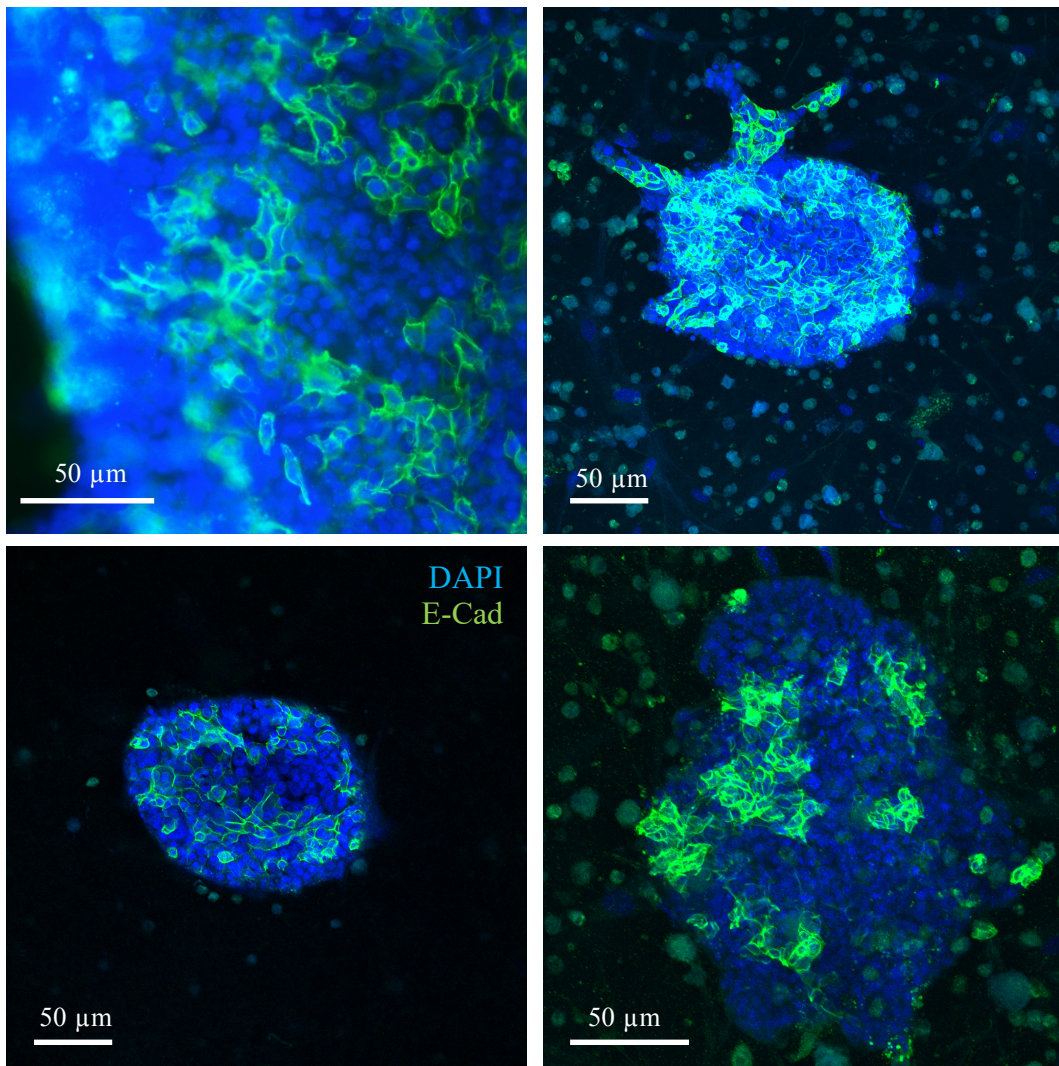


Figure 3.5 | Induced (KO) organoids display successful induction of Cdh1 knockout. All four organoids have been stained with an E-cadherin (488-green) antibody and DAPI (blue). Confocal microscopy images show that knockout occurs in clusters throughout the organoid and varies in efficacy between organoids. In all organoids there is a portion of cells that retain functional E-cadherin (green-488) localised to the adherens junctions. The variation in tones of green is caused by the overlay of green and blue staining from cells in different planes in collated confocal images.

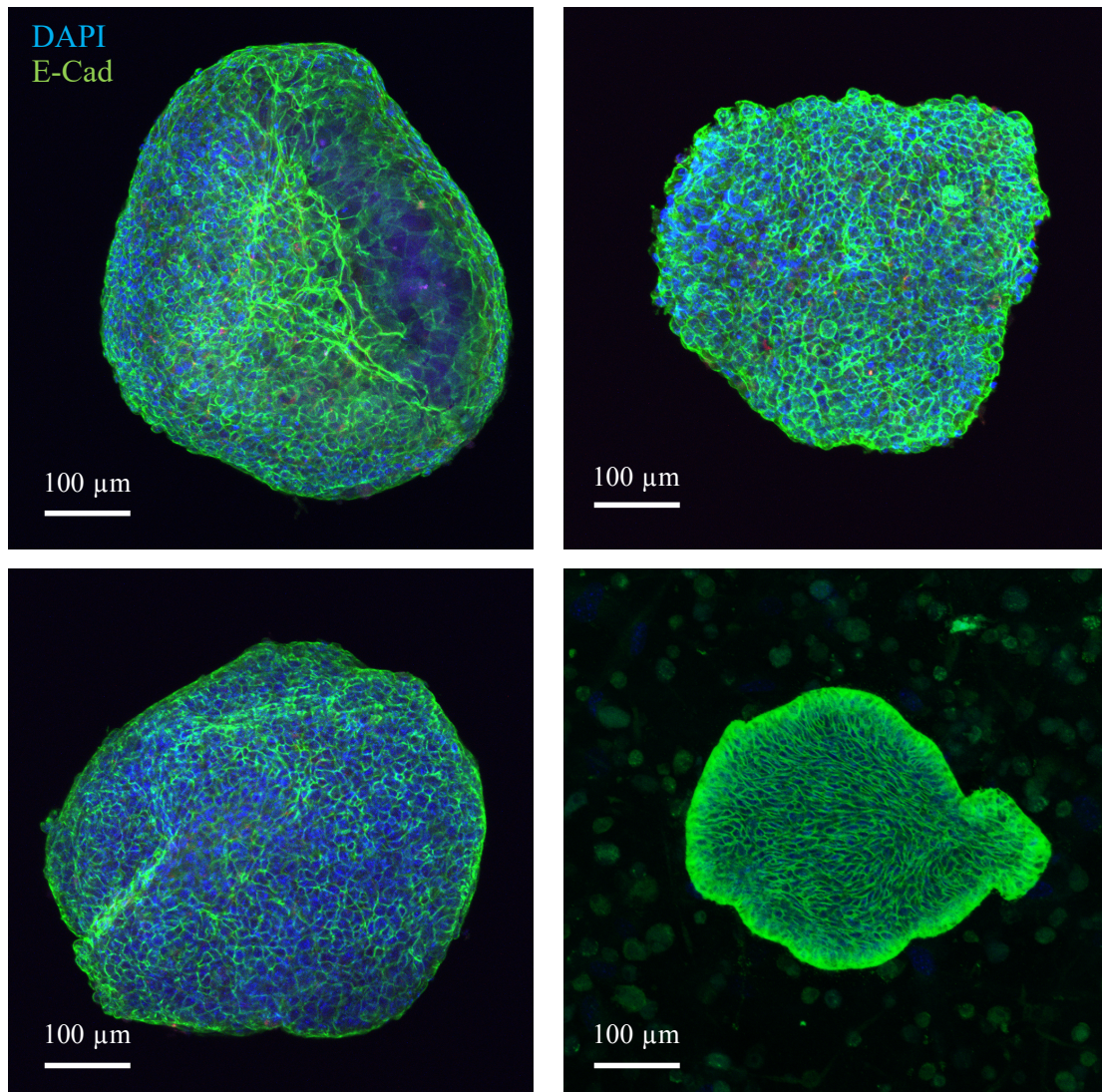


Figure 3.6 | Uninduced (WT) organoids show consistent E-cadherin expression. Confocal microscopy images of four typical organoids that have not been exposed to endoxifen in the media. E-cadherin staining is lattice-like and localised to the adherens junctions throughout the entire body of the organoids.

After inducing *Cre* expression in three biological replicate plates of organoids, the approximate percentage of E-cadherin-negative cells in a random sample of organoids was determined by calculating the relative area of *CDH1* negative cells as a percentage of the total area. This was completed for 10 slices through each organoid at different depths, and then the mean percentage knockout for the 10 slices was used as the average percentage knockout for the entire organoid.

This provided a reasonable estimate of the percentage of knocked out cells, and to what extent that number varied between organoids. Three examples are pictured in Table 3.1.

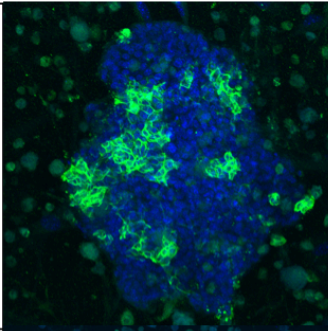
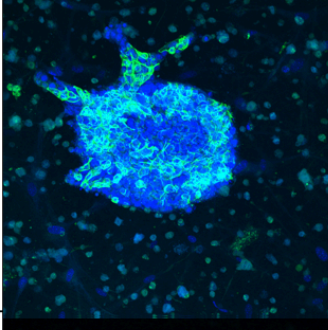
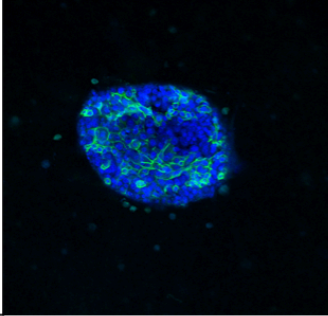
Org 19 82%	
Org 20 67%	
Org 22 71%	

Table 3.1 | Approximate percentage of knocked out cells in a sample of organoids. After immunofluorescence and confocal imaging, the approximate knockout efficiency percentage was determined by calculating the total area of E-cadherin deficient cells (no green E-cadherin staining) as a percentage of the total area of the organoid. Organoid 20 displays slightly different colouring due to the overlay of green and blue staining in different cell layers within the organoid.

Together, these results show that E-cadherin can be successfully inactivated in organoids derived from neonatal mice using an inducible *Cre* system under the *CD44* promoter. This happens in varying proportions of cells between different organoids. For the first time, this provides a novel model for the early stages of HDGC.

3.4 Establishment of TdTomato organoids

At this point in the project, mice harbouring a conditional *Cdh1* knockout with an endogenous TdTomato fluorescent protein became available (*CD44-cre/Cdh1^{-/-}/TdTomato*). TdTomato is a highly photostable tandem dimer that omits strong red fluorescence (emission wavelength 581) (Shaner, Steinbach, & Tsien, 2005). The TdTomato gene contains a short insertion that abrogates the fluorescence of the protein. The insertion is flanked by LoxP sites which, when deleted by cre recombinase, leads to fluorescence. Since *Cre* is expressed under the *CD44* promoter, *Cdh1* negative cells should co-localise with red fluorescence. The addition of an endogenous fluorescent protein allows for the knockout to be visualised in real-time under the fluorescence microscope, without having to fix the organoids and run immunofluorescence. The addition of TdTomato should not alter the growth or morphology of the organoids in any other way aside from the added fluorescence, however, it was unknown whether the behaviour of the organoids would remain unchanged, or if the TdTomato protein would have unforeseen effects on the growth or structure of the organoids.

To test the functionality of TdTomato, two dishes were set up, each with the tissue of one stomach from a 2 day old mouse seeded in the collagen. Endoxifen was added to the media of one dish from 0 hours post-seeding at a concentration of 5 μ M. organoids were then left to grow for 5 days.

On first observation, the TdTomato fluorescence was visible within 24 hours of induction and increased in intensity over time. Importantly, organoids generated from TdTomato mice did not appear to have a different growth pattern to non-TdTomato organoids (Fig. 3.7). This remained true through all three initial biological replicates of this TdTomato growth experiment, as well as with subsequent experiments using TdTomato organoids.

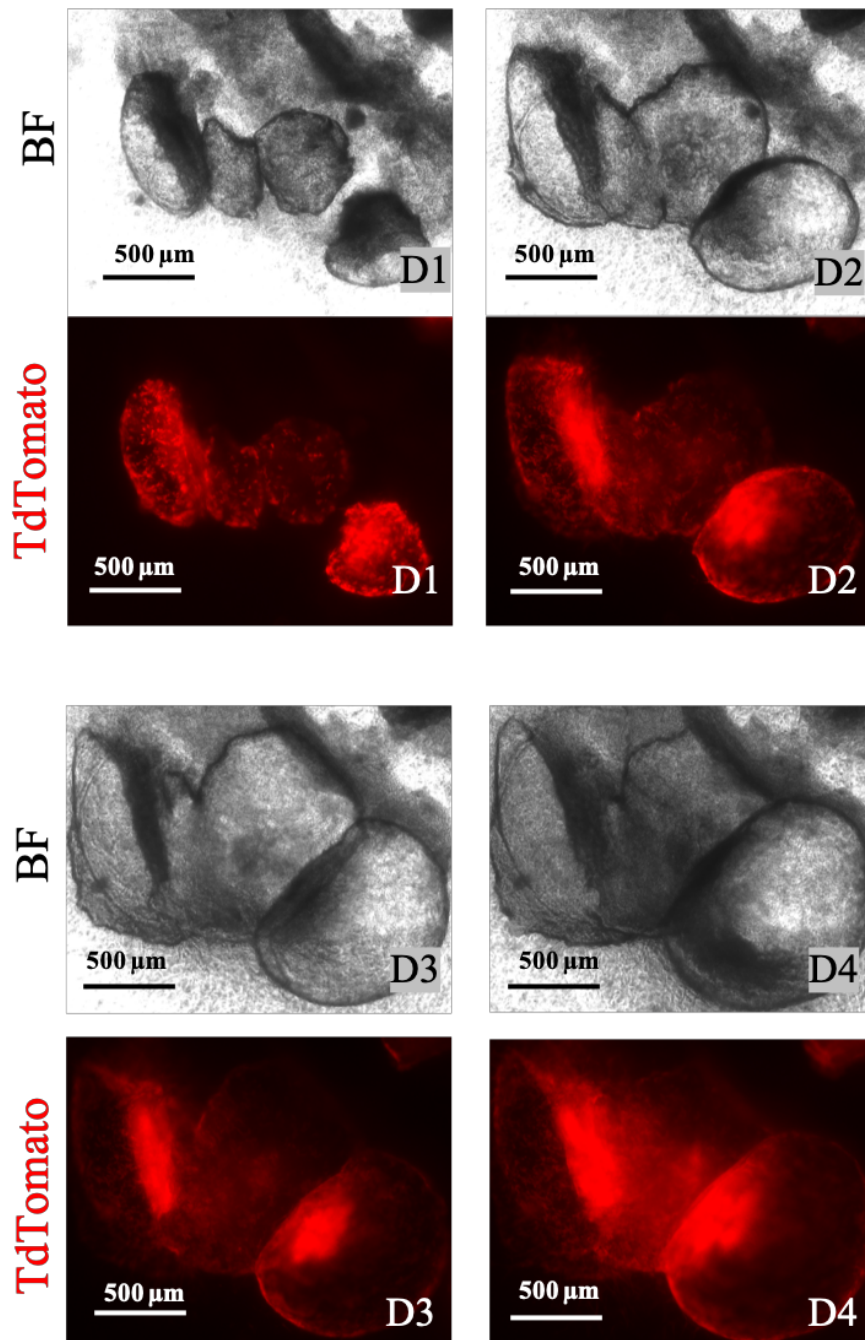


Figure 3.7 | Growth pattern of TdTomato-expressing organoids. Fluorescence imaging showing the growth and TdTomato expression of a cluster of four organoids from day 1-4. Brightfield imaging shows the organoids expanding in size, while fluorescence imaging using the TRIT-C filter shows the expression of TdTomato (red).

Following successful induction of the *Cdh1* knockout and TdTomato fluorescence, immunofluorescence experiments were carried out in order to validate the TdTomato fluorescence and ensure that cells positive for TdTomato were negative for E-cadherin staining. Immunofluorescence was carried out using an E-cadherin antibody (488-green) and DAPI and the protocol described in section 2.8. Organoids were then imaged using the confocal microscope to analyse TdTomato expression.

Confocal imaging of approximately 10 induced (KO) and 5 uninduced (WT) control organoids revealed that in general, there was virtually no co-staining of E-cadherin in TdTomato expressing cells and E-cadherin expressing cells. When looking at the collated image of all the Z-stack images, distinct patches of TdTomato positive, E-cadherin negative cells are visible, although the majority of cells on the outer surface of the organoid are E-cadherin positive (Fig. 3.8A). However, Z-stack images that expose the centre of the organoid show high numbers of TdTomato-positive, E-cadherin-negative cells infiltrating the inner lumen (Fig. 3.8B).

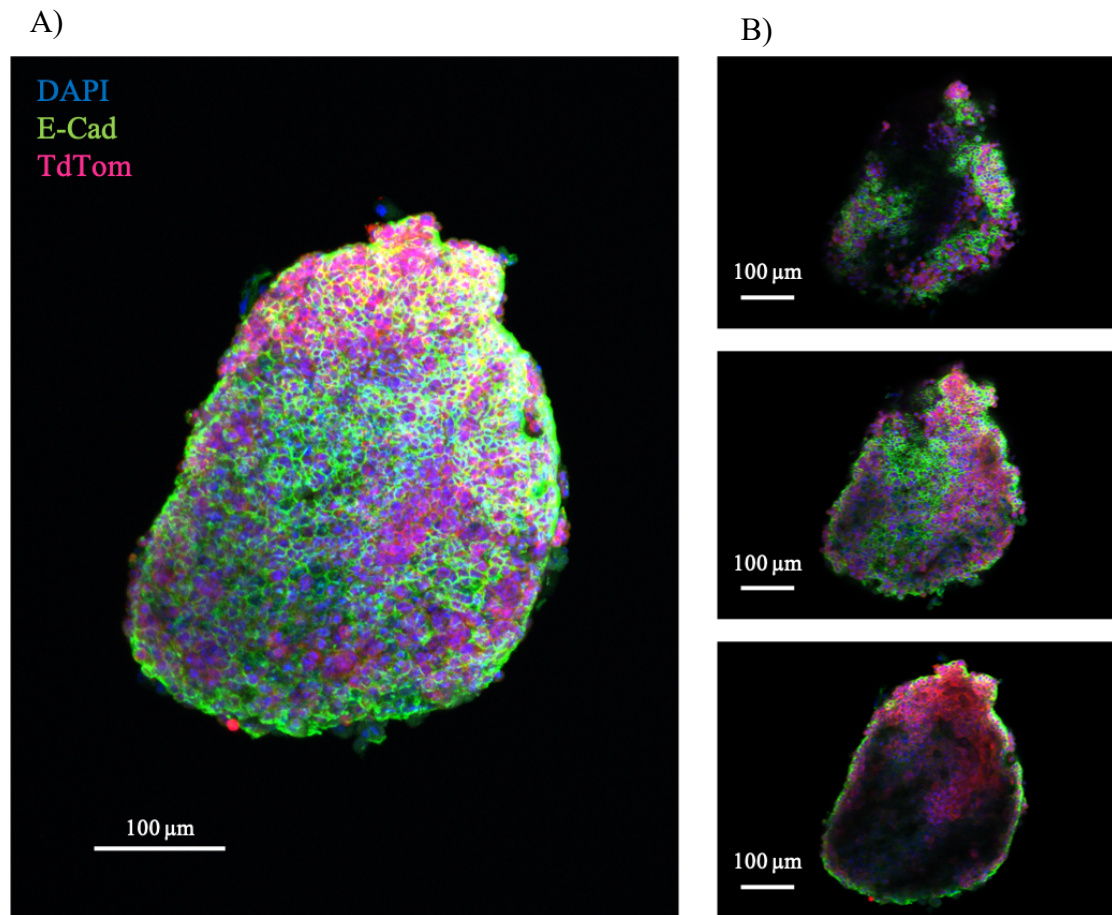


Figure 3.8 | Immunofluorescence of TdTomato-expressing organoids. Confocal images of an organoid, both collated (A) and single slices (B) after immunofluorescence with E-cadherin (488-green) and DAPI. Endogenous TdTomato fluorescence is also visible (red). The collated image shows patches of TdTomato expression on the organoid surface. The single slices (in order of increasing depth going downwards) show TdTomato-expressing E-cadherin negative cells are present deeper in the organoid.

Further investigation was done into the presence of TdTomato-expressing cells in the organoid lumen in order to gain a deeper understanding of what could be occurring. Confocal images of both uninduced (WT) and induced (KO) organoids were analysed, from both this and previous experiments, with a new focus on cells in the lumen (Fig. 3.9).

A closer examination of the lumen using a 3D reconstruction of the same organoid pictured in Figure 3.8 shows that the centre of the organoid is largely composed of E-cadherin negative cells (Fig. 3.9A). The cells appear adhered to the inner surface of the lumen, rather than detached. This phenomenon occurs in the majority of induced organoids, a selection of which are pictured in Figure 3.9B. This includes induced organoids without the TdTomato endogenous fluorescence. The vast majority of uninduced organoids have clear lumens with no cellular infiltration (Fig. 3.9C). This rich TdTomato core gives insight into how the organoids can have an outer surface which is primarily E-cadherin positive, but still have a high proportion of knocked out cells.

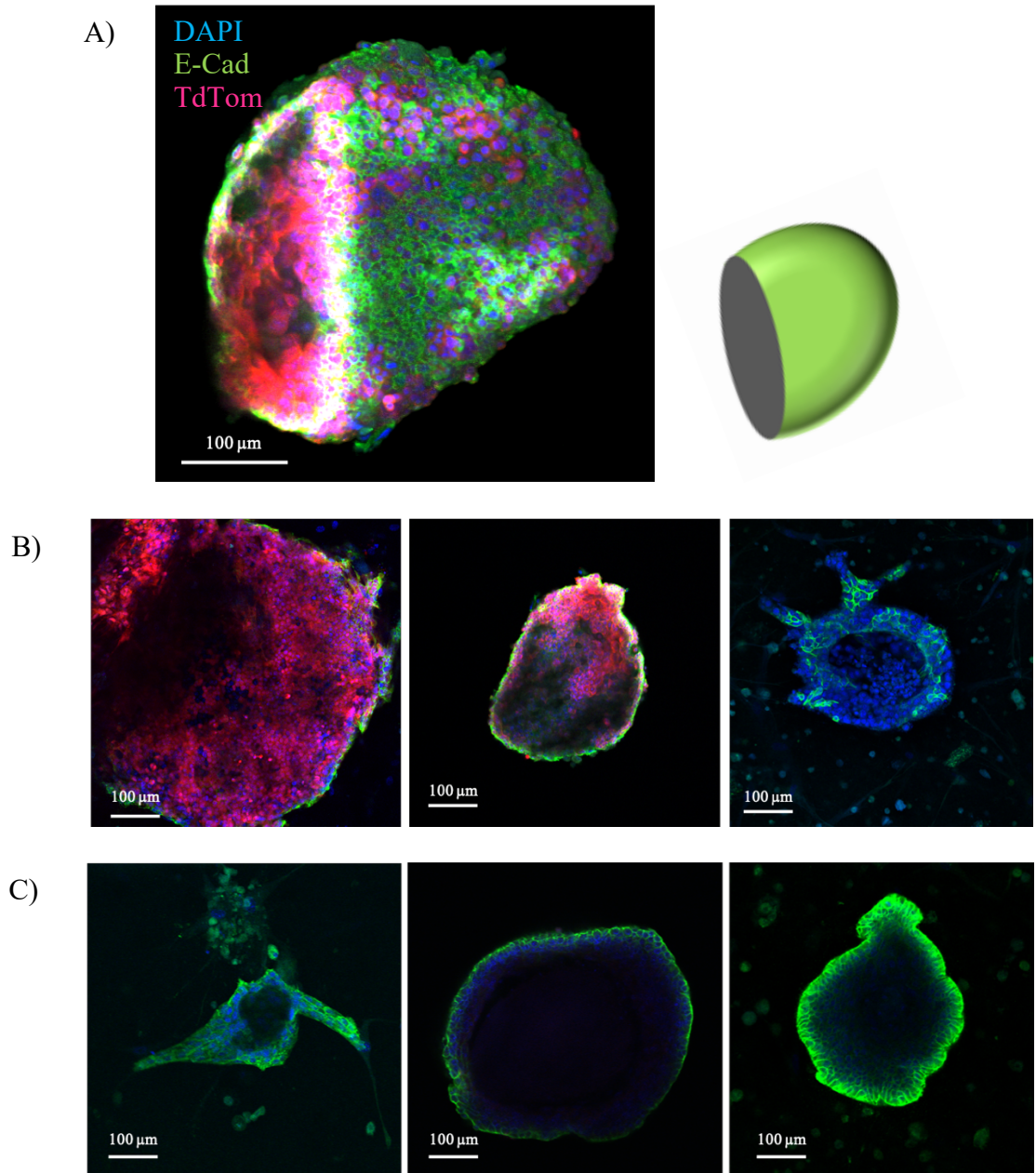


Figure 3.9 | E-cadherin deficient cells cluster in the inner lumen of the organoid. **A)** 3D confocal image of an induced (KO) organoid that is expressing TdTomato (red) and has been stained with an E-cadherin (488-green) antibody and DAPI. The end of the organoid has been digitally removed to show the lumen enriched with TdTomato-expressing cells (schematic of shape shown alongside image). The exposed lumen shown alongside the outer organoid surface emphasises the difference in amount of E-cadherin positive cells between the two areas of the organoid. **B)** Confocal image slices through the centre of several induced organoids. E-cadherin deficient cells clustering in the lumen occurs regularly in knockout organoids, including non-TdTomato organoids (far right). **C)** Non-induced organoids with a wildtype phenotype. These organoids show clear lumens harbouring few to no cells.

Through these experiments validating TdTomato, it was also observed that the endogenous fluorescence is continually expressed, significantly increasing in intensity over the first eight to ten days of culture. This is exemplified in Figure 3.10, which shows the progression of an organoid during the first 6 days of culture. When images are taken at the same exposure each day, the TdTomato fluorescence increases significantly in strength. This increase continues beyond day 6, not plateauing until approximately day 10.

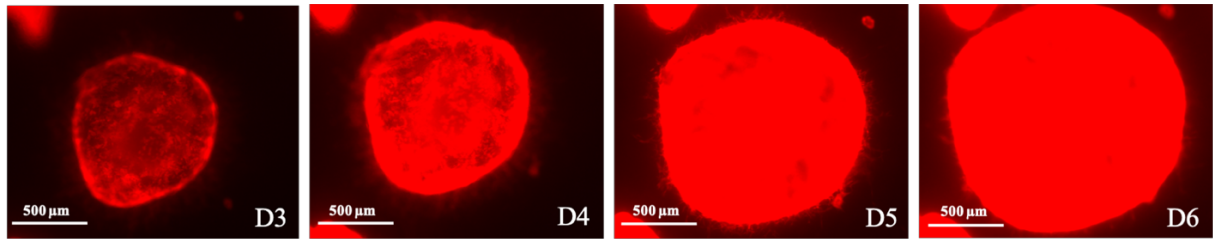


Figure 3.10 | TdTomato fluorescence increases over time. Fluorescence images of TdTomato expression (red) in the first 6 days of culture. The level of TdTomato fluorescence continues to increase over time.

Together, these results show that TdTomato organoids can have their E-cadherin inactivated in the same way as non-TdTomato organoids. Further, that there is virtually no cross over between E-cadherin positive cells and TdTomato-expressing cells, which accumulate in the inner lumen. Overall, this allows real-time observation of E-cadherin knockout in the organoids.

3.5 Immunofluorescence optimisation: collagenase

As part of the optimisation of the immunofluorescence protocol, an experiment was done in an attempt to increase the level of clarity seen in fluorescence and confocal imaging and reduce the amount of background fluorescence. Despite incorporating several wash steps, when staining organoids in collagen there is a certain amount of unavoidable background fluorescence present (Fig. 3.11A). Removing the collagen prior to staining is one way of potentially removing this background fluorescence.

To investigate this, collagen containing the organoid cultures was incubated in collagenase at a concentration of 1 mg/ml for 60 minutes at 37 °C prior to immunofluorescence staining on

day 5 of culture. Two dishes were used for this experiment, one induced and one uninduced, both containing approximately 10 organoids. After staining, organoids were imaged using fluorescence and confocal microscopy.

The collagenase was effective in removing any background immunofluorescence (Fig. 3.11B), however it produced its own complications. During immunofluorescence, the collagen had been acting as a protective layer around the organoids, so its removal exposed the delicate structures to damage during the staining process. As a result of this, the morphology of the organoids was often compromised, and the structures did not remain intact (Fig. 3.11C). Disruption appears to be most severe in induced (KO) organoids, possibly due to their reduced cell-cell adhesion properties. Due to these observations, collagenase was not used in any future experiments.

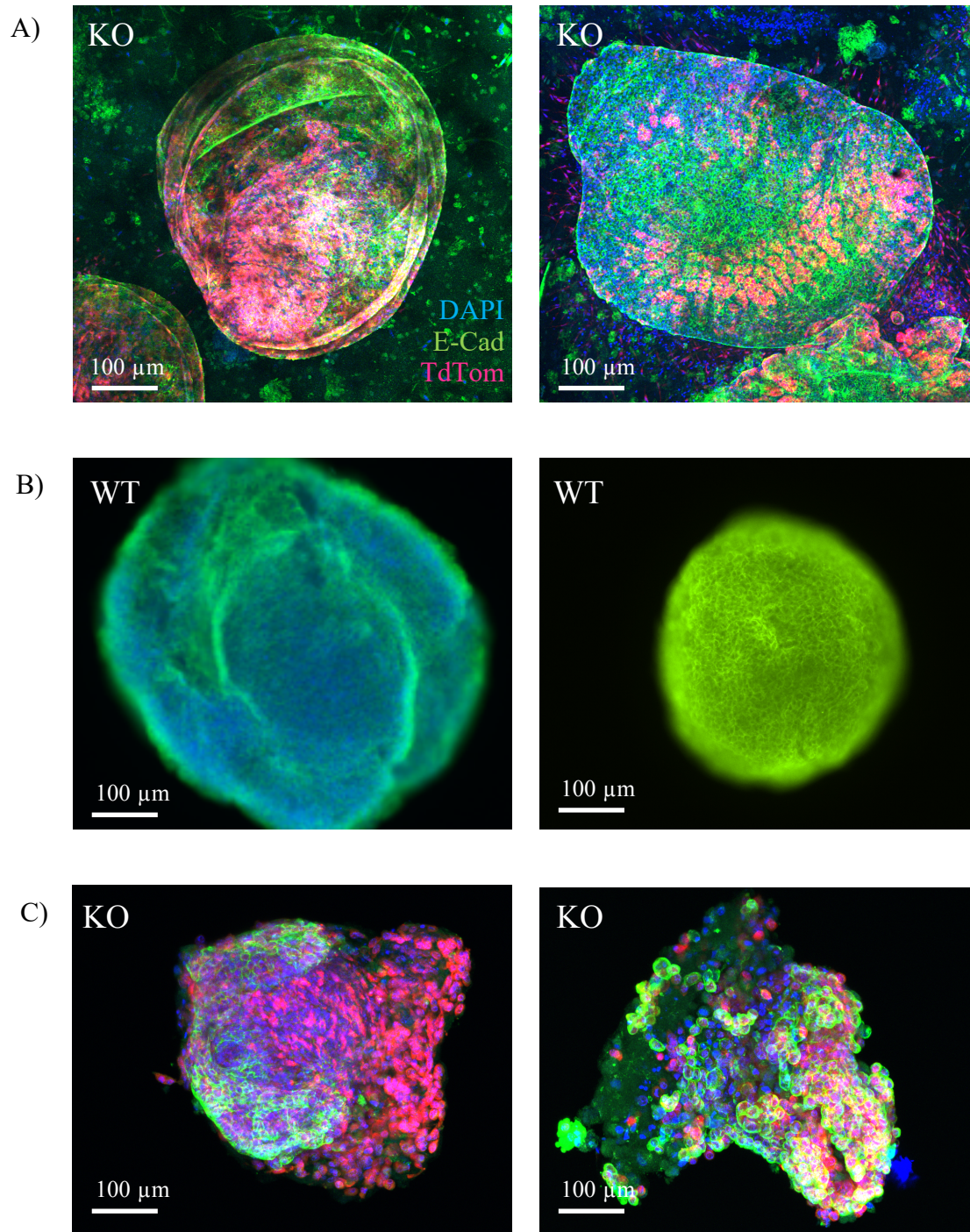


Figure 3.11 | Confocal images showing organoids with and without collagen. A) Images of two organoids displaying fluorescence associated with E-cadherin (488-green), TdTomato (red) and DAPI (blue) to demonstrate the level of background fluorescence seen when organoids remain in collagen. **B)** Two uninduced (WT) organoids with a clear background due to additional collagenase step. **C)** Two induced (KO) organoids demonstrating the level of morphological damage that can occur during immunofluorescence without collagen.

3.6 Ki67 Staining

Next, an investigation was undertaken to determine what proportion of cells in the organoids were actively proliferating and whether or not they were in a specific distribution or localised in any part of the organoid. Immunofluorescence was carried out using a Ki67 antibody (594) along with an E-cadherin antibody (488) and DAPI on two plates (one induced (KO) and one uninduced (WT)), both on day 7 of culture. Organoids were then imaged using a confocal microscope (Fig. 3.12).

From the confocal imaging, it can be observed that cells positive for Ki67 staining are dispersed throughout both the induced (KO) and uninduced (WT) organoids with no obvious patterning or localisation. Staining can be seen in both cells within the organoid and myofibroblast cells around the exterior of the main organoid body (Fig. 3.12B). Although it appears that Ki67 positive cells in the induced organoid are predominantly E-cadherin negative, there are E-cadherin positive cells in the uninduced (WT) organoid that are also positive for Ki67 staining.

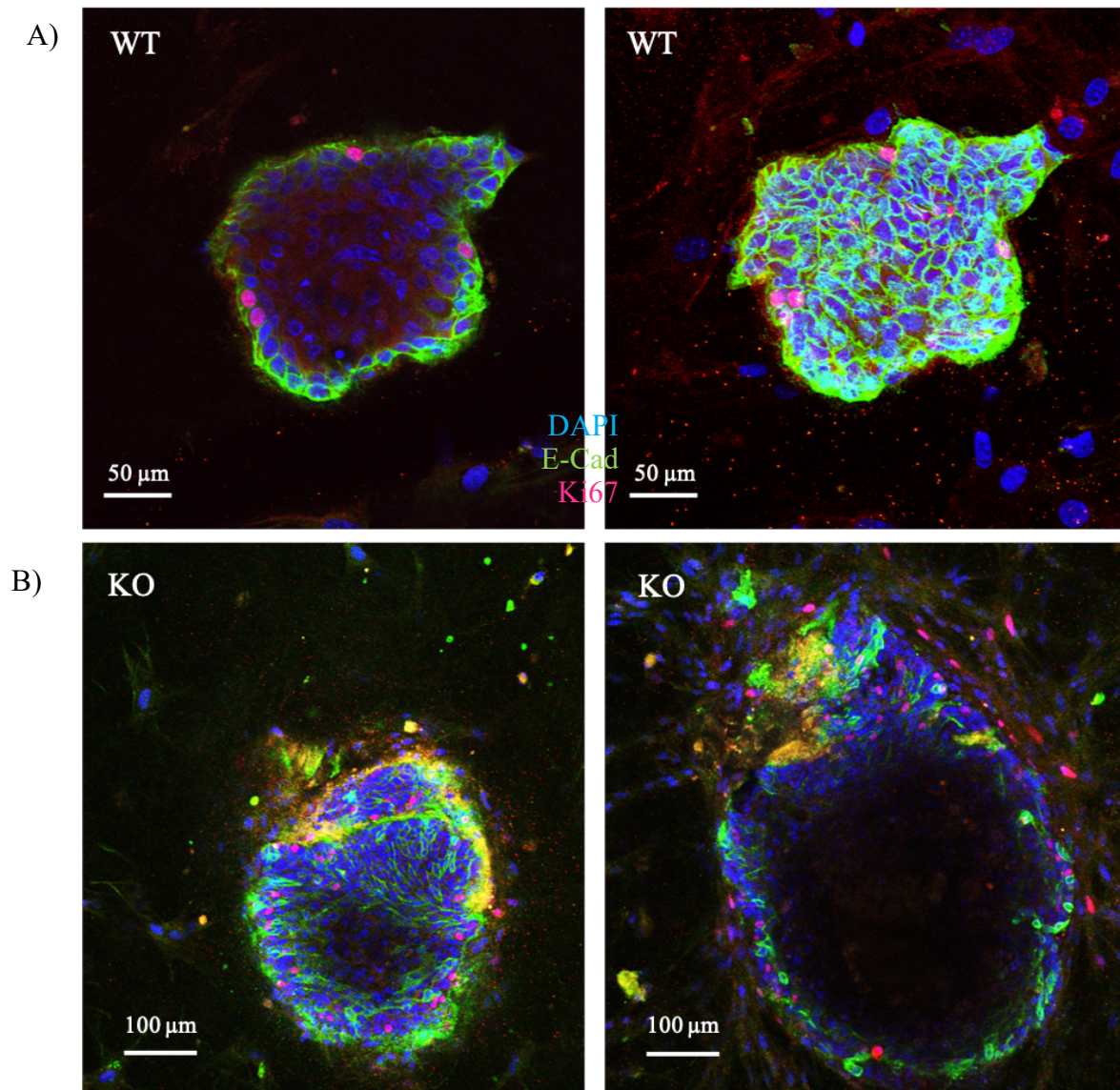


Figure 3.12 | Ki67 staining in organoids showing proliferating cells. A) Confocal images of an uninduced (WT) organoid showing positive Ki67 staining (594-red) in several cells, along with E-cadherin staining (488-green) and DAPI (blue). Ki67 staining is visible both on the surface and in the centre of the organoid. **B)** confocal images of an induced (KO) organoid with positive Ki67 staining. Ki67 positive cells are randomly dispersed throughout the organoid in no obvious pattern.

3.7 CD44 Staining

As a last characterisation step, an investigation was carried out into CD44 expression in the organoids. As noted earlier, the *Cre* recombinase is under the CD44 promoter, and therefore every cell expressing CD44 in theory has the potential to activate TdTomato fluorescence. To assess this, immunofluorescence was carried out on one dish of induced organoids after 6 days of culture using a CD44 antibody (488-green) and DAPI. Organoids were then imaged using the confocal microscope.

The CD44 staining for this experiment was not satisfactory due to poor antibody quality. Because of time restrictions, only one replicate was performed, and as a result there were no conclusive results. This is an experiment that will be optimised and repeated in future research.

3.8 Concluding Remarks

In summary, the optimisation phase of this project has provided powerful insight into the morphological characteristics and behaviours of our inducible E-cadherin knockout organoids. Although there are several important experiments still to be done, the results described above have provided enough of a foundation to confidently move forward into the drug screening phase of the wider project and affirm the organoids place as a novel model for early stage HDGC.

Chapter 4: Optimisation Discussion

Despite their inherent diversity, the growth patterns of the organoids were relatively consistent throughout all experiments. The growth pattern seen here reflected those observed in other models of a similar nature (Katano et al., 2015; Ootani et al., 2009), and although growth was not sustained beyond 20 days during this project, other groups have shown that it is possible to maintain organoid growth for as long as one year, though additional growth factors need to be supplemented into the media (Ootani et al., 2009). An investigation into the longevity of this specific HDGC organoid model is something that should be looked into in future research. This would provide important insight into the unique long-term growth patterns of the E-cadherin knockout organoids. For example, it has been shown that some organoid models are inconsistent in their growth rates, displaying alternating periods of rapid and slow growth over time (Ootani et al., 2009). Additionally, it would be of interest to look into how the composition of the different cell types change in the organoids over a prolonged period of time. For example, an investigation into whether some gastric cell types differentiate later in organoid development than others would be of value to the overall characterisation of the organoids. Another important research point would be to investigate whether long-term growth rate is determined by the size of the organoid's stem cell population at any given time. Answering these questions would provide valuable insights for the development of this and other organoid models.

When using the tissue from one mouse stomach per 35mm dish, anywhere between 5 and 20 true organoids could be expected to grow in each dish. Despite adhering to a strict protocol, this variation in organoid numbers could not be eliminated. It is possible that the main factor determining organoid growth is the composition of cells in each segment of primary tissue. For

the most part, this variation was mitigated by ensuring the tissue was minced the same amount for each experiment. However, it is not possible to control exactly what cell types are in each tissue segment and as a result some variation remains. Overall, this variation in organoid numbers did not pose any problems, apart from during drug testing when there was variation in organoid numbers both between replicates and in the different conditions within replicates.

When imaging the organoids, it was imperative that the techniques provided accurate and detailed visualisation of the complex organoid structures. This was somewhat challenging, as the 3D structures vary significantly in morphology. Firstly, an imaging technique was needed to visualise the growth of the live organoids. For this, regular brightfield imaging allowed for recording the organoids in sufficient detail to give insight into their growth behaviours. Early on, it became obvious through brightfield imaging that the organoids follow a growth pattern that was consistent across experiments. However, brightfield imaging could not provide insight into other important aspects of the organoids. For one, their 3D spherical morphology is not visible in brightfield. This meant that from the brightfield images alone, it could not be concluded that the organoids were cystic and contained a lumen. Secondly, when experiments looking at induction of the *Cdh1* knockout were to begin, the percentage of E-cadherin deficient cells would remain unknown after brightfield imaging.

The latter issue was overcome with the use of immunofluorescence staining and fluorescent imaging. By staining the organoids with an E-cadherin antibody and DAPI, then visualising them on the inverted fluorescent microscope, visualisation of the approximate number of cells with and without *Cdh1* expression was possible. This provided valuable insight into the relative success of our conditional knockout model. However, this technique was limited in that it still did not provide comprehensive information on the 3D morphology of the organoids.

Furthermore, it was limited in that the knockout could not be visualised in real-time, only as an endpoint analysis.

Confocal microscopy utilises a small pinhole to concentrate a laser at specific and changeable depths in a sample, resulting in the production of high resolution images at different cross-sections through a specimen. This allows for the visualisation of not only the outer surface of the organoid, but also the inner core and each layer of cells. With the use of a confocal, it was identified that the organoids were consistently cystic, containing a large lumen. By collating the multiple images taken at different depths in the organoid, it was also possible to visualise the organoid as a whole in great detail. This tool allowed for a much greater understanding of the organoids and their structure, adding extensively to both this specific objective as well as the wider project. However, confocal microscopy is both expensive and time consuming. Therefore, there is still a place for fluorescence microscopy in the workflow. The final sequence of imaging techniques for subsequent experiments was as follows: initial brightfield imaging to track organoid growth in real time, immunofluorescence and fluorescence microscopy to assess the quality of the staining and to establish which organoids would be most useful and representative for confocal imaging, and lastly confocal imaging of a selection of organoids from the sample for detailed visualisation. Together, these imaging techniques provided a comprehensive picture of the organoids for this project and provided an effective and efficient way to qualitatively assess the results of future experiments.

The organoids used throughout this project were generated from mice harbouring conditional *Cdh1* mutations. This system circumvents the issue of the embryonic lethal phenotype caused by a homozygous *Cdh1* knockout. It provides temporal and spatial control of the knockout, so that later embryonic or adult phenotypes can be accessed (Guo, Yang, & Lobe, 2002). Upon initial visualisation of the organoids, it was apparent that the knockout efficiency had not been

100% and varied significantly between organoids. These findings were not unexpected, as this *Cre*-inducible knockout system has been shown to harbour high amounts of variation in its knockout efficacy (Leonhard et al., 2008; Mirantes et al., 2013). This could be due to various components of the system. For example, endoxifen may not be reaching every cell in the organoid structure.

For 100% knockout, another method for inducing the mutation in the organoids would need to be adopted, such as a lentiviral system. However, 100% knockout is not necessarily the target for these organoids as a model for HDGC. *CDHI* mutation carriers are born with a heterozygous loss of the gene, later gaining homozygous loss through somatic mechanisms such as epigenetic silencing. This homozygous loss only occurs in a small subset of gastric cells, leading to the initiation of signet ring cell carcinomas (Guilford et al., 2010). Therefore, the organoids retaining a population of *CDHI* positive cells is an asset to their accuracy as a model for HDGC.

After doing initial optimisation and characterisation using the conditional knockout mice for *Cdh1*, mice that harboured an additional endogenous TdTomato fluorescent protein were analysed. TdTomato is a highly photostable tandem dimer that emits strong red fluorescence at a wavelength of 581. This protein is under the *CD44* promoter in the mice used for this project, and in theory should be exclusively expressed in cells which have also undergone *Cdh1* inactivation. The addition of an endogenous fluorescent protein allows for the visualisation and tracing of cells in real-time under the fluorescence microscope, without having to fix the organoids and run immunofluorescence.

An experiment was done to investigate whether or not there was a difference in percentage of knockout cells between organoids that were exposed to endoxifen continuously and those

exposed only for 48 hours before it was removed from the media (results not shown). Being able to remove the endoxifen from the media after 48 hours would be of benefit when it comes to drugging experiments later on, as ideally the organoids would not be exposed to endoxifen and the chosen drug simultaneously. From this investigation, it was concluded that the difference between knockout percentage of organoids exposed to endoxifen for 48 hours versus 96 hours was not significant, and therefore for subsequent experiments, it was acceptable to remove the endoxifen from the media after 48 hours of initial exposure.

When analysing confocal images of induced organoids, it was observed that many of these organoids contained an infiltration of TdTomato-expressing cells in their lumen. Further, E-cadherin negative cells also pooled in the centre of induced non-tomato organoids. One possible mechanism to explain this observation is that the E-cadherin negative cells with compromised cell-cell adhesion capabilities struggle to remain in the epithelial wall of the organoid and are pushed into the lumen. Meanwhile, the E-cadherin positive cells proliferate and maintain the structure of the organoid by holding the majority in the outer surface of the cystic epithelial structure. It is also possible that E-cadherin negative cells are not only pushed into the centre of the organoid, but also out into the collagen. The cells are predominantly pushed into the lumen as this area is void of collagen, so will be the path of least resistance.

It is unknown if the cells that are pushed into the organoid lumen are dead, dying or alive, however this would be an area of priority to look into in the future. If the cells are alive, this could mimic aspects of the tumour invasion process. On the other hand, the cells observed here could be dead or dying, which would explain their shedding into the lumen as a form of expulsion. This has been seen previously in gastric organoids, where high numbers of apoptotic cells were found in the inner lumen (Katano et al., 2013b).

Over all, the optimisation and characterisation of these organoids was both a challenging and informative process. An important direction for the future, is further investigation into different cell type markers. To gain a comprehensive understanding of these organoids, it is vital that their cell-type composition is known. To do this, markers for different gastric cell types – such as chief cells and parietal cells – should be used. Knowing what gastric cell types these organoids are comprised of, in what proportions and in what organisation, will elucidate further how accurate they are as a model for the *in vivo* gastric environment. In theory, they should harbour all the cell types present in a gastric gland, however it is unknown at what stage each cell type differentiates, or whether some do at all. Further characterisation should also be completed using additional techniques, such as classical histology. This would provide another perspective to the morphological analysis of the organoids, deepening our understanding of the model and the cells that comprise it.

In terms of longevity, it has been observed that growth slows down significantly after approximately 7 days. Therefore, it would be interesting to use a gastric stem cell marker, such as LGR5 (Barker et al., 2010), to investigate whether or not growth rate correlates with the size of the stem cell population in the organoid at any given time. If organoids with larger stem cell populations are growing faster, then this would be an indicator that the longevity of this model could be increased by maintaining the stem cell niche more effectively. At present, the primary method of stem cell niche maintenance is through the endogenous growth factors secreted by the myofibroblast cells. It is possible that to enhance the stem cell niche and increase the longevity of the model the media could be supplemented with additional growth factors, such as WNT and R-Spondin. Other groups have shown that with the addition of growth factors to the media, organoids can be maintained for upwards of one year (Ootani et al., 2009). This will be of great use in future projects when investigating the long-term consequences of HDGC in the organoids – for example, do they eventually develop signet ring cells?

There are other areas that should be optimised in order to improve this model, such as determining whether the organoids can be cryopreserved and resurrected without impacting their growth. Another area worth investigating is passaging of the organoids. Although passage was attempted multiple times throughout this project, satisfactory results were not achieved, as previously observed by others with this ALI model (Li et al., 2014). Having successful passage of the organoids would allow for expansion of the number of organoids being generated without having to use additional mice. This will be of benefit to all areas of this project, especially drug screening. Our laboratory is currently establishing a submerged model for HDGC organoids, to potentially use as a passageable model for drug screening to increase throughput. Even with this development, the ALI model will still be vital to the lab and this wider project, as it is known to be the model with the most accurate reflection of the *in vivo* environment (Pastuła et al., 2016).

The investigations that have been done into these organoids have provided valuable insight into their accuracy, usefulness and limitations as a model for HDGC, and enough of a foundation to confidently move forward into the drug screening phase of the wider project.

Chapter 5: Drug Screening Results

The usefulness of organoids is not limited to expanding our understanding of cancer progression and disease profile on a cellular level. Organoids can be used as a medium-throughput tool for drug screening – either in research to discover novel treatments or in a clinical setting as a tool for personalised medicine.

Within the scope of this project, the intention is to use them as a tool to screen compounds with the hopes of identifying drugs that impart a synthetic lethal effect on the conditional *Cdh1* knockout organoids. Four drugs were screened in total, chosen due to their promising results in 2D cell line screening conducted in our laboratory.

Qualitative and quantitative techniques were used to analyse the effectiveness of the drugs and determine whether or not they would be put forward into subsequent animal model screening. It was expected that drug screening in the organoids would not only provide insight into the effectiveness of the drugs, but also into the usefulness of the organoids as an intermediate screening step and model for HDGC cancer progression.

5.1 DMSO tolerance

Before drug testing could begin, an investigation into the tolerance threshold of organoids for DMSO was carried out. DMSO is a widely used drug solvent, which at high concentrations can have a toxic effect on cell cultures. In the 2D cell line drug screening done in our laboratory using MCF10A and NCI-N87 cells, 0.1% DMSO can be tolerated by the cells for a prolonged period of time.

For this experiment, four dishes of uninduced (WT) organoids were set up, each dish containing between 10-15 organoids. The four dishes were left to culture for 48 hours, and then exposed to four different concentrations of DMSO (0.2%, 0.1%, 0.05% and 0%) for 96 hours. Organoids were imaged in brightfield every 24 hours and observations recorded. It has been suggested that the DMSO tolerance threshold for other 3D cell cultures lies between 0.1% and 0.01% (Pal, Mamidi, Das, & Bhonde, 2012), so organoids were expected to have a similar result.

When exposed to 0.2% DMSO, the organoids did not display any significant growth over 48h. In addition to this, the cells that were there before DMSO exposure displayed characteristics suggestive of death 48h after exposure, such as disintegration, darkening and flattening (Fig. 5.1A). Organoids displayed these same traits when exposed to 0.1% DMSO (Fig. 5.1B), however they took slightly longer to take effect – 72 h versus 48 h at 0.2%. At 0.05% DMSO, no ‘death’ phenotypes were observed within the 96 h experiment timeframe (Fig. 5.1C). As a result, this concentration of DMSO was used in the future drug testing studies. Concentrations lower than this were generally not possible due to poor drug solubility below 0.05%.

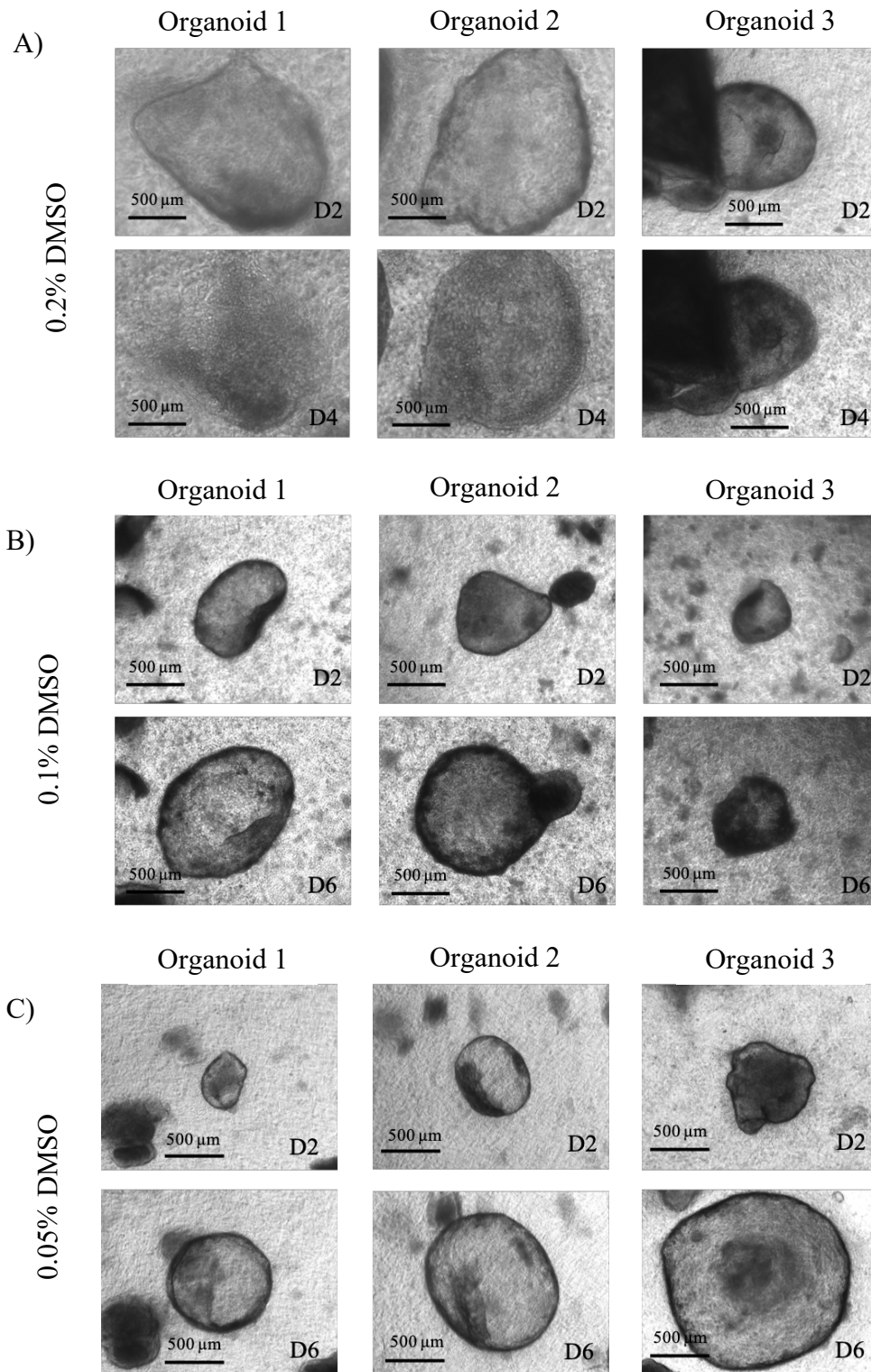


Figure 5.1 | DMSO tolerance screening in the organoids. **A)** Brightfield images of three organoids representative of the dish exposed to 0.2% DMSO on day 2 (0 hours post treatment) and day 4 (48 hours post treatment). Organoids have a darkened, flattened appearance and are beginning to disintegrate. **B)** Three organoids exposed to 0.1% DMSO for 96 hours. Also showing a darkened appearance on day 6. **C)** Three organoids exposed to 0.05% DMSO for 96 hours. Healthy, transparent appearance has been retained for >96 hours.

5.2 Drug Screening Protocol

For drug screening, four dishes were used for each experiment with the tissue of one neonatal mouse stomach in each. Primary tissue was seeded in the collagen and complete media added to the surrounding dish. For the two plates intending to house induced (KO) organoids, 5 μ M endoxifen was also added to the media. Organoids were left to grow without drug for 48 hours, after which the organoid media was changed, endoxifen removed and drug added to one induced (KO) dish and one uninduced (WT) dish and solvent control added to the remaining two dishes. After 6 days of total growth (4 days exposed to drug), organoids were fixed, stained and analysed using fluorescence and confocal microscopy.

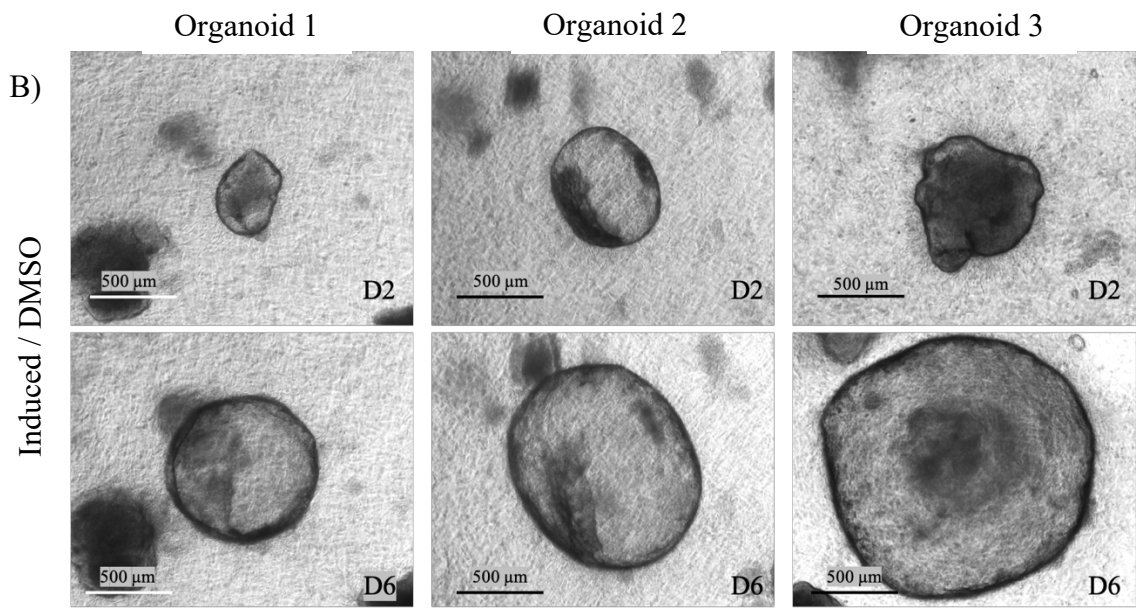
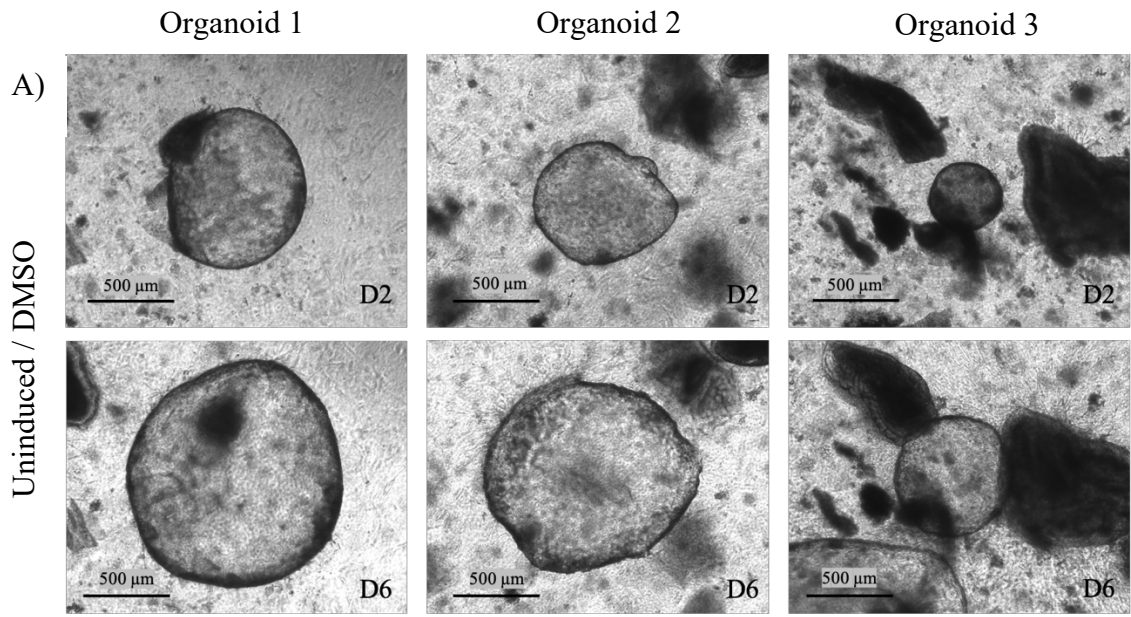
5.3 ARQ-092

Three replicates of the AKT inhibitor ARQ-092 were tested at a concentration of 5 μ M using the protocol described above. Notably, there was considerable variation between replicates in the number of organoids that grew in each dish, ranging from 5 to 20.

The uninduced DMSO control organoids for this experiment displayed normal growth and no signs of death (Fig. 5.2A). They increased in size significantly between day 2 and day 6 and, on day 6, showed no signs of disintegration, flattening or substantial darkening. The induced DMSO controls (Fig. 5.2B) were comparable, exhibiting strong growth and no death phenotypes. The uninduced organoids exposed to ARQ-092 displayed relatively normal growth, although some, such as organoid 1, showed darkening on both days 2 and 6 (Fig. 5.2C).

Induced organoids that were exposed to ARQ-092 for 96 hours exhibited distinct death phenotypes (Fig. 5.2D). By day 6, the organoids had lost their transparency, and were

instead comprised of darkened, grainy tissue. This darkening indicates necrotic cells, and the grainy texture along with the disrupted borders suggest that the organoids are beginning to lose their structure and break down.



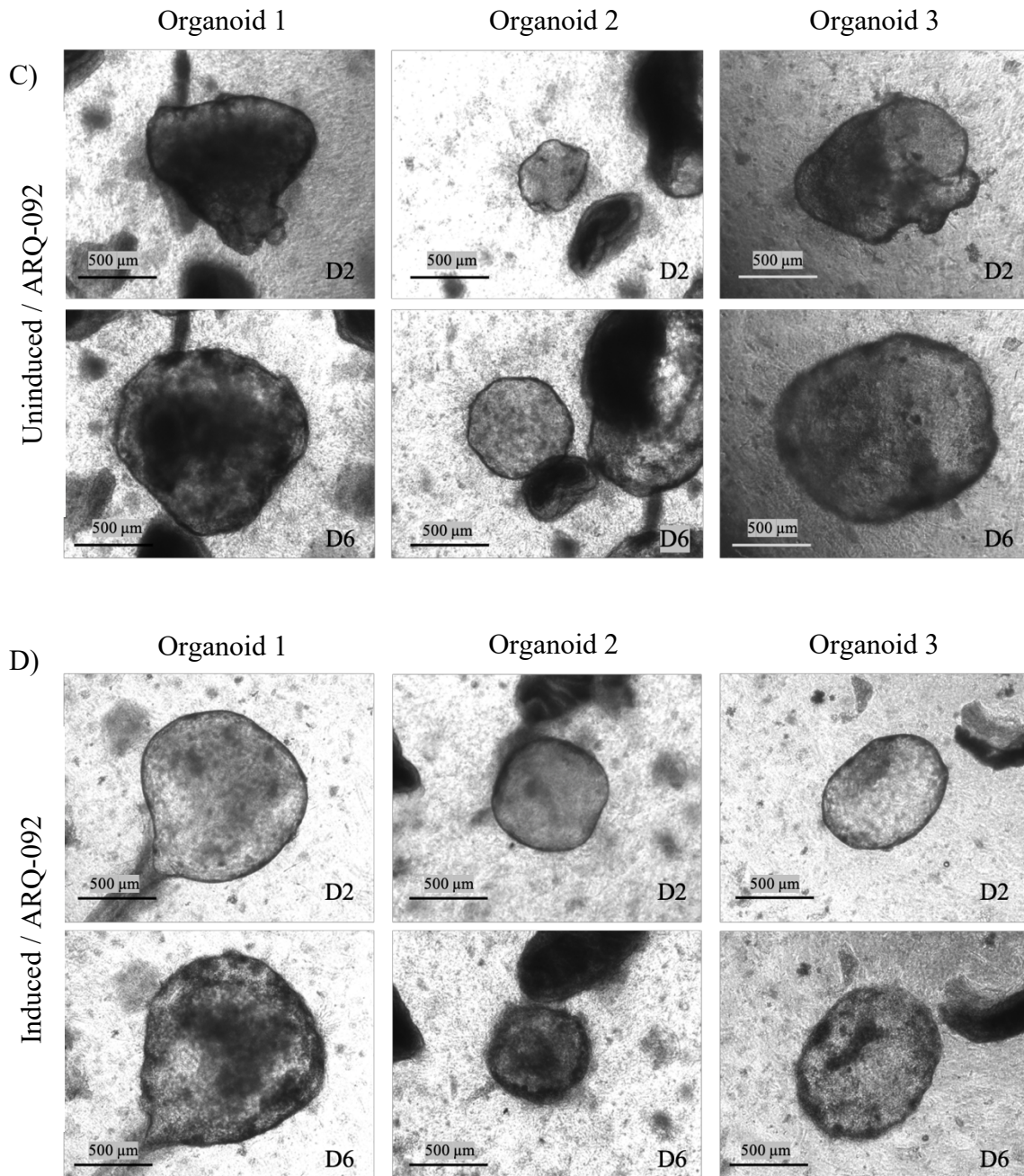


Figure 5.2 | Representative brightfield images of organoids exposed to ARQ-092 and controls. **A)** Three uninduced (WT) DMSO control organoids on day 2 and day 6. Healthy growth and appearance has been maintained. **B)** Three induced (KO) DMSO control organoids on day 2 and day 6. Also exhibiting normal growth and no signs of death. **C)** Three uninduced (WT) organoids exposed to ARQ-092 on day 2 and day 6. Look relatively healthy after 6 days of growth. **D)** Three induced (KO) organoids exposed to ARQ-092 on day 2 and day 6. Displaying a reduced growth rate and phenotypes signifying death (textured, grainy appearance and disrupted structure).

Change in area has been used in this thesis as the primary quantitative measure of drug effectiveness. To measure this, the total area of each organoid was calculated on day 2 and day 6, and the difference between the two calculated as a percentage change. By using percentage change, we were able to account for the high levels of variation in growth rate and starting size of the organoids. These values (from all three biological replicates) were then plotted on a line graph, where each line represents one organoid.

Figure 5.3A shows that for ARQ-092, both the induced (KO) and uninduced (WT) DMSO controls displayed normal growth that increased at comparable rates, however the uninduced organoids exposed to ARQ-092 grew at a reduced rate, almost as low as that of the induced ARQ-092 organoids. When viewed on a smaller scale (Fig. 5.3B), there are a larger number of induced (KO) organoids displaying less than a 50% total increase in size. Furthermore, 17% (5) induced drug-treated organoids reduced in size, an effect not observed in the uninduced/ARQ-092 condition. Statistically, the difference between the two conditions is significant ($p=0.012$).

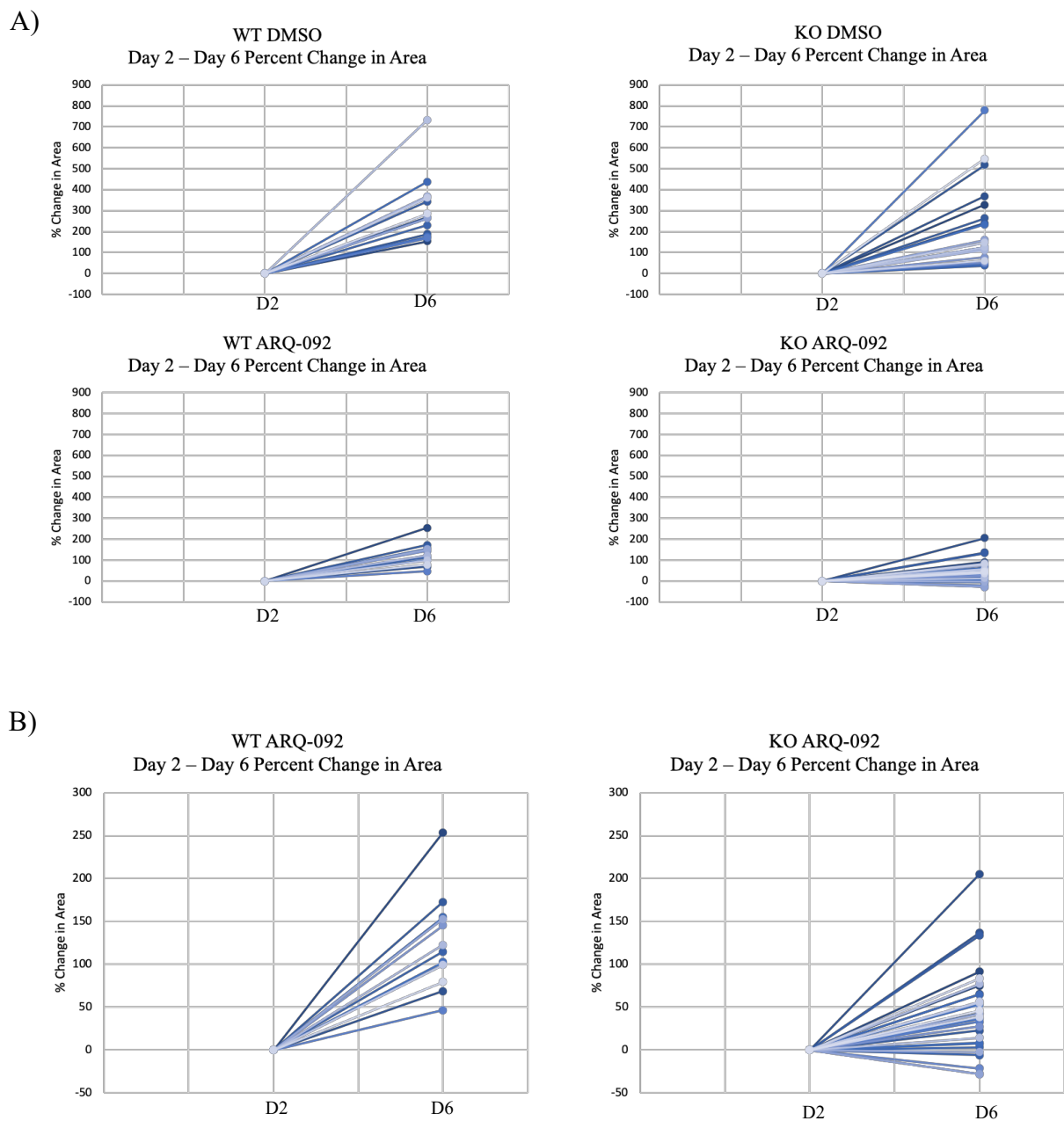


Figure 5.3 | Percentage change in area of organoids from day 2-6. **A)** Each graph displays the collated data from three biological replicates. Individual lines represent the change in area of a singular organoid over the 96 hours of drug/DMSO exposure. Uninduced (WT) and induced (KO) DMSO control organoids exhibit the highest rates of growth. Uninduced (WT) and induced (KO) organoids exposed to ARQ-092 display reduced growth. **B)** Close-up of percentage change in area for induced (KO) and uninduced (WT) graphs exposed to ARQ-092 shows that KO/ARQ-092 organoids have a reduced growth rate compared to WT/ARQ-092 organoids ($p=0.012$).

For each of the four conditions, the average percent change in area across all organoids was calculated and plotted on a bar graph (Fig. 9.3). Over 96 hours of treatment, uninduced (WT) organoids exposed to ARQ-092 have on average an 126% increase in size, whereas induced (KO) organoids show a 45% increase in size on average. This demonstrates a significant synthetic lethal effect ($p=0.012$).

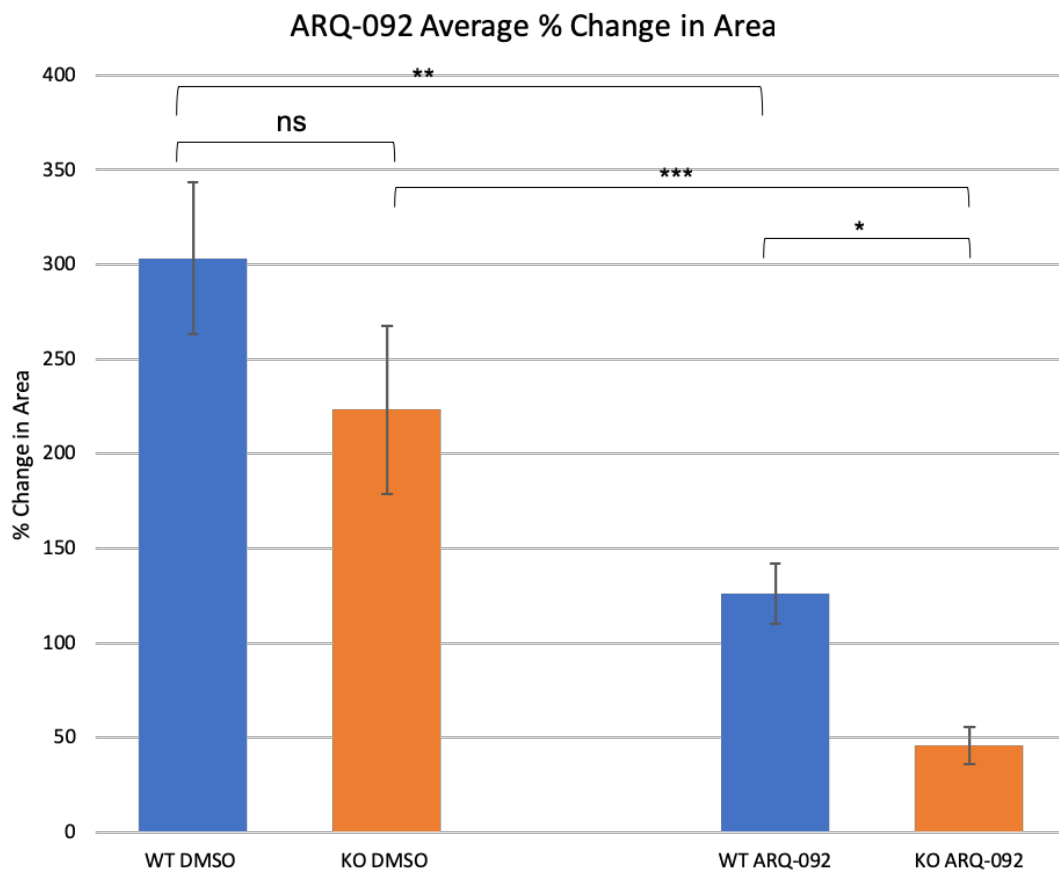


Figure 5.4 | Bar graph showing % Change in area of organoids exposed to ARQ-092 for 96 h (Mean \pm S.E). Graph displaying combined data for three biological replicates. Uninduced (WT)/ARQ-092 organoids ($n=13$) increase in area by 126% on average. Induced (KO)/ARQ-092 organoids ($n=30$) increase in area by 45% on average, displaying a significantly reduced amount of growth ($p=0.012$). The uninduced (WT) ($n=25$) and induced (KO) ($n=29$) DMSO controls increase by 303% and 223%, respectively.

Confocal microscopy was used to capture more detailed images of the organoids and their morphology after drug screening. To do this, all four organoid dishes were fixed and stained with an E-cadherin antibody (488-green) and DAPI (blue) using the immunofluorescence protocol in section 2.8. The organoids were then examined using fluorescence microscopy and four organoids from each dish chosen for confocal imaging.

Two DMSO control organoids (Fig. 5.5) are pictured below as a reference for changes to morphology induced by the drugs. Both the induced (KO) and uninduced (WT) DMSO control organoids displayed intact morphology with a spherical shape and regular cellular organisation. These images will be referred back to as DMSO control images for all confocal imaging from drug screening experiments as they are representative of the general morphology of DMSO control organoids.

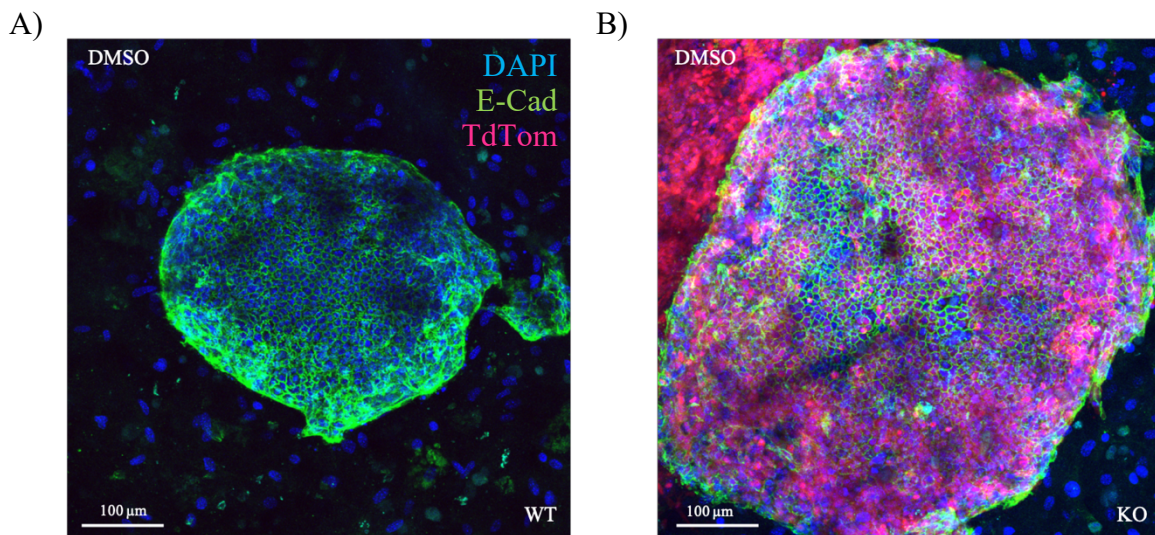


Figure 5.5 | Confocal images of DMSO control organoids. Confocal imaging showing (A) uninduced (WT) and (B) induced (KO) DMSO control organoids displaying immunofluorescence associated with E-cadherin (488-green) and DAPI (blue). Red fluorescence in induced (KO) organoid is TdTomato. Both have intact structures and normal, spherical morphology. Dark patches on uninduced organoid are artefacts from the imaging process (likely to be obstruction from primary tissue) rather than damage to the organoid itself.

Figure 5.6 shows confocal images of uninduced (WT) organoids that have been exposed to ARQ-092. Regardless of any growth inhibition that has taken place, the morphology of organoid 1 is largely normal. Its intact, regular morphology is comparable to the DMSO control seen in Figure 5.5. Organoid 2 is an abnormal shape, harbouring a doughnut-like hole in the centre. Although relatively rare, this shape does occasionally occur in normal organoids under standard growth conditions.

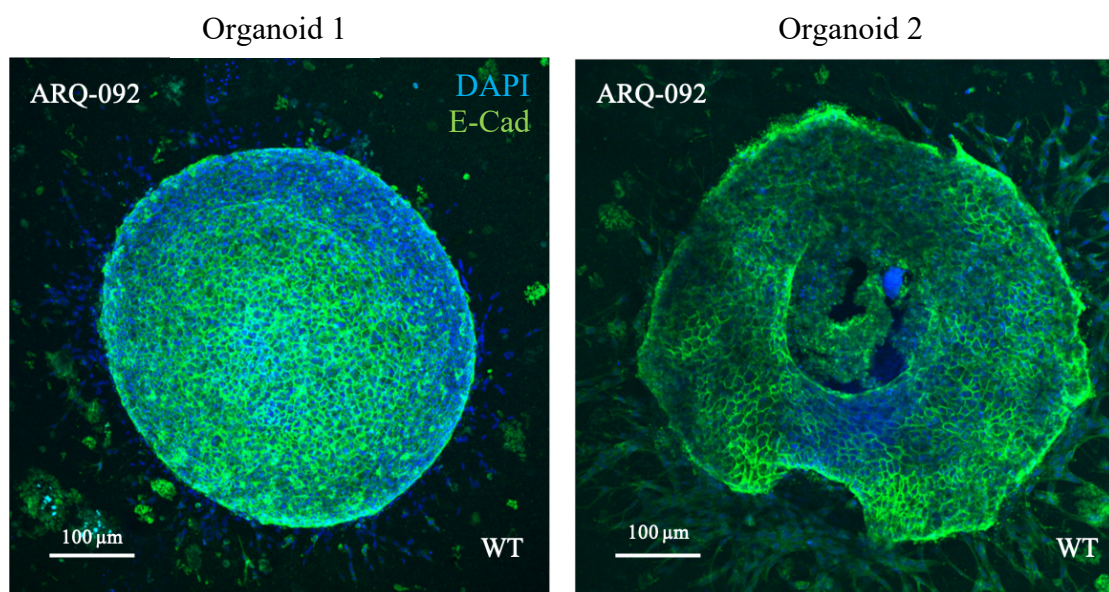


Figure 5.6 | Confocal images of uninduced (WT) organoids exposed to ARQ-092. Organoids were stained with an E-cadherin (488-green) antibody and DAPI (blue) after 6 days of growth. The organoids pictured are positive for lattice-like E-cadherin staining localised to the adherens junctions and demonstrate intact structures with clear borders and organised cells. Organoid 2 has a doughnut-like shape, which although rare, can occur in normal organoids under standard growth conditions.

Four induced organoids that were exposed to ARQ-092 for 96 hours are shown in Figure 5.7. The structure and organisation of all four organoids is highly disrupted, although to a variable extent. Organoid 1 in this series is smaller and remains relatively undisrupted in its bottom half. However, the top segment of the organoid has begun to disintegrate, visible in the major disruption of the structure and displacement of cells out of the main organoid body. This disfigured section of the organoid is where the majority of the TdTomato-expressing E-cadherin negative cells are localised, suggesting they are more susceptible to the effects of the drug.

Organoid 2 is arguably displaying the most disrupted morphology of the four organoids. The structure is highly disorganised with no definitive boundaries and an abundance of cells being displaced from the body of the organoid. Amongst this disruption, there is a sheet of E-cadherin positive cells that have remained intact.

Organoids 3 and 4 remain relatively intact after exposure to ARQ-092, although these organoids are displaying signs of disruption in comparison to the induced (KO) DMSO control in Figure 5.5. Their borders are less defined, indicating that cells are being dislodged from the main organoid body and disintegration is starting to occur. In organoid 3, once again disruption appears to be primarily occurring in the segment of the organoid containing the majority of the E-cadherin-negative cells.

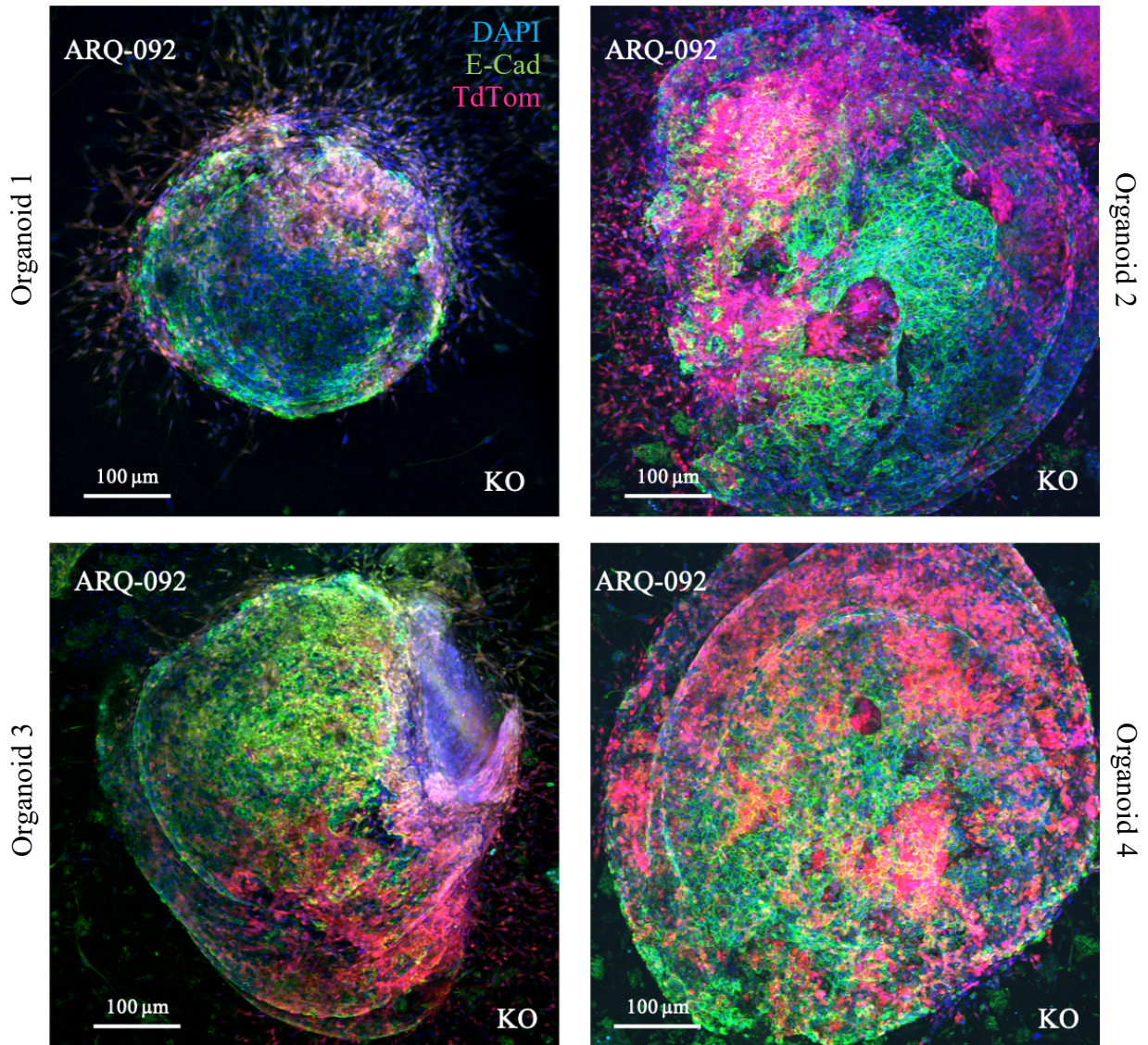


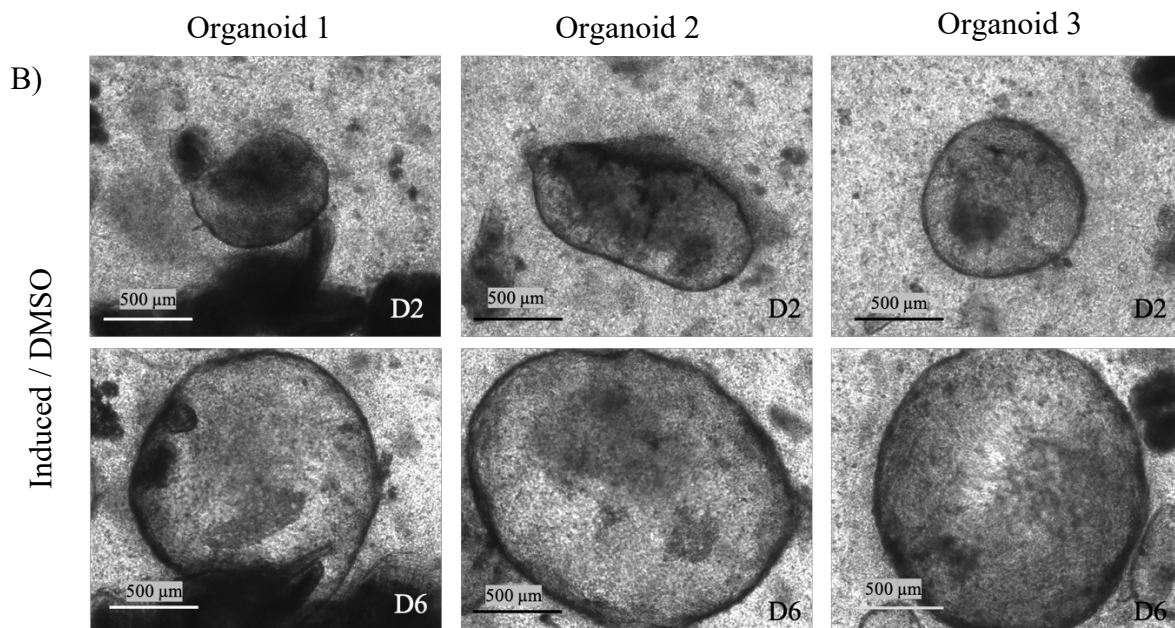
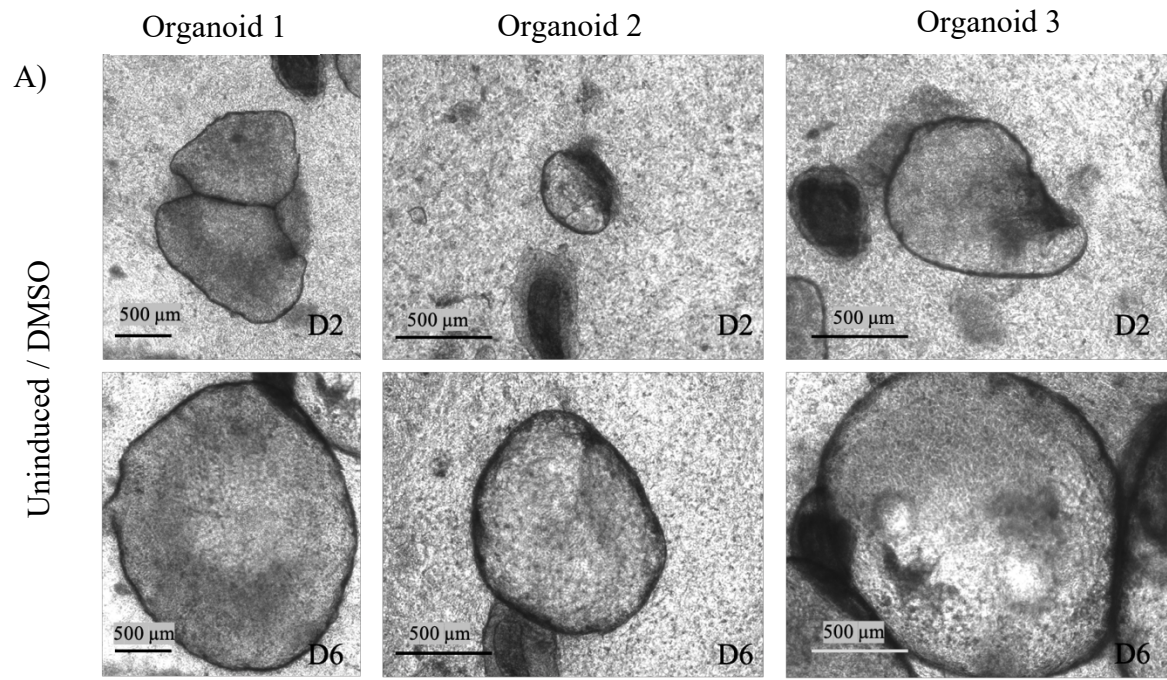
Figure 5.7 | Confocal images of induced organoids exposed to ARQ-092. All four organoids have been exposed to ARQ-092 for 96 hours and stained with DAPI and an E-cadherin antibody (488-green). Endogenous TdTomato fluorescence (red) is also visible. They contain varying levels of E-cadherin negative cells (TdTomato expression) as well as varying levels of morphological disruption. The cystic structures have started to break down and cells are becoming disorganised and scattered around the exterior of the organoid – seen most severely in organoids 1 and 2.

In summary, ARQ-092 has emerged as an effective drug for inhibiting growth and inducing death in the E-cadherin-negative organoids and shows promise as a chemopreventative treatment for HDGC. Future experiments will test ARQ-092 at a range of concentrations, and in combination with other compounds, in order to enhance the differential between WT and KO organoids.

5.4 MK2206

The next drug candidate tested was MK2206, another pan-AKT inhibitor that produced promising results in the prior 2D cell line screens. Three replicates of this experiment were carried out using the protocol described in section 2.9 at a concentration of 6.25 μ M. Once again, there was considerable variation between the replicates in the number of organoids that grew in each dish, ranging from approximately 5-20.

Both the uninduced (WT) and induced (KO) DMSO controls displayed healthy growth, as visible in the brightfield images in Figure 5.8A and 5.8B. On day 6, these organoids were considerably larger than on day 2, and had retained their healthy, transparent, intact phenotypes. Uninduced (WT) organoids that had been exposed to MK2206, shown in Figure 5.8C, showed no obvious signs of death on day 6, 96 hours after initial drug exposure. In contrast, the brightfield images of the induced (KO) organoids that were exposed to MK2206 showed a marked effect on the growth rate and general health of the organoids (Fig. 5.8D).



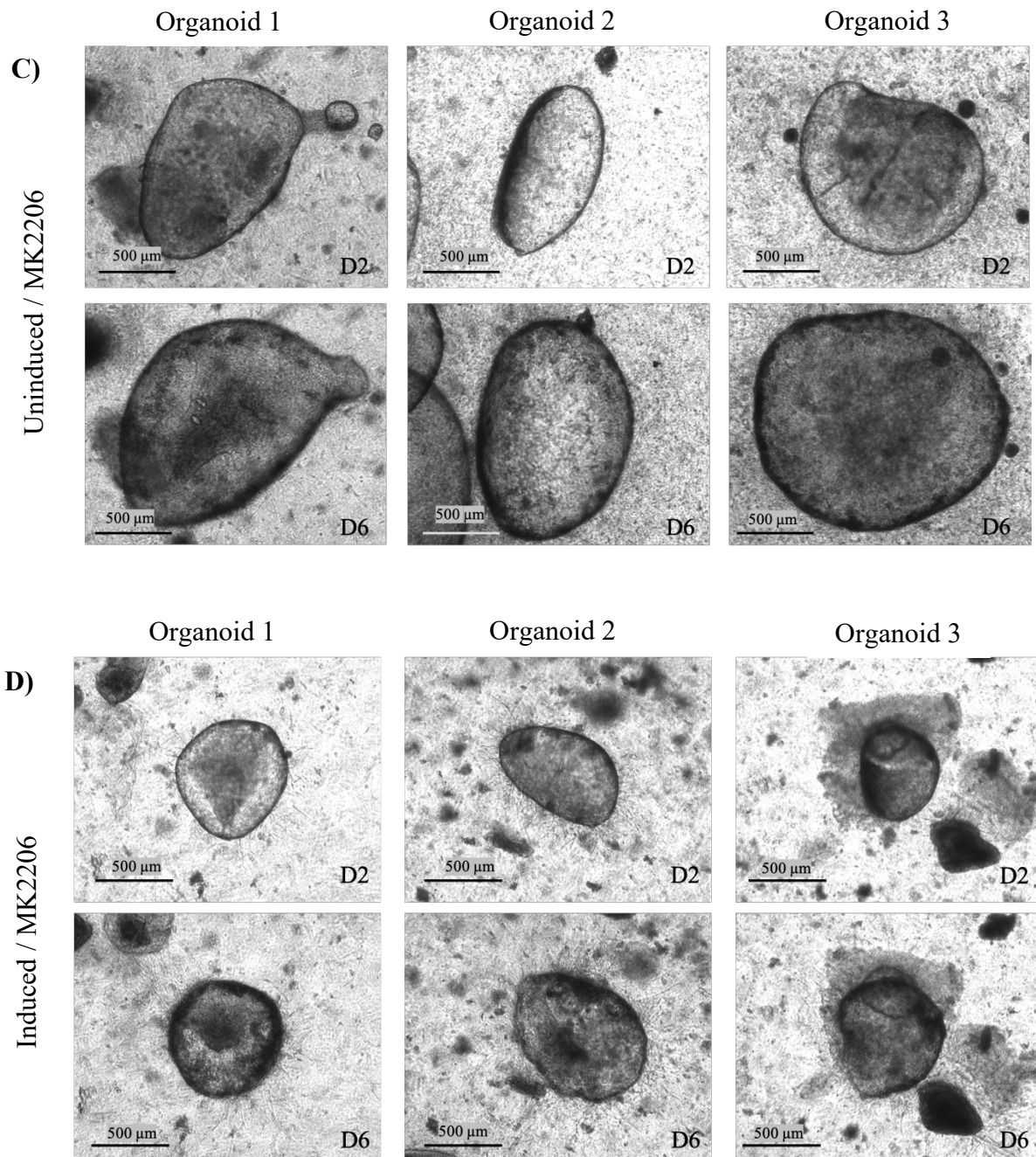


Figure 5.8 | Representative brightfield images of organoids exposed to MK2206 and controls. A) Uninduced (WT) DMSO control organoids on day 2 and day 6. Healthy levels of growth are seen, and no death phenotypes occur. B) Induced (KO) DMSO control organoids on day 2 and day 6. Also exhibiting normal growth and no signs of death. C) Uninduced (WT) organoids exposed to MK2206 for 96 hours. Healthy appearance maintained after 6 days of growth. D) Induced (KO) organoids exposed to MK2206 for 96 hours. These organoids have a highly reduced growth rate and are displaying phenotypes signifying death. All three organoids have a textured, grainy and darkened appearance.

The percentage change in organoid size from day 2 to day 6 is shown in Figure 5.9. Both the induced (KO) and uninduced (WT) DMSO controls displayed normal growth rates. Interestingly, induced (KO) DMSO control organoids grew at a slightly reduced rate in comparison to the uninduced (WT) DMSO control organoids. This is most likely to be due to the slower growth rate of E-cadherin-deficient cells, as observed in the isogenic MCF10A cell line (Chen et al., 2014).

The uninduced (WT) organoids exposed to MK2206 appeared to grow at a slightly reduced rate, however the induced (KO) organoids exposed to MK2206 showed a striking reduction in growth rate (Fig. 5.9). Statistically, the difference between the two conditions is significant ($p=0.0005$).

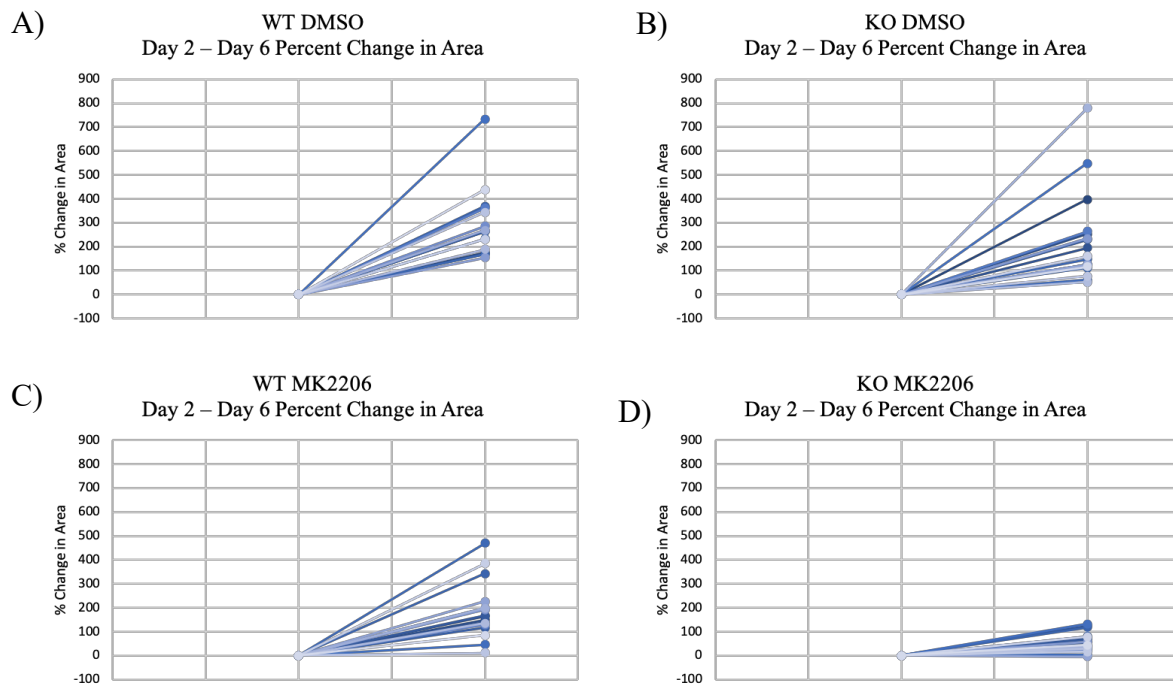


Figure 5.9 | Data showing the percentage change in area of organoids from day 2-6. Each graph displays the collated data from three biological replicates. Individual lines represent the change in area of a singular organoid over the 96 hours of drug/DMSO exposure. Uninduced (WT) (A) and induced (KO) (B) DMSO control organoids exhibit the highest rates of growth. Uninduced (WT) organoids exposed to MK2206 (C) display slightly reduced growth. Induced (KO) organoids exposed to MK2206 (D) have a highly reduced growth rate compared to WT/MK2206 organoids ($p=0.0005$) – the maximum increase being 132% compared to 469% in uninduced (WT) MK2206 organoids.

For each of the four conditions, the average percent change in area across all organoids was calculated and plotted on a bar graph (Fig. 5.10). Over 96 hours of treatment, uninduced (WT) organoids exposed to MK2206 have on average an 185% increase in size, whereas induced (KO) organoids show a 52% increase in size on average. This demonstrates a significant synthetic lethal effect ($p=0.0005$).

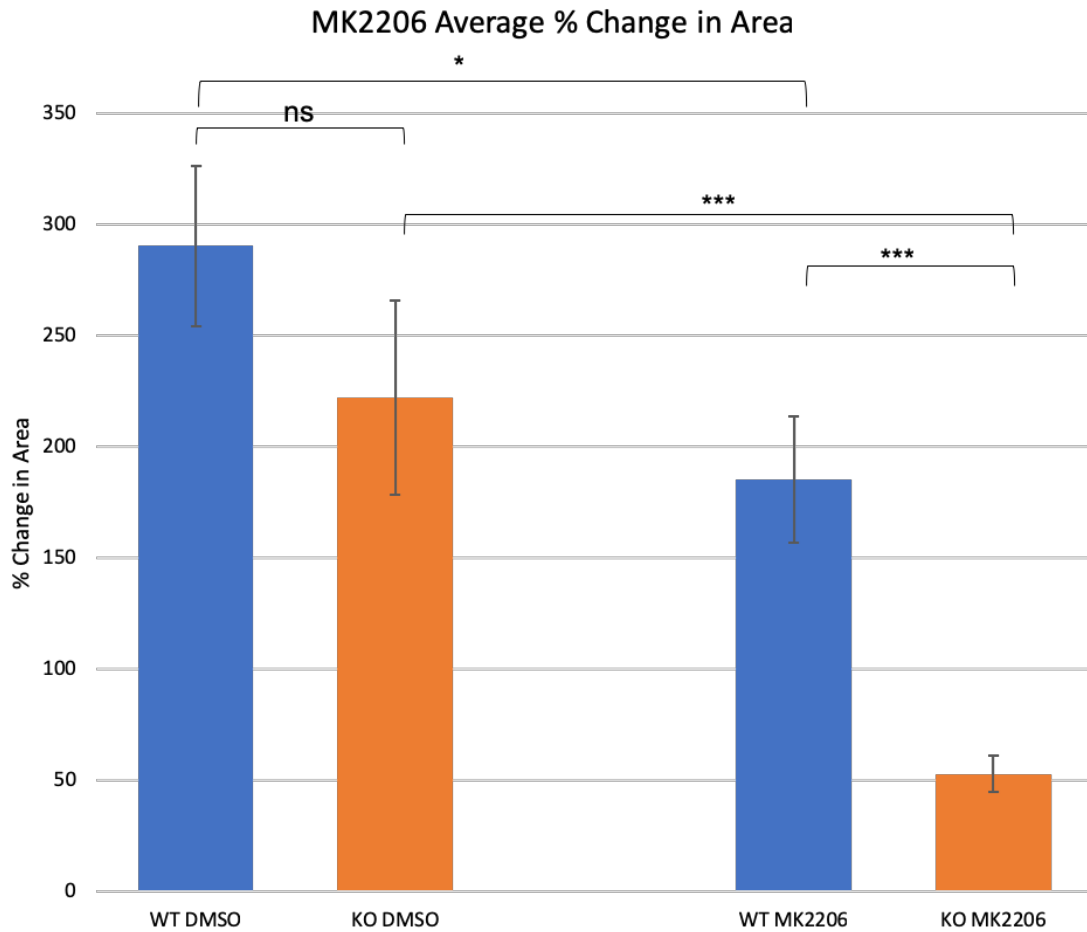


Figure 5.10 | Bar graph showing Change in area of organoids exposed to MK2206 for 96 h (Mean \pm S.E). Graph displaying combined data for three biological replicates. Uninduced (WT)/MK2206 (n=18) organoids increase in area by 185% on average. Induced (KO)/MK2206 (n=22) organoids increase in area by 52% on average, displaying a significantly reduced amount of growth (p=0.0005). The uninduced (WT) (n=23) and induced (KO) DMSO (n=28) controls increase by 290% and 222%, respectively.

Once again, confocal imaging was carried out in order to gain a more detailed picture of organoid morphology. The two dishes containing uninduced (WT) and induced (KO) organoids exposed to MK2206 were fixed and stained with an E-cadherin antibody (488-green) and DAPI (blue) using the immunofluorescence protocol in section 2.8. The organoids were then

examined using fluorescence microscopy and four organoids from each dish chosen for confocal imaging, the cleanest of which are displayed below.

The uninduced organoid treated with MK2206 looked relatively intact despite 96 hours of drug exposure (Fig 5.11). The E-cadherin staining (488-green) appeared faint around the outer edges of the organoid, however this is likely due to limitations with exposure times during imaging. Overall, this organoid appeared structurally intact with clean borders, suggesting that MK2206 is not causing significant morphological disruption in uninduced (WT) organoids.

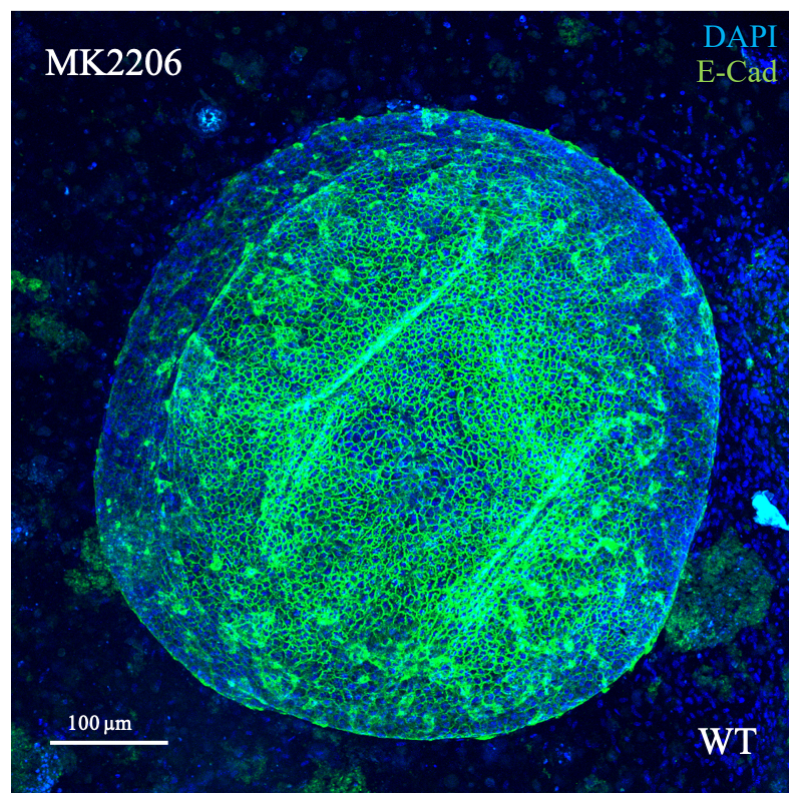


Figure 5.11 | Confocal image of an uninduced (WT) organoid exposed to MK2206. The organoid pictured has been stained with an E-cadherin antibody (488-green) and DAPI (blue) 96 hours after drug treatment. The organoid has retained an intact structure with clear borders and organised cells.

Induced (KO) organoids that were exposed to MK2206 displayed some morphological disruption (Fig. 5.12), however not to the same extent as the damage caused by ARQ-092 (Fig. 5.7). These organoids were relatively intact, although there was a significant number of cells expelled from the main organoid body, especially in organoid 2. It should be noted that much of the debris surrounding the organoids in these images is from the primary tissue and other organoids in the dish, rather than debris from the organoids themselves. The E-cadherin positive cells are growing out of the organoids as nodules in both organoids, but more prominently in organoid 2.

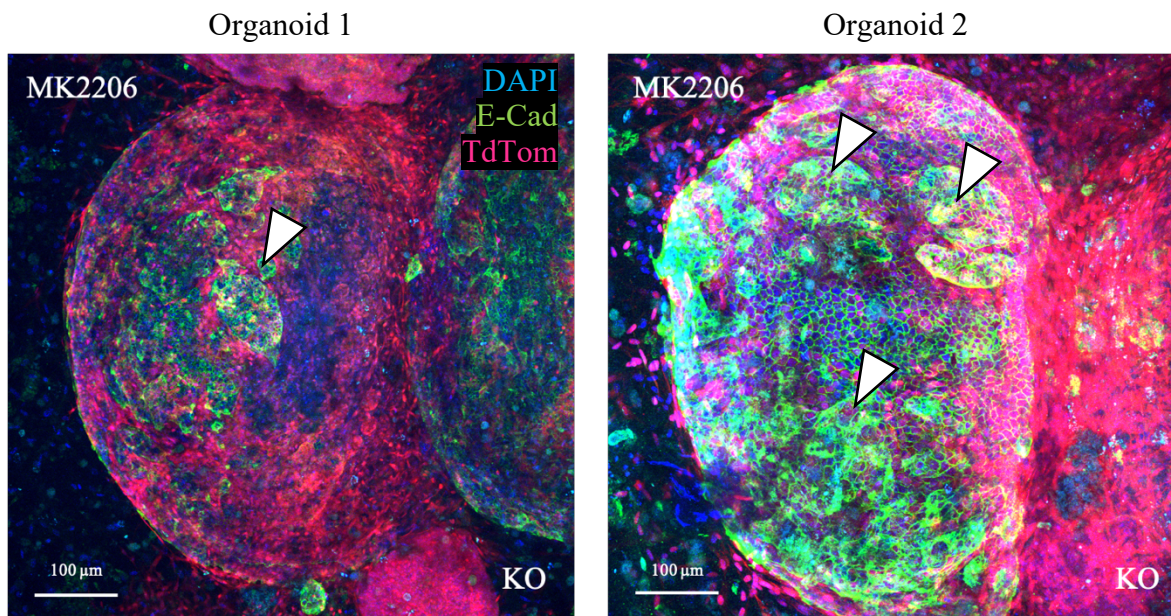


Figure 5.12 | Confocal images of induced organoids exposed to MK2206. Organoids 1 and 2 have been stained with an E-cadherin antibody (488-green) and DAPI 96 hours after drug treatment. Endogenous TdTomato fluorescence is also visible (red). Some morphological disruption is present, however organoid borders have remained relatively intact. Patches of E-cadherin positive cells are growing out of the organoids as nodules (white arrows), particularly organoid 2.

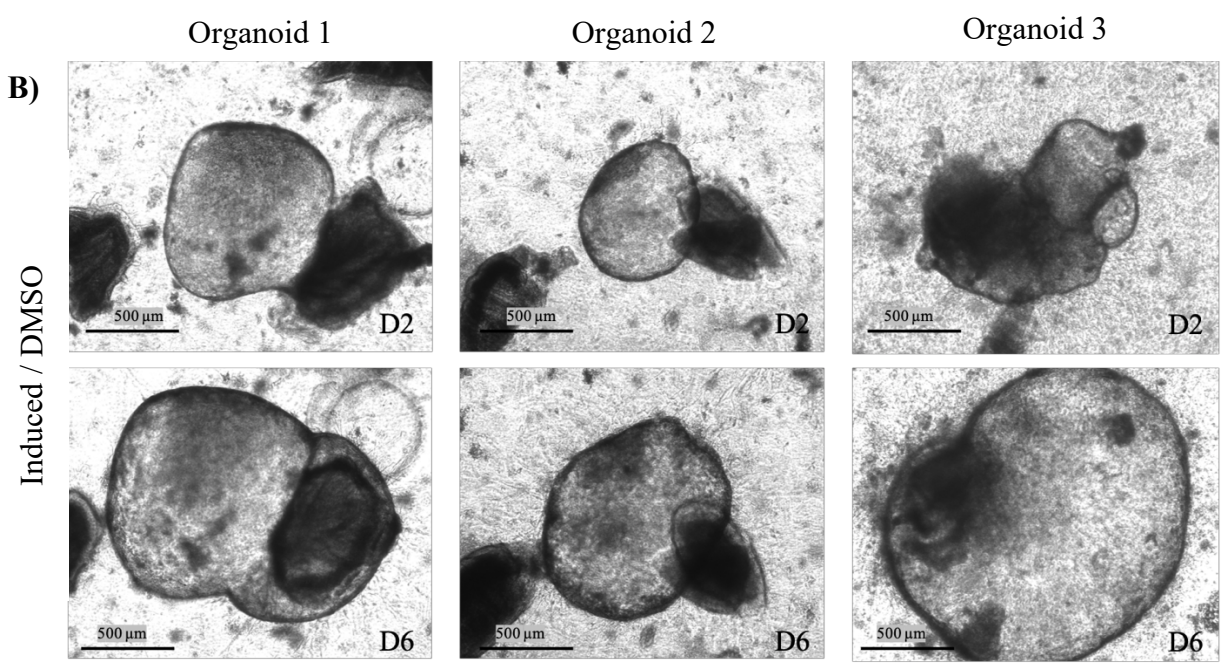
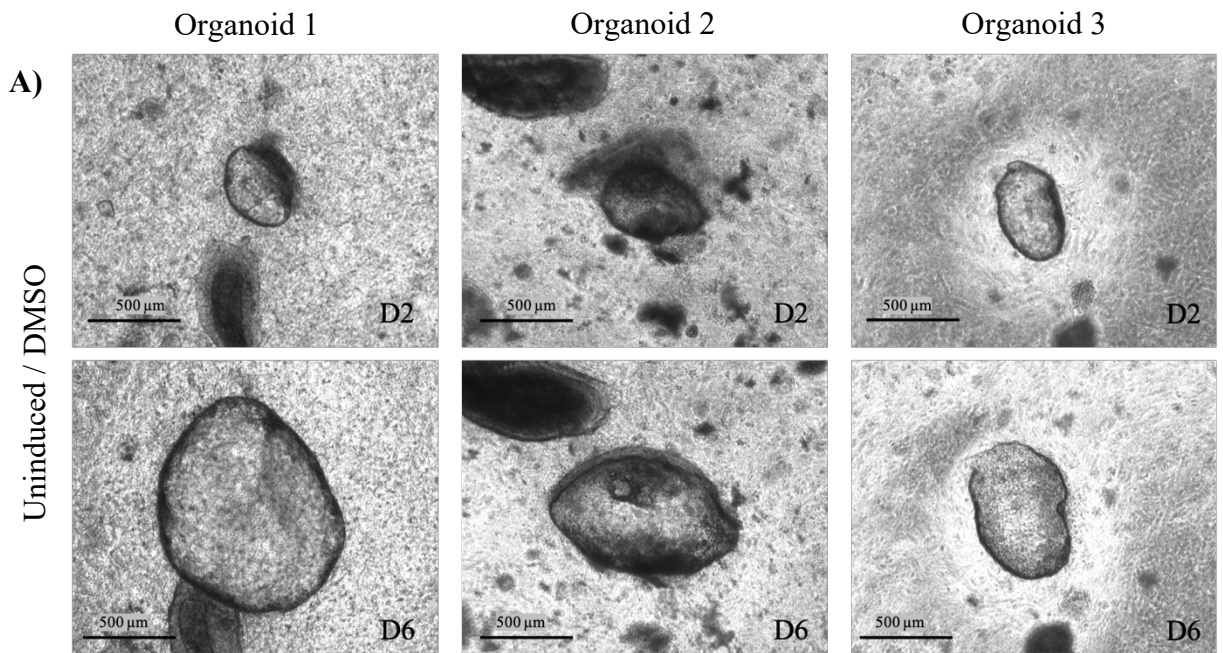
Overall, quantitative and qualitative analysis supports the possibility that MK2206 induces growth inhibition preferentially in the KO organoids.

5.5 Vorinostat

The third drug screened was Vorinostat, also known as suberanilohydroxamic acid (SAHA), a histone deacetylase (HDAC) inhibitor that showed evidence of E-cadherin-related synthetic lethality in the previous 2D cell line screening. Vorinostat has a history of use in psychiatry and neurology, however more recently it has been used in anticancer therapy (Bubna, 2015).

For drug screening, Vorinostat was used at a concentration of 1.5 μ M in the protocol described in section 2.9. Due to time restrictions, only one replicate of this experiment was able to be performed. There were between 5-15 organoids per dish for this experiment.

The induced (KO) organoids that were exposed to Vorinostat (Fig. 5.13D) exhibited relatively normal growth and no death phenotypes. Their growth appeared to be comparable to that of the DMSO controls (Fig. 5.13A and 5.13B) and the uninduced organoids exposed to the drug (Fig. 5.13C). The tissue of induced (KO) organoids that have been exposed to Vorinostat is transparent, and the organoids have retained their 3D, spherical structure with no disintegration. This suggests that at this concentration (1.5 μ M), Vorinostat has not had a visible effect on the organoids.



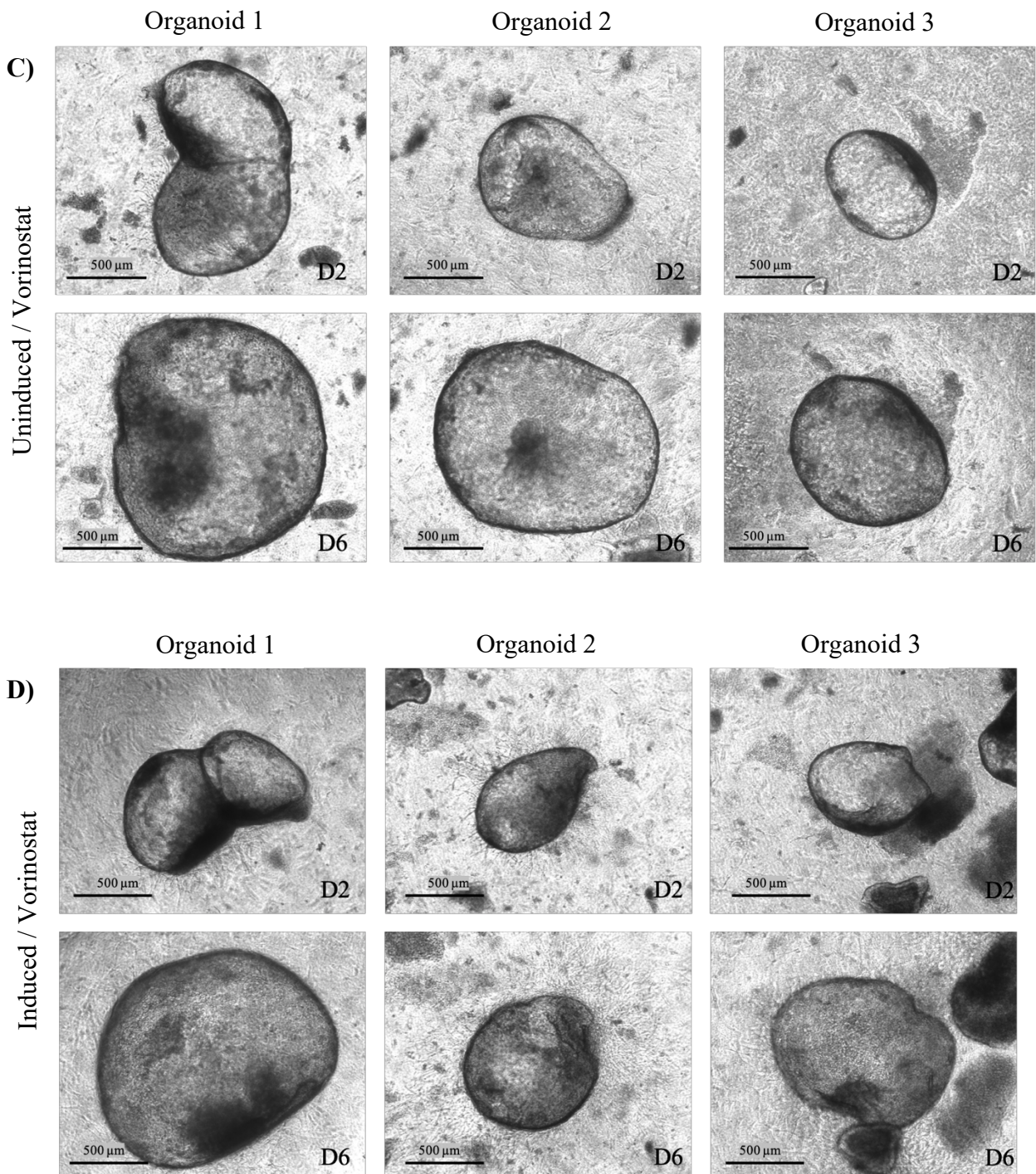


Figure 5.13 | Brightfield images of organoids exposed to Vorinostat and controls. A) Uninduced (WT) DMSO control organoids on day 2 and day 6. Organoids display healthy levels of growth and no death phenotypes. **B)** Induced (KO) DMSO control organoids on day 2 and day 6. Also exhibit normal growth and no signs of death. **C)** Uninduced (WT) organoids exposed to Vorinostat on day 2 and day 6. Organoids have retained healthy phenotypes. **D)** Induced (KO) organoids exposed to Vorinostat on day 2 and day 6. These organoids also appear relatively healthy with no darkening or degradation.

The two dishes containing uninduced (WT) and induced (KO) organoids exposed to Vorinostat were fixed and stained with an E-cadherin antibody (488-green) and DAPI (blue) using the immunofluorescence protocol in section 2.8. The organoids were then examined using fluorescence microscopy and four organoids from each dish chosen for confocal imaging, the cleanest of which are pictured below.

Confocal imaging of the uninduced (WT) organoid exposed to Vorinostat also showed no obvious signs of morphological disruption or death (Fig. 5.14). Induced (KO) organoids that have been exposed to Vorinostat (Fig. 5.15) harboured high levels of variation in both morphology and percentage of E-cadherin-negative cells. For example, organoids 2 and 4 have a significantly higher number of E-cadherin-positive cells in comparison to organoid 3. Regardless, they also retained a relatively healthy morphology.

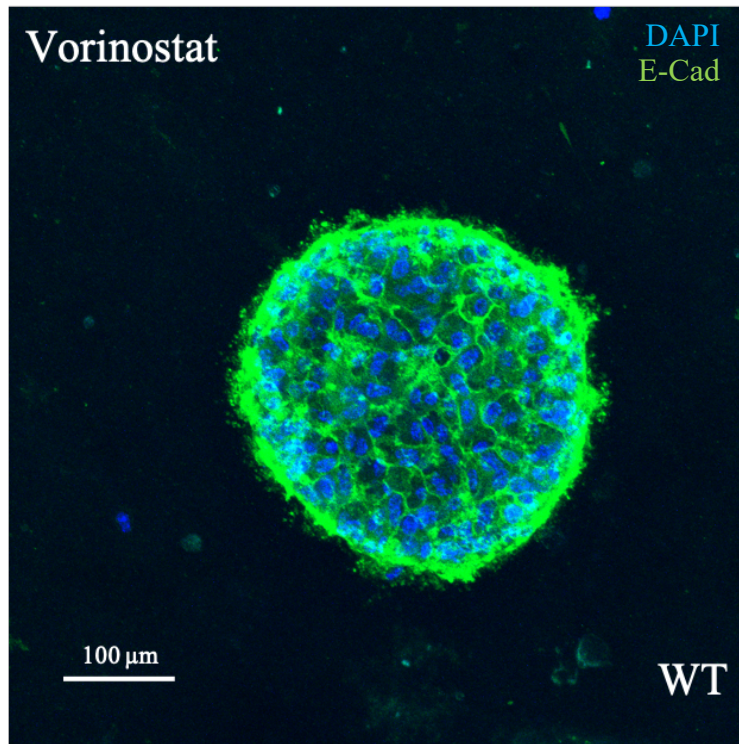


Figure 5.14 | Confocal image of an uninduced (WT) organoid exposed to Vorinostat. The organoid was stained with an E-cadherin antibody (488-green) and DAPI (blue) after 96 hours of drug exposure. The structure of the organoid has remained intact, implying that Vorinostat has not had a significant impact on morphology. The borders of the organoid look slightly undefined, however this is an issue with staining, rather than with the morphology of the organoid itself.

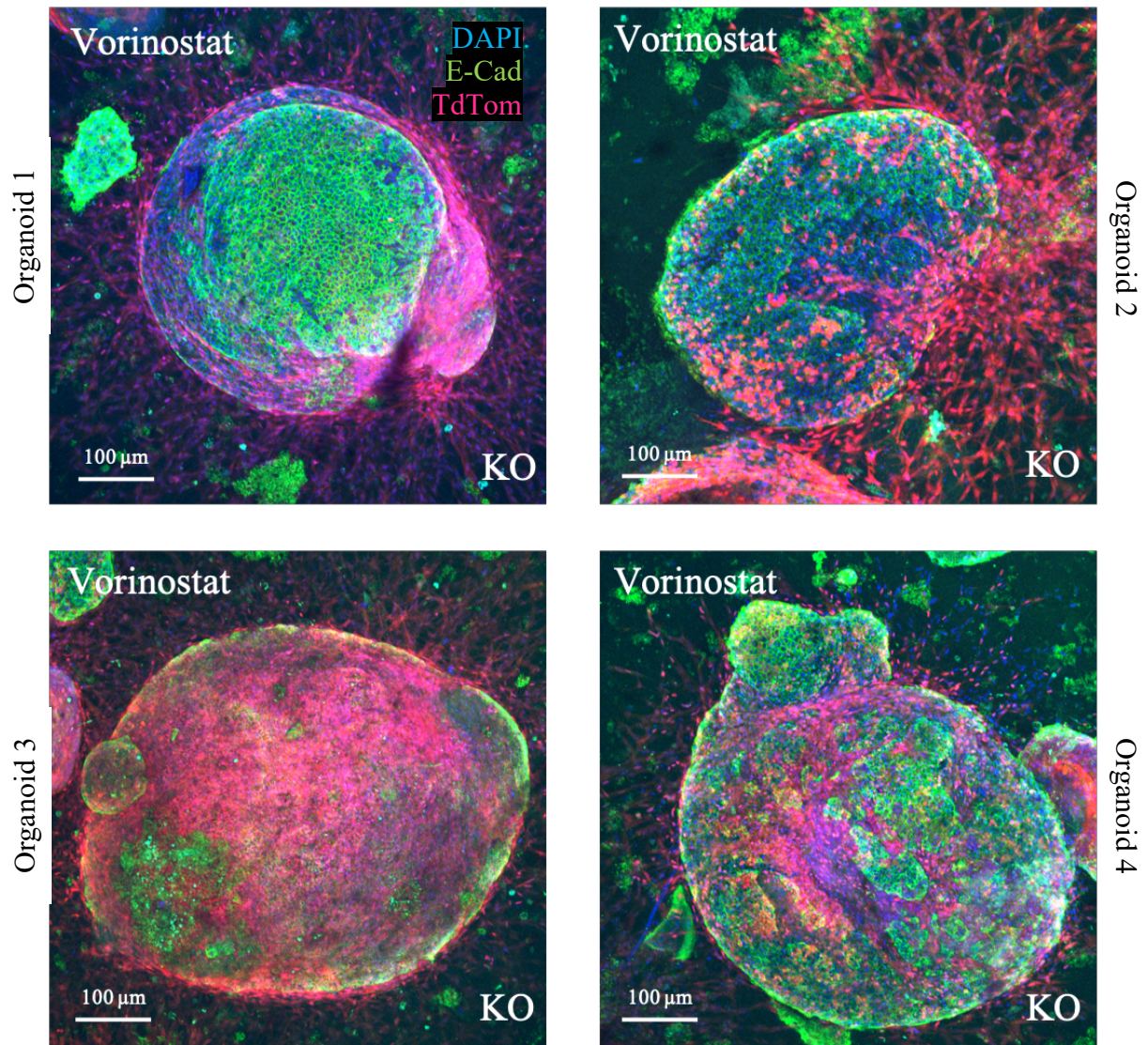


Figure 5.15 | Confocal images of induced organoids exposed to Vorinostat. All four organoids have been exposed to Vorinostat for 96 hours and stained with DAPI (blue) and an E-cadherin antibody (488-green). The general structure of the organoids is relatively intact, suggesting that Vorinostat has not induced any major morphological damage. All four organoids are displaying higher than usual numbers of myofibroblast-like cells around their exterior.

The organoids in Figure 5.15 all display high levels of elongated, mesenchymal-like TdTomato-expressing cells that are projecting out of the main organoid body. This phenomenon occurs relatively frequently, particularly, but not exclusively, in organoids exposed to drug. The biological basis of this effect is somewhat unknown, but it is suggestive of an outgrowth of mesenchymal-like cells from the organoid to aid in structural support and growth factor production (Katano et al., 2013b; Ootani et al., 2009).

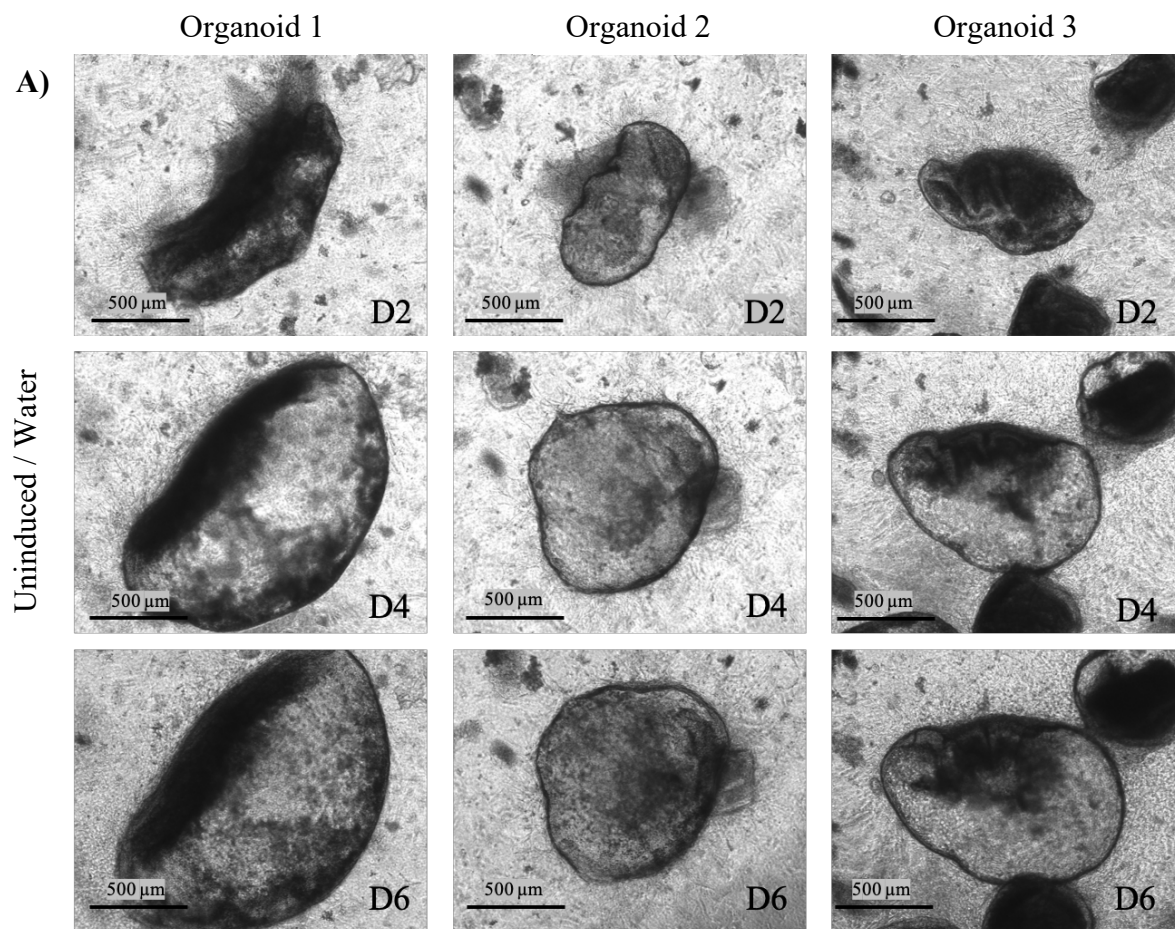
These experiments have shown that at 1.5 μ M, Vorinostat has no visible effect on both induced (KO) and uninduced (WT) organoids. Repetition of this experiment at a range of higher concentrations may provide a differential. If a clear differential can be achieved, Vorinostat will be passed on to animal models as a potential drug treatment for the chemoprevention of HDGC. Due to only one replicate being performed, which only generated a small number of organoids, quantitative analysis was not carried out on the Vorinostat-treated organoids. This will be done once three reps of Vorinostat have been completed at a higher concentration.

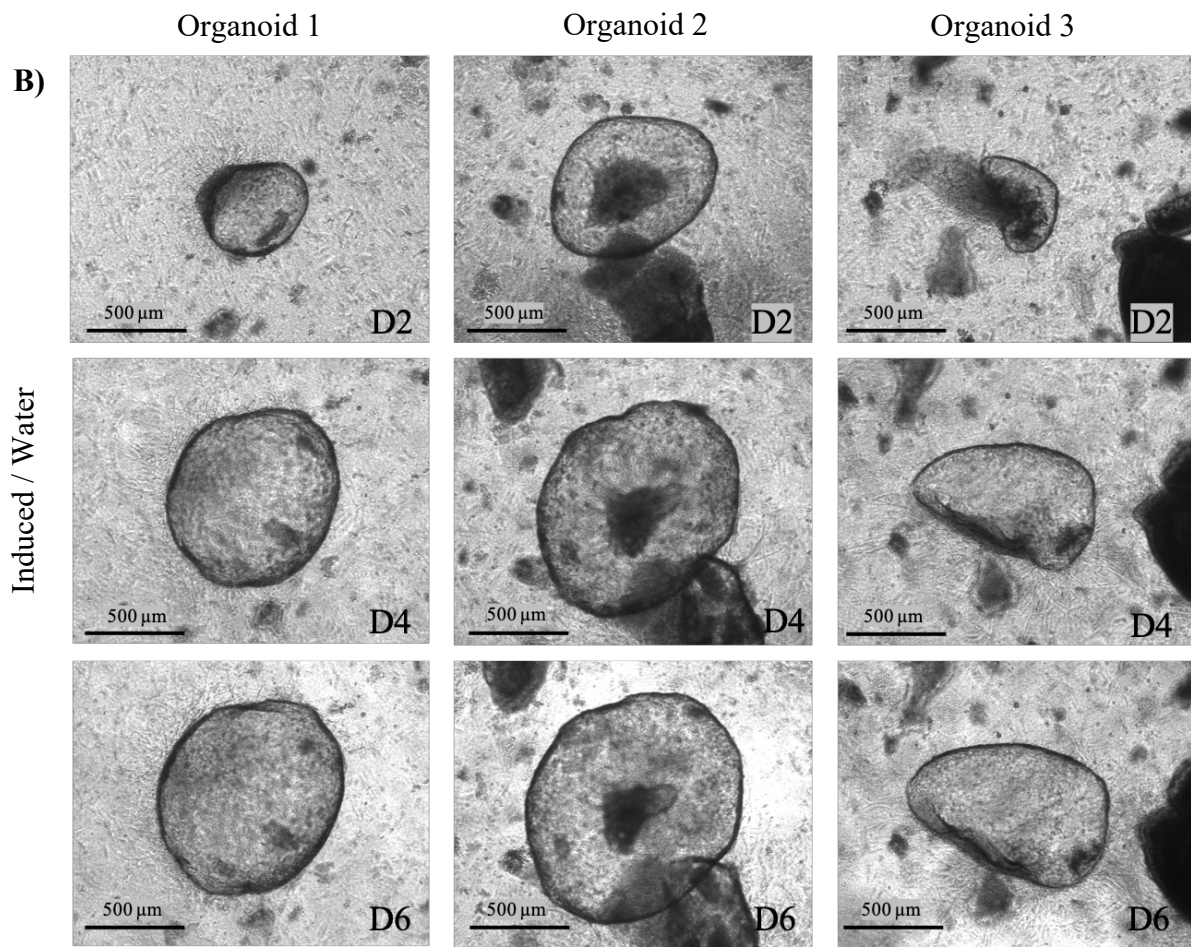
5.6 MBCD

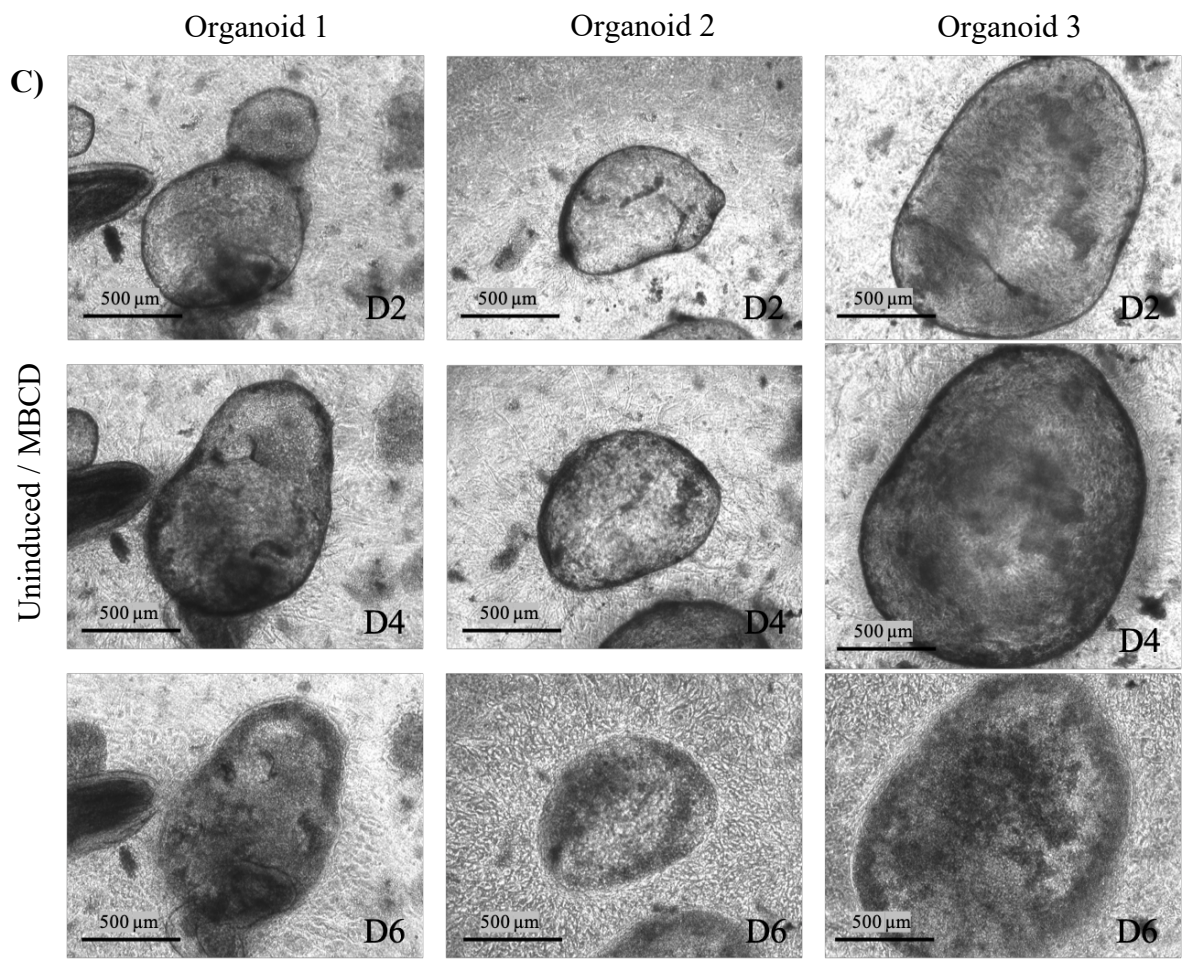
The final drug screened during this project was MBCD, a cholesterol sequestering agent used experimentally for lipid raft disruption (Larbi et al., 2004) that had shown promising results in our 2D screens. MBCD was screened using the protocol described in section 2.9 at a concentration of 5 mM. Unlike the three drugs screened previously, MBCD is reconstituted in water rather than DMSO. As with Vorinostat, only one replicate of MBCD was able to be carried out due to time restrictions. There were between 5-15 organoids generated per dish for this experiment.

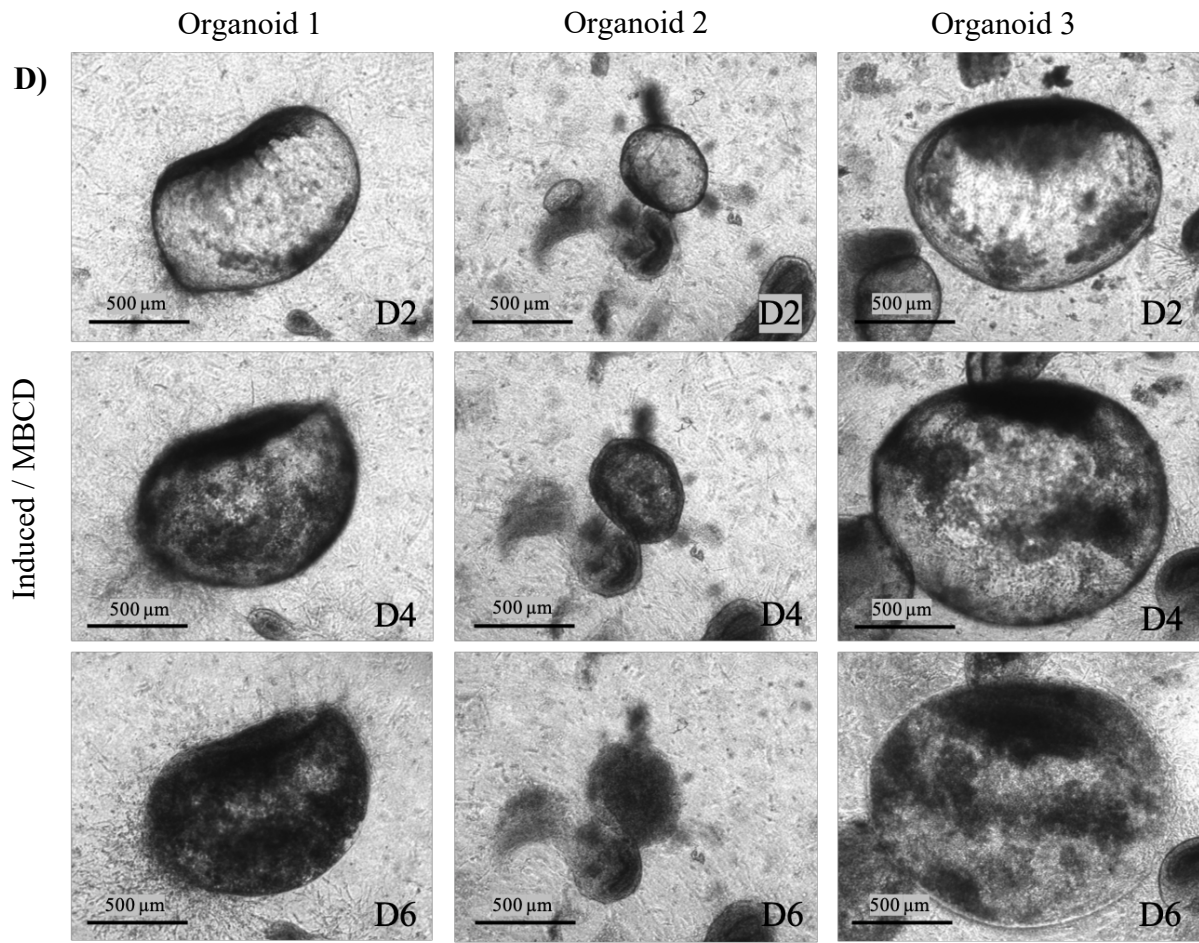
Both the induced and uninduced water controls displayed normal growth and little sign of consistent death phenotypes (Fig. 5.16A and 5.16B). By day 4 (48 hours after drug treatment), both the uninduced (WT) (Fig. 5.16C) and induced (KO) (Fig. 5.16D) organoids had begun to display death phenotypes. By day 6 in both conditions, these death phenotypes had increased in severity. The uninduced (WT) MBCD-treated organoids (Fig. 5.16C) showed a grainy, flattened appearance and have started to disintegrate. This was also observed in the induced (KO) MBCD-treated organoids (Fig. 5.16D), in addition to severe darkening, especially in organoid 1.

Figure 5.16E, which directly compares both the induced (KO) and uninduced (WT) organoids on day 4, highlights the increased intensity of the darkened and grainy texture of the induced (KO) organoids at this timepoint. Although the uninduced (WT) organoids are starting to display death phenotypes on day 4, they still look relatively healthy in terms of their colour, texture and 3D shape in comparison to the induced (KO) organoids.









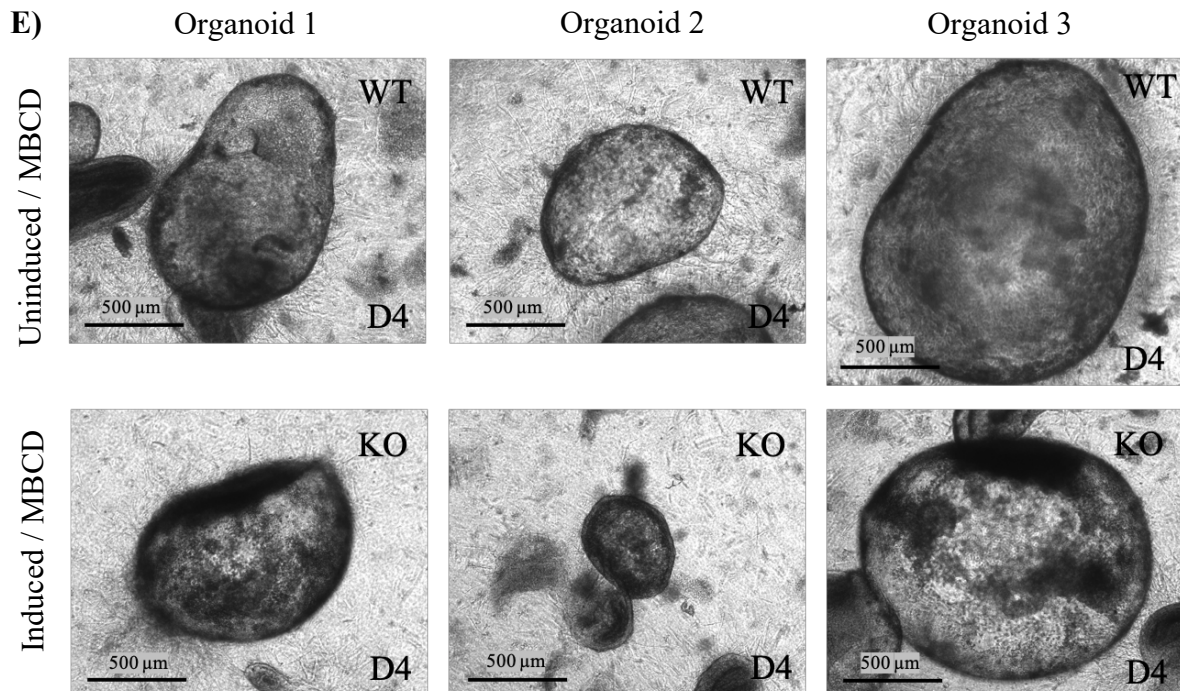


Figure 5.16 | Brightfield images of organoids exposed to MBCD and controls. A) Uninduced (WT) water control organoids display healthy levels of growth and no death phenotypes after 6 days of culture. **B)** Induced (KO) water control organoids also exhibit normal growth and no signs of death after 6 days of culture. **C)** Uninduced (WT) organoids exposed to MBCD have a flattened, grainy appearance after 6 days of culture, indicating degradation and death. **D)** Induced (KO) organoids exposed to MBCD also have a flattened, grainy and darkened appearance, signifying death. **E)** Comparison between the uninduced (WT) and induced (KO) organoids on day 4 shows that death occurs in the induced organoids slightly earlier than the uninduced organoids under the same conditions.

All four dishes used in this experiment were fixed and stained with an E-cadherin antibody (488-green) and DAPI (blue) using the immunofluorescence protocol in section 2.8. The organoids were then examined using fluorescence microscopy and four organoids from each dish chosen for confocal imaging. Due to poor quality staining/imaging, only one organoid from both the induced (KO)/water and uninduced (WT)/MBCD condition are shown below, and no uninduced (WT)/water organoids are pictured.

Figure 5.17 shows an induced (KO) organoid from the water control dish. The structure of the organoid looks intact and the overall morphology is normal. Figure 5.18 and 5.19 show an uninduced (WT) organoid (Fig. 5.18) and two induced (KO) organoids (Fig. 5.19) that have been exposed to MBCD for 96 hours. The level of damage visible from the confocal images in both these conditions surpasses that of any other drug seen so far. The structural disruption is severe, and large numbers of cells can be seen surrounding the organoids, which are possibly a combination of mesenchymal-like cell projections and epithelial cells that are beginning to break away from the main organoid body as a product of organoid disintegration.

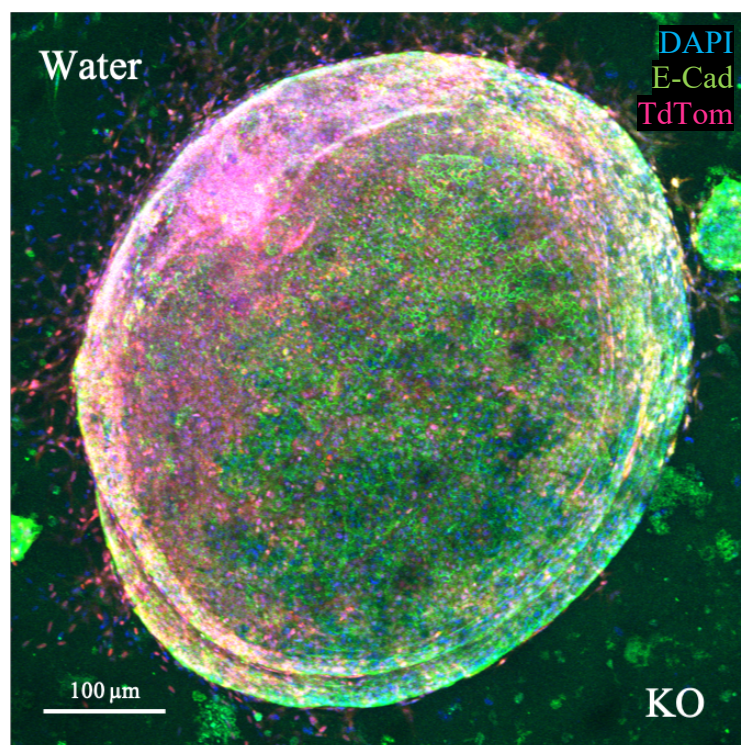


Figure 5.17 | Confocal image showing an induced (KO) water control organoid after 6 days of growth. The organoid has been stained with an E-cadherin antibody (488-green) and DAPI (blue). TdTomato fluorescence is also visible (red). Morphology looks intact and relatively healthy with defined borders. No signs of morphological disruption are present.

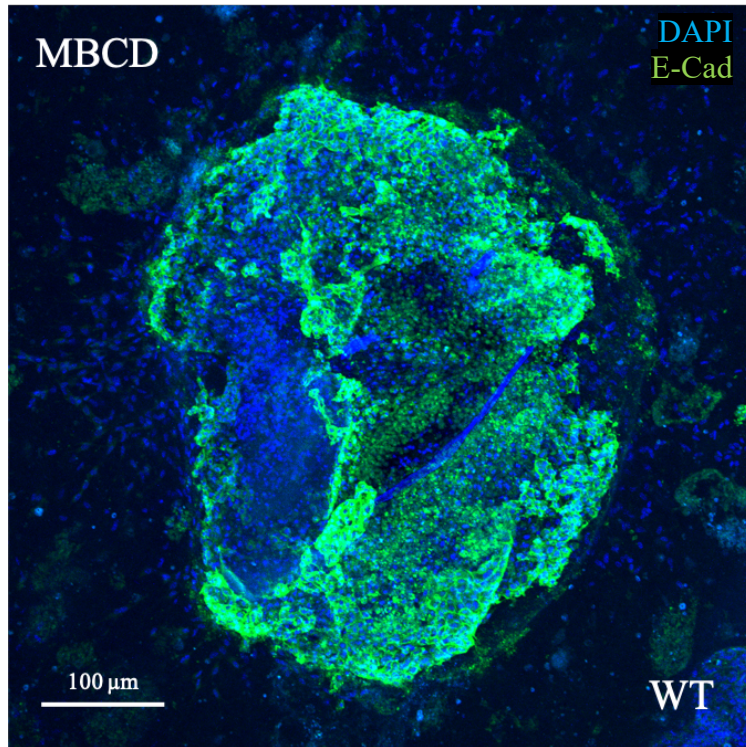


Figure 5.18 | Confocal image of an uninduced (WT) organoid exposed to MBCD. The organoid has been stained with an E-cadherin antibody (488-green) and DAPI (blue) 96 hours after treatment with MBCD. Drug-induced damage has caused the organoid to lose its intact structure and defined borders. High levels of degradation and morphological damage are visible.

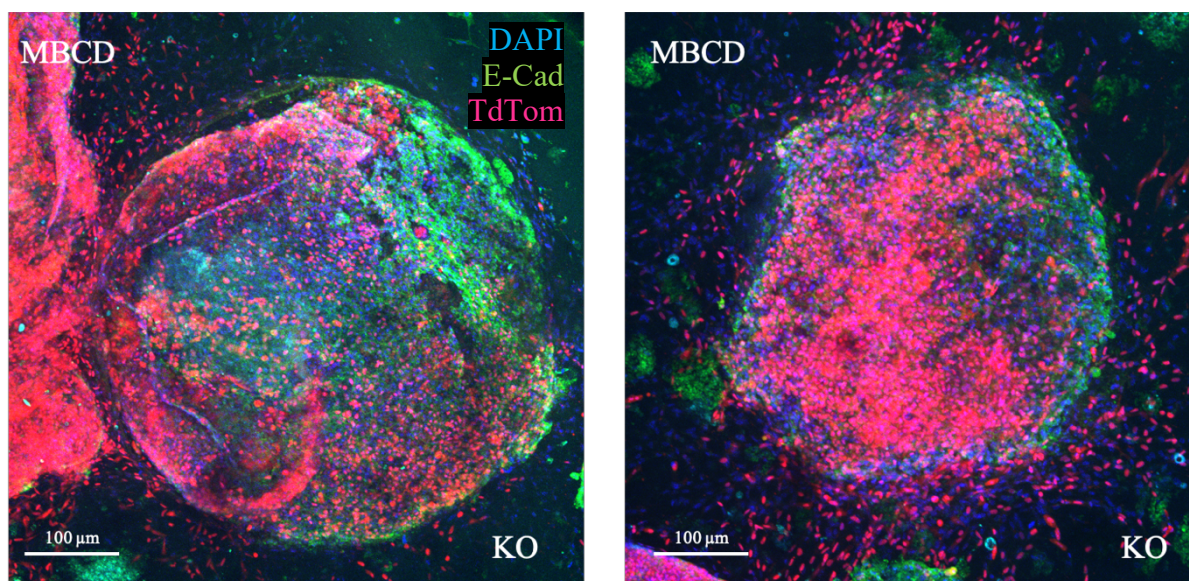


Figure 5.19 | Confocal imaging of induced (KO) organoids after being exposed to MBCD.

The organoids have been stained with an E-cadherin antibody (488-green) and DAPI (blue) after 96 hours of exposure to MBCD. TdTomato fluorescence is also visible (red). Both organoids are exhibiting clear signs of death. There is intense morphological damage occurring, with TdTomato-expressing cells surrounding the exterior of the organoid in a disorganised manner, possibly indicating the organoid has started to degrade, expelling cells and debris from its core.

These experiments have shown that at 5 mM, MBCD is highly toxic to both induced (KO) and uninduced (WT) organoids, however, there is a suggestion of a greater impact on induced (KO) organoids. Repetition of this experiment at a range of lower concentrations may provide a clearer differential. If a clear differential can be achieved, MBCD will be passed on to animal models as a potential drug treatment for the chemoprevention of HDGC. Due to only one replicate being performed, which only generated a small number of organoids, quantitative analysis was not carried out on the MBCD-treated organoids. This will be carried out once three complete reps of MBCD have been completed at a lower concentration.

5.7 Concluding remarks

Overall, the drug screening phase of this project has produced diverse and promising results. The two AKT inhibitors, ARQ-092 and MK2206, have proved to be effective at inducing morphological damage and growth inhibition that was more severe in the E-cadherin-null organoids. Both drugs, after closer examination of the optimal dose, will be passed on to animal model screening. Vorinostat and MBCD will be screened at a range of different concentrations in an attempt to demonstrate a synthetic lethal effect in this model. Ultimately, all four drugs have provided valuable insight into the organoids, highlighting their advantages, limitations and usefulness as the first early-stage model for HDGC.

Chapter 6: Drug screening Discussion

Drug screening using the organoids has provided valuable insight into both the drug candidates themselves as well as the ALI organoids and their usefulness as a model for HDGC. Four drug candidates were screened in total, all chosen because of their promising results in 2D screens carried out in two isogenic cell lines with and without E-cadherin: MCF10A, an epithelial breast cell line, and NCI-N87, a gastric cancer cell line.

The first drug, ARQ-092, is a pan-*AKT* inhibitor that inhibits all three *AKT* isoforms. It is currently involved in several clinical trials as a therapeutic drug for overgrowth disorders and cancers, including a phase 1 study for the overgrowth disorder, Proteus syndrome, and a phase 1b study in combination with hormonal treatment for advanced endometrial cancer (Brown & Banerji, 2017). ARQ-092 suppresses the *PI3K/AKT* pathway by both binding AKT to prevent it from localising at the membrane and activating, and binding active AKT to directly inhibit its function (Yu et al., 2015).

Brightfield and confocal imaging showed induced organoids that had been exposed to ARQ-092 for 96 hours exhibited distinct death phenotypes, such as darkened, grainy tissue. Notably, confocal imaging revealed populations of E-cadherin positive cells within the organoids that had remained intact, suggesting they are less susceptible to the drug. Imaging, in conjunction with quantitative analysis, revealed that ARQ-092 was also having a growth inhibiting effect on uninduced organoids. However this effect, on average, is greater in the induced organoids ($p=0.012$), consistent with our prior 2D cell line data.

Although the overall trend was for greater sensitivity of the induced organoids to the drug, there was considerable variability between organoids receiving the same treatment. Variation in drug response could be due to a multitude of contributing factors. For example, position of

the organoid in the collagen may have an impact on drug delivery and accessibility. Additionally, the exact cellular composition and relative numbers of each cell type in the organoid may have an impact on drug response. This will vary depending on the original cell population that generated the organoid. This could affect drug response as different gastric cell types could vary in their drug sensitivity. Another contributing factor to level of drug response will be the percentage of E-cadherin negative cells within the organoid. As discussed previously, the percentage of knockout cells can range anywhere between 50-90% in any given organoid. In theory, ARQ-092 should have a greater effect on E-cadherin negative cells. Therefore, the higher the percentage of E-cadherin negative cells in an organoid, the more pronounced the drug effect would be expected to be. Once more repeat studies have been carried out, we will be able to test this possibility by correlating the level of TdTomato expression with the observed drug response.

Overall, ARQ-092 has emerged as a promising drug candidate for the chemoprevention of HDGC. However, the observation that the uninduced (WT) organoids exposed to ARQ-092 had a reduced growth rate in comparison to the DMSO control demonstrates that toxicity in healthy tissue will need to be reduced or managed. As the *PI3K/AKT* pathway is involved in such integral cellular functions, such as cell growth, proliferation and survival signalling, it is not surprising that a drug inhibiting this pathway will have some toxicity and negative downstream effects, even in healthy cells with functional E-cadherin. Therefore, testing promising drugs, such as ARQ-092, at different concentrations will be an important future direction for this project. It is possible that the general toxicity of this drug might be greater in the organoids in comparison to the 2D cell lines previously tested, regardless of concentration. This variance highlights the importance of the organoids as a complementary model system for drug screening.

Although to our knowledge there has been no data yet published reporting screening results of ARQ-092 in organoids, promising results have been described in other models. Along with reports of strong antiproliferative activity in several cancer cell lines, ARQ-092 was shown to reduce tumour activity by 90% in xenograft models of endometrial cancer and show good activity in breast cancer (Yu et al., 2015). Studies such as these, along with the work described here, suggest that this drug may prove to have valuable clinical utility.

MK2206, also a pan-AKT inhibitor, was the second drug screened on the organoids. It works by inhibiting both auto-phosphorylation of AKT, as well as AKT-mediated phosphorylation of downstream signalling molecules. It is currently involved in a number of phase 1 and phase 2 clinical trials for a wide range of cancers and yielding promising results (Brown & Banerji, 2017).

Brightfield and confocal imaging of induced (KO) organoids exposed to MK2206 displayed a considerably reduced growth rate as well as morphological signs of death, including darkened and grainy tissue. This is in stark contrast to the uninduced (WT) organoids, which displayed normal growth and healthy tissue. These observations were backed up with quantitative data, which showed significantly reduced growth in the induced organoids ($p=0.0005$). This indicates that MK2206 is inducing death in a synthetic lethal manner – a finding that reflects the 2D cell line screens, further validating the organoids as a drug screening tool for HDGC.

MK2206 is one of the most highly tested AKT inhibitors on the market and is yielding promising results. In one study that included MK2206, intestinal organoid drug responses were shown to accurately reflect the results of a parallel clinical trial, further validating their usefulness as a disease model (Vlachogiannis et al., 2018). MK2206 will likely continue to show therapeutic potential for various cancers in the future.

In summary, both AKT inhibitors, ARQ-092 and MK2206, produced a synthetic lethal effect in the organoids, although ARQ-092 was slightly more toxic. In future experiments, both drugs will be screened at a range of concentrations and in different combinations to find the optimum point for maximal synthetic lethality as well as minimal toxicity. Following this, the drugs will be put forward for screening in the animal models.

The remaining two drugs that were screened, Vorinostat and MBCD, did not produce results as conclusive as the previous two. As this organoid model is relatively low throughput, drugs were only screened at one concentration initially. This concentration was chosen using the IC50 values from the 2D screen. Although the 2D screens can give a suitable concentration range, effective concentrations may not always translate between 2D and 3D screening models. This drawback was illustrated by the Vorinostat and MBCD studies which appeared to have been used at too low and too high concentrations respectively.

Both these drugs will be screened at a range of concentrations to elucidate whether or not they have the ability to induce synthetic lethal death in the organoids. If successful, they will be passed on to animal models. Despite failing to validate the synthetic lethality of these drugs, they provided valuable insight into other aspects of the model, such as organoid-derived myofibroblast growth (discussed below) and the morphological changes that occur during organoid death – seen in the highly toxic effects of MBCD.

Drug screening in organoids, both for drug discovery and as a pre-clinical tool for drug selection using patient derived organoids is increasing in popularity globally. Studies have shown that in drug discovery, organoids are closely reflecting the results of animal model screens and human trials (Jabs et al., 2017). Further, in drug selection, patient derived

organoids closely mirror patient response – as seen with metastatic gastrointestinal cancers (Vlachogiannis et al., 2018). The drugs screened as part of this project add to the ever-expanding list of potential therapies for which organoids have contributed to the discovery and clinical application of, further emphasising their value in the field.

Imaging throughout the various drugging experiments revealed that many of the organoids contained large amounts of elongated, TdTomato-expressing cell projections. This occurs to the largest extent in induced organoids under drugged conditions, as well as in induced DMSO controls and occasionally in uninduced organoids under drugged conditions. As these cells are expressing TdTomato in the induced organoids, they must be generated from the organoids themselves, rather than from the myofibroblast cells present in the collagen. This could be a sign of dysregulated asymmetric division of stem cells within the organoid, or cells gaining migratory potential, however neither option explains why the cells have a highly elongated phenotype or exist in uninduced organoids. The most likely explanation is that the organoids are projecting out mesenchymal-like cells, a process that occurs naturally in small numbers (Katano et al., 2013b; Ootani et al., 2009) but is enhanced under stress-inducing conditions such as drug or DMSO exposure (Lahar et al., 2011). The production of additional mesenchymal-like cells may reduce the impact of the environment by promoting regrowth of the epithelium and enhancing barrier function (McKaig, Makh, Hawkey, Podolsky, & Mahida, 1999).

The challenges faced during this phase of the project were numerous, and not all were overcome. The high levels of variation in organoid size and numbers made quantitative assessment difficult, however once the various ways of displaying the data had been established, this was for the most part overcome. A major challenge of this model, highlighted by the screening of Vorinostat and MBCD, is only being able to test one concentration at a

time. Due to the size of the dishes and the time restraints in mouse culling/tissue seeding, the amount of conditions per experiment is limited. This is somewhat problematic, however the initial concentration used will often be able to provide a good indication of what concentrations to test in the future. The submerged organoid model (Barker et al., 2010), currently under development in our laboratory, is higher throughput due to the dish size used, and therefore will be able to aid in solving this problem. However, the ALI model will still be needed in drug screening due to its higher accuracy in recapitulating the *in vivo* HDGC environment. A possible workflow will be to do initial screening using the submerged model of a range of concentrations for each drug before subsequently screening the most effective concentration on the ALI organoids as a final step before animal model screening.

Another useful future experiment will be to do immunofluorescence using the proliferation marker Ki67 on organoids that have been exposed to growth-inhibiting drugs. Ki67 staining will allow for the visualisation of the differences in rates of cell proliferation between organoids that are displaying reduced growth rates and organoids that are growing normally, further validating the effects of the drugs. In addition to this, experiments using a live dead stain could be done as an additional quantitative measure of drug effectiveness alongside change in area. These future experiments will provide a more definitive answer on whether the drugs are inflicting primarily a cytostatic or cytotoxic effect. In addition to this, comparison of the E-cadherin-positive and E-cadherin-negative areas within a single organoid, and how they respond to any given drug, is a potentially valuable area of future investigation. This comparison would control for potentially confounding variables between organoids, such as exposure to different drug concentrations due to their position in the collagen, which contains a diffusional gradient.

Chapter 7: Concluding remarks and Project Significance

At the outset of this project, two main objectives were identified: firstly, to optimise culture techniques and characterise the conditional *Cdh1* knockout organoids. Secondly, to use this model as a medium-throughput drug screening tool for the chemoprevention of HDGC. Over the duration of this project, many challenges arose, and not all were overcome. However, the insight gained from the various experiments has been of great value and clear pathways have emerged for future investigation.

The characterisation and optimisation of the organoids taught us a lot about their growth, behaviour and morphology. The successful induction of the *Cdh1* knockout validated the organoids as a model for HDGC and provided insight into how the organoids might demonstrate disease progression, such as with the pooling of E-cadherin negative cells in the lumen.

As detailed in chapter 4, additional experiments will need to be carried out in the future in order to complete the characterisation of these organoids. Arguably, the most important of which is a thorough investigation into the gastric cell types present in the organoids and their organisation. This will aid in determining how accurate of a gastric model the organoids are. These experiments can be done using further fluorescent microscopy with various gastric cell type markers, as well as through histological techniques such as haematoxylin and eosin (H&E) staining. Other aspects of the model, such as its longevity and passage potential should also be explored.

The drug screening phase of this project yielded promising results, identifying two drug candidates (ARQ-092 and MK2206) with the ability to consistently display strong synthetic lethal effects in the conditional *Cdh1* knockout organoids. Two more candidates (Vorinostat and MBCD) were also screened, but these drugs will require dose titrations before any conclusions on their potential utility can be made. In addition to this, the drug screening provided valuable insights into organoid death processes, DMSO tolerance and the various ways organoids react to stress, such as the proliferation of mesenchymal-like cells.

As well as performing dose titrations, further work will be done to provide a more detailed assessment on the effects of the drugs screened throughout this project. These experiments will include both Ki67 staining and live/dead assays in order to elucidate whether the effects of the drugs are primarily cytostatic/growth inhibiting or cytotoxic/death inducing. Once this additional analysis has been done, drugs with a significant synthetic lethal effect will be forwarded on to animal models.

This project has the potential to directly impact the care of over 500 HDGC families and thousands of *CDHI* mutation carriers worldwide. Moreover, the knowledge gained will also be of potential use for research into treatments for sporadic DGC. As it stands, gastric cancer is consistently the second highest cause of cancer-related death worldwide (Nadauld & Ford, 2013) and standard chemotherapies provide little benefit for DGC patients (Smalley et al., 2012). The detrimental effects of gastric cancer are especially prominent in New Zealand, where our Māori and Pasifika populations harbour a 3-fold higher incidence compared to the global average (Ministry of Health, 2015). Therefore, there is an urgent domestic and international need for new drugs for the chemoprevention and treatment of the familial and sporadic forms of this disease. The work described in this thesis provides an exciting direction for drug development that we are confident will reduce the impact of this devastating cancer.

References

- Barber, M., Murrell, A., Ito, Y., Maia, A. T., Hyland, S., Oliveira, C., ... Fitzgerald, R. C. (2008). Mechanisms and sequelae of E-cadherin silencing in hereditary diffuse gastric cancer. *Journal of Pathology*, *216*(3), 295–306. <https://doi.org/10.1002/path.2426>
- Barker, N., Huch, M., Kujala, P., van de Wetering, M., Snippert, H. J., van Es, J. H., ... Clevers, H. (2010). Lgr5+ve Stem Cells Drive Self-Renewal in the Stomach and Build Long-Lived Gastric Units In Vitro. *Cell Stem Cell*, *6*(1), 25–36. <https://doi.org/10.1016/j.stem.2009.11.013>
- Berx, G., Staes, K., Van Hengel, J., Molemans, F., G Bussemakers, M. J., Van Bokhoven, A., & Frans Van Roy, I. (1995). Cloning and Characterization of the Human Invasion Suppressor Gene E-Cadherin (CDH1). *Genomics*, *26*(2), 281-289. [https://doi.org/10.1016/0888-7543\(95\)80212-5](https://doi.org/10.1016/0888-7543(95)80212-5)
- Brieher, W. M., & Yap, A. S. (2013). Cadherin junctions and their cytoskeleton(s). *Current Opinion in Cell Biology*, *25*(1), 39–46. <https://doi.org/10.1016/J.CEB.2012.10.010>
- Brown, J. S., & Banerji, U. (2017). Maximising the potential of AKT inhibitors as anti-cancer treatments. *Pharmacology and Therapeutics*, *172*, 101-115. <https://doi.org/10.1016/j.pharmthera.2016.12.001>
- Bryant, H. E., Schultz, N., Thomas, H. D., Parker, K. M., Flower, D., Lopez, E., ... Helleday, T. (2005). Specific killing of BRCA2-deficient tumours with inhibitors of poly(ADP-ribose) polymerase. *Nature*, *434*(7035), 913–917. <https://doi.org/10.1038/nature03443>
- Bubna, A. (2015). Vorinostat-An overview. *Indian Journal of Dermatology*, *60*(4), 419. <https://doi.org/10.4103/0019-5154.160511>
- Caponigro, G., & Sellers, W. R. (2011). Advances in the preclinical testing of cancer therapeutic hypotheses. *Nature Reviews Drug Discovery*, *10*, 179-187. <https://doi.org/10.1038/nrd3385>

- Carneiro, F., Huntsman, D. G., Smyrk, T. C., Owen, D. A., Seruca, R., Pharoah, P., ...
Sobrinho-Simões, M. (2004). Model of the early development of diffuse gastric cancer in E-cadherin mutation carriers and its implications for patient screening. *Journal of Pathology*, 203(2), 681–687. <https://doi.org/10.1002/path.1564>
- Carneiro, P., Fernandes, M. S., Figueiredo, J., Caldeira, J., Carvalho, J., Pinheiro, H., ...
Seruca, R. (2012). E-cadherin dysfunction in gastric cancer - Cellular consequences, clinical applications and open questions. *FEBS Letters*, 586(18), 2981–2989.
<https://doi.org/10.1016/j.febslet.2012.07.045>
- Chan, D. A., Sutphin, P. D., Nguyen, P., Turcotte, S., Lai, E. W., Banh, A., ... Giaccia, A. J.
(2011). Targeting GLUT1 and the Warburg effect in renal cell carcinoma by chemical synthetic lethality. *Science Translational Medicine*, 3(94).
<https://doi.org/10.1126/scitranslmed.3002394>
- Charlton, A., Blair, V., Shaw, D., Parry, S., Guilford, P., & Martin, I. G. (2004). Transitional Zone. *Gut*, 53, 814–820. <https://doi.org/10.1136/gut.2003.010447>
- Chen, A., Beetham, H., Black, M. A., Priya, R., Telford, B. J., Guest, J., ... Guilford, P. J.
(2014). E-cadherin loss alters cytoskeletal organization and adhesion in non-malignant breast cells but is insufficient to induce an epithelial-mesenchymal transition. *BMC Cancer*, 14(1), 552. <https://doi.org/10.1186/1471-2407-14-552>
- Deng, C. X. (2012). The use of Cre-loxP technology and inducible systems to generate mouse models of cancer. *Genetically Engineered Mice for Cancer Research: Design, Analysis, Pathways, Validation and Pre-Clinical Testing* (pp. 17–36). New York, NY: Springer New York. https://doi.org/10.1007/978-0-387-69805-2_2
- Dobzhansky, T. (1946). Genetics of natural populations; recombination and variability in populations of *Drosophila pseudoobscura*. *Genetics*, 31(3), 269–290. Retrieved from <http://www.ncbi.nlm.nih.gov/pubmed/20985721>
- Dunbier, A., & Guilford, P. (2001). Hereditary diffuse gastric cancer. *Advances in Cancer*

Research, 83, 55–65. Retrieved from

https://www.sciencedirect.com/science/article/pii/S0065230X01830025/pdf?md5=340d532c9181b77540ae0b32fc24c66d&pid=1-s2.0-S0065230X01830025-main.pdf&_valck=1

Egeblad, M., Nakasone, E. S., & Werb, Z. (2010). Tumors as organs: Complex tissues that interface with the entire organism. *Developmental Cell*, 18(6), 884-901.

<https://doi.org/10.1016/j.devcel.2010.05.012>

Eiraku, M., Watanabe, K., Matsuo-Takasaki, M., Kawada, M., Yonemura, S., Matsumura, M., ... Sasai, Y. (2008). Self-Organized Formation of Polarized Cortical Tissues from ESCs and Its Active Manipulation by Extrinsic Signals. *Cell Stem Cell*, 3(5), 519–532.

<https://doi.org/10.1016/j.stem.2008.09.002>

Farmer, H., McCabe, H., Lord, C. J., Tutt, A. H. J., Johnson, D. A., Richardson, T. B., ...

Ashworth, A. (2005). Targeting the DNA repair defect in BRCA mutant cells as a therapeutic strategy. *Nature*, 434(7035), 917–921. <https://doi.org/10.1038/nature03445>

Fatehullah, A., Tan, S. H., & Barker, N. (2016). Organoids as an in vitro model of human development and disease. *Nature Cell Biology*, 18(3), 246-254.

<https://doi.org/10.1038/ncb3312>

Ferlay, J., Shin, H. R., Bray, F., Forman, D., Mathers, C., & Parkin, D. M. (2010). Estimates

of worldwide burden of cancer in 2008: GLOBOCAN 2008. *International Journal of Cancer*, 127(12), 2893-2917. <https://doi.org/10.1002/ijc.25516>

Ferrari, E., Lucca, C., & Foiani, M. (2010). A lethal combination for cancer cells: Synthetic

lethality screenings for drug discovery. *European Journal of Cancer*, 46(16), 2889-2895. <https://doi.org/10.1016/j.ejca.2010.07.031>

Fitzgerald, R. C., Hardwick, R., Huntsman, D., Carneiro, F., Guilford, P., Blair, V., ...

Caldas, C. (2010). Hereditary diffuse gastric cancer: Updated consensus guidelines for clinical management and directions for future research. *Journal of Medical Genetics*,

47(7), 436–444. <https://doi.org/10.1136/jmg.2009.074237>

- Grunwald, G. B. (1993). The structural and functional analysis of cadherin calcium-dependent cell adhesion molecules. *Current Opinion in Cell Biology*, 5(5), 797–805. [https://doi.org/10.1016/0955-0674\(93\)90028-O](https://doi.org/10.1016/0955-0674(93)90028-O)
- Guilford, P. (1999). E-cadherin downregulation in cancer: Fuel on the fire? *Molecular Medicine Today*, 5(4), 172-177. [https://doi.org/10.1016/S1357-4310\(99\)01461-6](https://doi.org/10.1016/S1357-4310(99)01461-6)
- Guilford, P., Hopkins, J., Harraway, J., McLeod, M., McLeod, N., Harawira, P., ... Reeve, A. E. (1998). E-cadherin germline mutations in familial gastric cancer. *Nature*, 392(6674), 402–405. <https://doi.org/10.1038/32918>
- Guilford, P., Humar, B., & Blair, V. (2010). Hereditary diffuse gastric cancer: Translation of CDH1 germline mutations into clinical practice. *Gastric Cancer*, 13(1), 1-10. <https://doi.org/10.1007/s10120-009-0531-x>
- Guilford, P. J., Hopkins, J. B. W., Grady, W. M., Markowitz, S. D., Willis, J., Lynch, H., ... Reeve, A. E. (1999). E-cadherin germline mutations define an inherited cancer syndrome dominated by diffuse gastric cancer. *Human Mutation*, 14(3), 249–255. [https://doi.org/10.1002/\(SICI\)1098-1004\(1999\)14:3<249::AID-HUMU8>3.0.CO;2-9](https://doi.org/10.1002/(SICI)1098-1004(1999)14:3<249::AID-HUMU8>3.0.CO;2-9)
- Guo, C., Yang, W., & Lobe, C. G. (2002). A Cre recombinase transgene with mosaic, widespread tamoxifen-inducible action. *Genesis*, 32(1), 8–18. <https://doi.org/10.1002/gene.10021>
- Hakkaart, C., Ellison-Loschmann, L., Day, R., Sporle, A., Koea, J., Harawira, P., ... Guilford, P. (2018). Germline CDH1 mutations are a significant contributor to the high frequency of early-onset diffuse gastric cancer cases in New Zealand Māori. *Familial Cancer*, 18(1), 83-90. <https://doi.org/10.1007/s10689-018-0080-8>
- Hansford, S., Kaurah, P., Li-Chang, H., Woo, M., Senz, J., Pinheiro, H., ... Huntsman, D. G. (2015). Hereditary Diffuse Gastric Cancer Syndrome. *JAMA Oncology*, 1(1), 23. <https://doi.org/10.1001/jamaoncol.2014.168>

- Hinz, B., Phan, S. H., Thannickal, V. J., Galli, A., Bochaton-Piallat, M. L., & Gabbiani, G. (2007). The myofibroblast: One function, multiple origins. *American Journal of Pathology*, *170*(6), 1807-1816. <https://doi.org/10.2353/ajpath.2007.070112>
- Huntsman, D. G., Carneiro, F., Lewis, F. R., MacLeod, P. M., Hayashi, A., Monaghan, K. G., ... Caldas, C. (2001). Early Gastric Cancer in Young, Asymptomatic Carriers of Germ-Line E-Cadherin Mutations. *New England Journal of Medicine*, *344*(25), 1904–1909. <https://doi.org/10.1056/NEJM200106213442504>
- Iglehart, J. D., & Silver, D. P. (2009). Synthetic Lethality — A New Direction in Cancer-Drug Development. *New England Journal of Medicine*, *361*(2), 189–191. <https://doi.org/10.1056/NEJMe0903044>
- Jabs, J., Zickgraf, F. M., Park, J., Wagner, S., Jiang, X., Jechow, K., ... Conrad, C. (2017). Screening drug effects in patient-derived cancer cells links organoid responses to genome alterations. *Molecular Systems Biology*, *13*(11), 955. <https://doi.org/10.15252/msb.20177697>
- Kaelin, W. G. (2005). The concept of synthetic lethality in the context of anticancer therapy. *Nature Reviews Cancer*, *5*(9), 689-698. <https://doi.org/10.1038/nrc1691>
- Kaelin, W. G. (2009). Synthetic lethality: A framework for the development of wiser cancer therapeutics. *Genome Medicine*, *1*(10), 99. <https://doi.org/10.1186/gm99>
- Kamb, A. (2005). What's wrong with our cancer models? *Nature Reviews Drug Discovery*, *4*(2), 161–165. <https://doi.org/10.1038/nrd1635>
- Katano, T., Ootani, A., Mizoshita, T., Tanida, S., Tsukamoto, H., Ozeki, K., ... Joh, T. (2013a). Establishment of a long-term three-dimensional primary culture of mouse glandular stomach epithelial cells within the stem cell niche. *Biochemical and Biophysical Research Communications*, *432*(4), 558–563. <https://doi.org/10.1016/j.bbrc.2013.02.051>
- Katano, T., Ootani, A., Mizoshita, T., Tanida, S., Tsukamoto, H., Ozeki, K., ... Joh, T.

- (2015). Gastric mesenchymal myofibroblasts maintain stem cell activity and proliferation of murine gastric epithelium in vitro. *American Journal of Pathology*, *185*(3), 798-807. <https://doi.org/10.1016/j.ajpath.2014.11.007>
- Kemler, R. (1993). From cadherins to catenins: cytoplasmic protein interactions and regulation of cell adhesion. *Trends in Genetics*, *9*(9), 317-321. [https://doi.org/10.1016/0168-9525\(93\)90250-L](https://doi.org/10.1016/0168-9525(93)90250-L)
- Kim, N.-G., Koh, E., Chen, X., & Gumbiner, B. M. (2011). E-cadherin mediates contact inhibition of proliferation through Hippo signaling-pathway components. *Proceedings of the National Academy of Sciences*, *108*(29), 11930–11935. <https://doi.org/10.1073/pnas.1103345108>
- Lahar, N., Lei, N. Y., Wang, J., Jabaji, Z., Tung, S. C., Joshi, V., ... Dunn, J. C. Y. (2011). Intestinal subepithelial myofibroblasts support in vitro and in vivo growth of human small intestinal epithelium. *PLoS ONE*, *6*(11), e26898. <https://doi.org/10.1371/journal.pone.0026898>
- Lancaster, M. A., Renner, M., Martin, C. A., Wenzel, D., Bicknell, L. S., Hurles, M. E., ... Knoblich, J. A. (2013). Cerebral organoids model human brain development and microcephaly. *Nature*, *501*(7467), 373–379. <https://doi.org/10.1038/nature12517>
- Larbi, A., Douziech, N., Khalil, A., Dupuis, G., Gheraïri, S., Guérard, K. P., & Fülöp, T. (2004). Effects of methyl- β -cyclodextrin on T lymphocytes lipid rafts with aging. In *Experimental Gerontology*, *39*, 551–558. <https://doi.org/10.1016/j.exger.2003.10.031>
- Lauren, P. (1965). The two histological main types of gastric carcinoma: diffuse and so-called intestinal-type carcinoma. An attempt at a histo-clinical classification. *Acta Pathologica et Microbiologica Scandinavica*, *64*(1), 31–49. <https://doi.org/10.1111/apm.1965.64.1.31>
- Lecuit, T., & Yap, A. S. (2015). E-cadherin junctions as active mechanical integrators in tissue dynamics. *Nature Cell Biology*, *17*(5), 533-539. <https://doi.org/10.1038/ncb3136>

- Leonhard, W. N., Roelfsema, J. H., Lantinga-Van Leeuwen, I. S., Breuning, M. H., & Peters, D. J. M. (2008). Quantification of Cre-mediated recombination by a novel strategy reveals a stable extra-chromosomal deletion-circle in mice. *BMC Biotechnology*, *8*, 18. <https://doi.org/10.1186/1472-6750-8-18>
- Li, X., Nadauld, L., Ootani, A., Corney, D. C., Pai, R. K., Gevaert, O., ... Kuo, C. J. (2014). Oncogenic transformation of diverse gastrointestinal tissues in primary organoid culture. *Nature Medicine*, *20*(7), 769-777. <https://doi.org/10.1038/nm.3585>
- Lord, C. J., Tutt, A. N. J., & Ashworth, A. (2015). Synthetic Lethality and Cancer Therapy: Lessons Learned from the Development of PARP Inhibitors. *Annual Review of Medicine*, *66*(1), 455–470. <https://doi.org/10.1146/annurev-med-050913-022545>
- Luo, J., Manning, B. D., & Cantley, L. C. (2003, October 1). Targeting the PI3K-Akt pathway in human cancer: Rationale and promise. *Cancer Cell*, *4*(4), 257-262. [https://doi.org/10.1016/S1535-6108\(03\)00248-4](https://doi.org/10.1016/S1535-6108(03)00248-4)
- Mahe, M. M., Aihara, E., Schumacher, M. A., Zavros, Y., Montrose, M. H., Helmrich, M. A., ... Shroyer, N. F. (2013). Establishment of Gastrointestinal Epithelial Organoids. In *Current Protocols in Mouse Biology*, *3*, 217–240. Hoboken, NJ, USA: John Wiley & Sons, Inc. <https://doi.org/10.1002/9780470942390.mo130179>
- McCracken, K. W., Catá, E. M., Crawford, C. M., Sinagoga, K. L., Schumacher, M., Rockich, B. E., ... Wells, J. M. (2014). Modelling human development and disease in pluripotent stem-cell-derived gastric organoids. *Nature*, *516*, 400–404. <https://doi.org/10.1038/nature13863>
- McKaig, B. C., Makh, S. S., Hawkey, C. J., Podolsky, D. K., & Mahida, Y. R. (1999). Normal human colonic subepithelial myofibroblasts enhance epithelial migration (restitution) via TGF-beta3. *Am. J. Physiol. Gastrointest. Liver Physiol.*, *276*(5 Pt 1), G1087–G1093. [https://doi.org/10.1016/S0016-5085\(98\)84217-0](https://doi.org/10.1016/S0016-5085(98)84217-0)
- Menke, A., & Giehl, K. (2012). Regulation of adherens junctions by Rho GTPases and p120-

- catenin. *Archives of Biochemistry and Biophysics*, 524(1), 48–55.
<https://doi.org/10.1016/j.abb.2012.04.019>
- Ministry of Health. (2015). *Cancer: New registrations and deaths 2012*. Wellington.
- Mirantes, C., Eritja, N., Dosil, M. A., Santacana, M., Pallares, J., Gatus, S., ... Dolcet, X. (2013). An inducible knockout mouse to model the cell-autonomous role of PTEN in initiating endometrial, prostate and thyroid neoplasias. *Disease Models & Mechanisms*, 6(3), 710–720. <https://doi.org/10.1242/dmm.011445>
- Nadauld, L. D., & Ford, J. M. (2013). Molecular profiling of gastric cancer: Toward personalized cancer medicine. *Journal of Clinical Oncology*, 31(7), 838-839.
<https://doi.org/10.1200/JCO.2012.47.1714>
- Nadauld, L. D., Garcia, S., Natsoulis, G., Bell, J. M., Miotke, L., Hopmans, E. S., ... Ji, H. P. (2014). Metastatic tumor evolution and organoid modeling implicate TGFBR2 as a cancer driver in diffuse gastric cancer. *Genome Biology*, 15(8), 428.
<https://doi.org/10.1186/s13059-014-0428-9>
- Neal, J. T., & Kuo, C. J. (2016). Organoids as Models for Neoplastic Transformation. *Annual Review of Pathology: Mechanisms of Disease*, 11(1), 199–220.
<https://doi.org/10.1146/annurev-pathol-012615-044249>
- Norton, J. A., Ham, C. M., Dam, J. Van, Jeffrey, R. B., Longacre, T. A., Huntsman, D. G., ... Ford, J. M. (2007). CDH1 truncating mutations in the E-cadherin gene: An indication for total gastrectomy to treat hereditary diffuse gastric cancer. *Annals of Surgery*, 245(6), 873–879. <https://doi.org/10.1097/01.sla.0000254370.29893.e4>
- Oliveira, C., Sousa, S., Pinheiro, H., Karam, R., Bordeira-Carriço, R., Senz, J., ... Seruca, R. (2009). Quantification of Epigenetic and Genetic 2nd Hits in CDH1 During Hereditary Diffuse Gastric Cancer Syndrome Progression. *Gastroenterology*, 136(7), 2137-2148.
<https://doi.org/10.1053/j.gastro.2009.02.065>
- Ootani, A., Li, X., Sangiorgi, E., Ho, Q. T., Ueno, H., Toda, S., ... Kuo, C. J. (2009).

- Sustained in vitro intestinal epithelial culture within a Wnt-dependent stem cell niche. *Nature Medicine*, 15(6), 701–706. <https://doi.org/10.1038/nm.1951>
- Pal, R., Mamidi, M. K., Das, A. K., & Bhone, R. (2012). Diverse effects of dimethyl sulfoxide (DMSO) on the differentiation potential of human embryonic stem cells. *Archives of Toxicology*, 86(4), 651–661. <https://doi.org/10.1007/s00204-011-0782-2>
- Parkin, D. M. (2006). The global health burden of infection-associated cancers in the year 2002. *International Journal of Cancer*, 118(12), 3030–3044. <https://doi.org/10.1002/ijc.21731>
- Pastuła, A., Middelhoff, M., Brandtner, A., Tobiasch, M., Höhl, B., Nuber, A. H., ... Quante, M. (2016). Three-Dimensional Gastrointestinal Organoid Culture in Combination with Nerves or Fibroblasts: A Method to Characterize the Gastrointestinal Stem Cell Niche. *Stem Cells International*, 2016, 1–16. <https://doi.org/10.1155/2016/3710836>
- Pece, S., Chiariello, M., Murga, C., & Gutkind, J. S. (1999). Activation of the protein kinase Akt/PKB by the formation of E-cadherin-mediated cell-cell junctions. Evidence for the association of phosphatidylinositol 3-kinase with the E-cadherin adhesion complex. *Journal of Biological Chemistry*, 274(27), 19347–19351. <https://doi.org/10.1074/jbc.274.27.19347>
- Pompaiah, M., & Bartfeld, S. (2017). Gastric organoids: An emerging model system to study *Helicobacter pylori* pathogenesis. In *Current Topics in Microbiology and Immunology* 400, 149–168. https://doi.org/10.1007/978-3-319-50520-6_7
- Poultides, G., & Norton, J. A. (2015). Hereditary Diffuse Gastric Cancer. In V. E. Strong (Ed.), *Gastric Cancer: Principles and Practice* (pp. 251–254). Cham: Springer International Publishing. https://doi.org/10.1007/978-3-319-15826-6_18
- Reaper, P. M., Griffiths, M. R., Long, J. M., Charrier, J. D., MacCormick, S., Charlton, P. A., ... Pollard, J. R. (2011). Selective killing of ATM- or p53-deficient cancer cells through inhibition of ATR. *Nature Chemical Biology*, 7(7), 428–430.

<https://doi.org/10.1038/nchembio.573>

Rock, J. R., Onaitis, M. W., Rawlins, E. L., Lu, Y., Clark, C. P., Xue, Y., ... Hogan, B. L. M. (2009). Basal cells as stem cells of the mouse trachea and human airway epithelium.

Proceedings of the National Academy of Sciences, 106(31), 12771-12775.

<https://doi.org/10.1073/pnas.0906850106>

Ruzankina, Y., Schoppy, D. W., Asare, A., Clark, C. E., Vonderheide, R. H., & Brown, E. J.

(2009). Tissue regenerative delays and synthetic lethality in adult mice after combined deletion of Atr and Trp53. *Nature Genetics*, 41(10), 1144–1149.

<https://doi.org/10.1038/ng.441>

Sangster-Guity, N., Conrad, B. H., Papadopoulos, N., & Bunz, F. (2011). ATR mediates cisplatin resistance in a p53 genotype-specific manner. *Oncogene*, 30(22), 2526–2533.

<https://doi.org/10.1038/onc.2010.624>

Schlaermann, P., Toelle, B., Berger, H., Schmidt, S. C., Glanemann, M., Ordemann, J., ...

Meyer, T. F. (2016). A novel human gastric primary cell culture system for modelling *Helicobacter pylori* infection in vitro. *Gut*, 65(2), 202-213.

<https://doi.org/10.1136/gutjnl-2014-307949>

Schwenk, F., Baron, U., & Rajewsky, K. (1995). A cre-transgenic mouse strain for the ubiquitous deletion of loxP-flanked gene segments including deletion in germ cells.

Nucleic Acids Research 23(24), 5080-5081. <https://doi.org/10.1093/nar/23.24.5080>

Seidlitz, T., Merker, S. R., Rothe, A., Zakrzewski, F., Von Neubeck, C., Grützmann, K., ...

Stange, D. E. (2018). Human gastric cancer modelling using organoids. *Gut*, pp. 1–11.

<https://doi.org/10.1136/gutjnl-2017-314549>

Senbanjo, L. T., & Chellaiyah, M. A. (2017). CD44: A Multifunctional Cell Surface Adhesion Receptor Is a Regulator of Progression and Metastasis of Cancer Cells. *Frontiers in Cell*

and Developmental Biology, 5, 18. <https://doi.org/10.3389/fcell.2017.00018>

Shaner, N. C., Steinbach, P. A., & Tsien, R. Y. (2005). A guide to choosing fluorescent

- proteins. *Nature Methods*, 2(12), 905–909. <https://doi.org/10.1038/nmeth819>
- Simian, M., Hirai, Y., Navre, M., Werb, Z., Lochter, A., & Bissell, M. J. (2001). The interplay of matrix metalloproteinases, morphogens and growth factors is necessary for branching of mammary epithelial cells. *Development* 128(16), 3117-3131. <https://doi.org/10.1016/j.pestbp.2011.02.012>.Investigations
- Smalley, S. R., Benedetti, J. K., Haller, D. G., Hundahl, S. A., Estes, N. C., Ajani, J. A., ... Macdonald, J. S. (2012). Updated analysis of SWOG-directed intergroup study 0116: A phase III trial of adjuvant radiochemotherapy versus observation after curative gastric cancer resection. *Journal of Clinical Oncology* 30(19), 2327-2333. <https://doi.org/10.1200/JCO.2011.36.7136>
- Takeichi, M. (1991). Cadherin cell adhesion receptors as a morphogenetic regulator. *Science*, 251(5000), 1451–1455. <https://doi.org/10.1126/science.2006419>
- Tapia, O., Riquelme, I., Leal, P., Sandoval, A., Aedo, S., Weber, H., ... Roa, J. C. (2014). The PI3K/AKT/mTOR pathway is activated in gastric cancer with potential prognostic and predictive significance. *Virchows Archiv*, 465(1), 25–33. <https://doi.org/10.1007/s00428-014-1588-4>
- Telford, B. J., Chen, A., Beetham, H., Frick, J., Brew, T. P., Gould, C. M., ... Guilford, P. (2015). Synthetic Lethal Screens Identify Vulnerabilities in GPCR Signaling and Cytoskeletal Organization in E-Cadherin-Deficient Cells. *Molecular Cancer Therapeutics*, 14(5), 1213–1223. <https://doi.org/10.1158/1535-7163.MCT-14-1092>
- Torre, L., Bray, F., Siegel, R. L., Ferlay, J., Lortet-tieulent, J., & Jemal, A. (2015). Global Cancer Statistics, 2012. *CA: A Cancer Journal of Clinicians*, 65(2), 87-108. <https://doi.org/10.3322/caac.21262>
- Van De Wetering, M., Francies, H. E., Francis, J. M., Bounova, G., Iorio, F., Pronk, A., ... Clevers, H. (2015). Prospective derivation of a living organoid biobank of colorectal cancer patients. *Cell*, 161(4), 933–945. <https://doi.org/10.1016/j.cell.2015.03.053>

- Van der Post, R. S., Vogelaar, I. P., Carneiro, F., Guilford, P., Huntsman, D., Hoogerbrugge, N., ... Fitzgerald, R. C. (2015). Hereditary diffuse gastric cancer: updated clinical guidelines with an emphasis on germline CDH1 mutation carriers. *Journal of Medical Genetics*, 52(6), 361–374. <https://doi.org/10.1136/jmedgenet-2015-103094>
- Vlachogiannis, G., Hedayat, S., Vatsiou, A., Jamin, Y., Fernández-Mateos, J., Khan, K., ... Valeri, N. (2018). Patient-derived organoids model treatment response of metastatic gastrointestinal cancers. *Science*, 359(6378), 920-926. <https://doi.org/10.1126/science.aao2774>
- Xu, H., Lyu, X., Yi, M., Zhao, W., Song, Y., & Wu, K. (2018). Organoid technology and applications in cancer research. *Journal of Hematology and Oncology*, 11(1), 116. BioMed Central. <https://doi.org/10.1186/s13045-018-0662-9>
- Yang, J., & Weinberg, R. A. (2008). Epithelial-Mesenchymal Transition: At the Crossroads of Development and Tumor Metastasis. *Developmental Cell*, 14(6), 818-829. <https://doi.org/10.1016/j.devcel.2008.05.009>
- Ye, B., Jiang, L. L., Xu, H. T., Zhou, D. W., & Li, Z. S. (2012). Expression of pi3k/akt pathway in gastric cancer and its blockade suppresses tumor growth and metastasis. *International Journal of Immunopathology and Pharmacology*, 25(3), 627–636. <https://doi.org/10.1177/039463201202500309>
- Yin, X., Mead, B. E., Safaei, H., Langer, R., Karp, J. M., & Levy, O. (2016). Engineering Stem Cell Organoids. *Cell Stem Cell*, 18(1), 25-38. <https://doi.org/10.1016/j.stem.2015.12.005>
- Yu, Y., Savage, R. E., Eathiraj, S., Meade, J., Wick, M. J., Hall, T., ... Schwartz, B. (2015). Targeting AKT1-E17K and the PI3K/AKT pathway with an allosteric AKT inhibitor, ARQ 092. *PLoS ONE*, 10(10), e0140479. <https://doi.org/10.1371/journal.pone.0140479>

Appendix A

A.1 Reagent preparations

A.1.1 Antibody diluting buffer

Antibody diluting buffer for immunofluorescence consisted of 10% FHS and 2% FBS in PBS.

A.1.2 Blocking buffer

Blocking buffer for immunofluorescence consisted of 10% FHS in PBS.

A.1.3 Phosphate buffered saline (PBS)

PBS was made by dissolving one PBS tablet per 100mL H₂O, then autoclaving to sterilise.

A.1.4 Myofibroblast freezing medium

Freezing medium for myofibroblast cells (MFB11) consisted of 80% complete culture media, 10% additional FBS and 10% DMSO.

A.1.5 Trypsin preparation

0.05% trypsin was made by diluting 0.5% Trypsin at a 1:10 ratio with PBS.